2021

The Taste of Blood

Veronica Jove

THE TASTE OF BLOOD

A Thesis Presented to the Faculty of

The Rockefeller University

in Partial Fulfillment of the Requirements for

the degree of Doctor of Philosophy

by

Veronica Jové

June 2021

THE TASTE OF BLOOD

Veronica Jové, Ph.D.

The Rockefeller University 2021

Human blood and floral nectar are both appetizing meals to a hungry female mosquito, yet each meal fulfills a distinct nutritional requirement. While protein obtained from blood is required for females to develop eggs and successfully reproduce, carbohydrates supplied from plant nectar are sufficient for energy metabolism in both females and males. To procure essential nutrients from these distinct food sources, females employ two mutually exclusive feeding programs with unique sensory appendages, meal sizes, digestive tract targets, and metabolic fates. When a female is ready to reproduce, she must selectively seek the taste of blood and ignore the sweet taste of nectar. How does she flexibly modify her preference for the taste of blood to select the feeding program that satisfies her current metabolic needs?

Here we investigated the syringe-like blood-feeding appendage, the stylet, and discovered a population of sexually dimorphic chemosensory neurons that are the first neurons to contact blood as a mosquito bites her victim. Using pan-neuronal GCaMP calcium imaging, we found that stylet neurons robustly respond to blood and its components but are insensitive to nectar-specific sugars. The complex mixture of blood is detected by four functionally distinct stylet neuron classes, each tuned to specific blood components associated with diverse taste qualities. Surprisingly, one subset

contained polymodal “Integrator” neurons that responded only to mixtures of blood components belonging to distinct taste qualities.

What functional role does taste quality integration play in *Ae. aegypti*? We discovered that Integrator neurons selectively respond to physiological levels of blood glucose only in the presence of additional blood components like NaCl and $NaHCO_3$. Integrator neurons, like all remaining stylet neurons, are insensitive to nectar-specific sugars. Since glucose is the only redundant cue in blood and nectar, this unconventional taste coding mechanism confers context-specific information to distinguish between glucose present in blood versus nectar. Together these experiments reveal that specialized stylet neurons innately encode the distinction between blood and nectar at the very first level of sensory detection. This innate ability to recognize blood is the basis of global vector-borne disease transmission and is a remarkable example of how specialists can adopt exceptional neural coding strategies to thrive in their niche.

To my parents,

who taught me that a meaningful experiment is one that

asks a question for which we cannot predict the answer.

Als meus estimats avis,

gràcies per guiar-me per tal de portar

una vida amb seny i una mica de rauxa.

To Paul,

whose love has supported, challenged, and inspired me

to grow individually and together in our partnership.

Thank you for making this journey worthwhile.

ACKNOWLEDGMENTS

Thank you to my family, friends, colleagues, and mentors who have filled these last seven years with the extraordinary memories not captured in these pages.

I am deeply indebted to Leslie Vosshall for her support as my thesis advisor and head cheerleader. Leslie's extraordinary mentorship has left a deep impact on me that extends far beyond how to choose the right experiment or give a sensational presentation. Starting from when she nudged the timid rotation student to voice a question at the Friday lectures, Leslie has unfailingly demonstrated her confidence in me to grow as a scientist. Leslie encouraged me to burst into her office with exciting (and very raw) data and always entertained my latest crazy idea, which promised to be even more "brilliant" than the last. To this day, Leslie would have broken into Caspary to ensure this mid-pandemic defense is an affair to remember!

I am grateful for the unwavering support of my fabulous committee members, Vanessa Ruta and Winrich Freiwald. Their tremendous scientific knowledge spans protein crystallization to primate cognition, making every FAC meeting an exciting opportunity to receive insightful advice. Thank you Vanessa and Winrich for shaping my scientific trajectory and encouraging me to find the light at the end of the tunnel. Your shared enthusiasm for great science continues to inspire me as I navigate the next chapter of my career!

Thank you Ardem Patapoutian for the interest you have taken in our story and your insightful feedback along the way. As I started to imagine how the taste of blood might be recognized, I repeatedly returned to Ardem's elegant work as a paradigm for how to discover the identity and function of novel sensory receptors. I am thrilled to have Ardem serve as the external examiner and I am truly grateful for the time he has committed to join us for the defense.

Many thanks to Andrea, Cris, Emily, Kristen, Marta, Sid, and Stephanie in the Dean's Office for their dedication to the David Rockefeller Graduate Program. I am so grateful for the opportunity to attend international conferences, study at the Marine Biology Laboratory, and always have a computer fast enough to process all my data! Thank you all for cutting through the fluff so that we can focus on the science.

This thesis represents the culmination of many years of work for me and my fantastic collaborators. A special thank you to Zhongyan Gong, Felix Hol, Zhilei Zhao, Trevor Sorrells, Thomas Carroll, and Lindy McBride, all of whom contributed key data to the work presented here. Thank you all for your creativity and generosity that helped shaped this project. I also appreciate the support from the Rockefeller Resource Centers and our commercial partners, including Alison North, Christina Pyrgaki, Dan Gross, Jim Petrillo, Connie Zhao, Bin Zhang, Gavin Jeffries, Rob Harrell, Andrew Gerson, and Tasos Siskoglou.

I am grateful for the opportunity to do my PhD in the vibrant Vosshall Lab. Each person, past and present, has played an important role in making the lab such a wonderful place to do science. Thank you to Gloria Gordon, Libby Mejia, and Barbara Ghelardi for their steadfast support that makes our lab feel like a family. I would also like to highlight the former and current Vosshall Lab members who have mentored me at various points throughout my PhD. Thank you to Nilay Yapaci and Emily Dennis, who helped me to develop the initial project proposal, and to Ellen De Obaldia and Meg Younger, who mentored me as a rotation student and have provided key feedback along the way. I am indebted to Takeshi Morita and Laura Duvall who have been extremely generous in sharing their expansive knowledge of experimental techniques and scientific prowess. Finally, thank you to Ben Matthews for enabling all of us to ask real neuroscience questions in *Aedes aegypti*. During the time that we overlapped in the Vosshall lab, Ben was a second PI to me and I truly enjoyed our banter to refine the "right" experiment. Thank you for shaping the way that I think as a scientist!

Perhaps one of the greatest surprises of graduate school is the opportunity to work with so many talented scientists who have also become close friends. Given the social distancing restrictions at the time of writing, it is hard to believe that Margo Herre, Trevor Sorrells, Nipun Basrur, Krithika Venkataraman, and I have worked within six feet of each other for five years. Together, we've witnessed all of the news worth sharing- from popping our heads over the bay to ask, "wanna see something cool?!", to comforting each other when the mutants have no phenotype, to cheering each other on when the paper is accepted or when you land the dream job. I would also like to thank

Marc, Maria José, and baby Nil, along with Roey and Aster, and their humans, Elisabeth, Annie and Kevin, Amy, and the whole gang from NYU- Simón, Anthony, Korey, Deana, Lisa, Vangel, Kristina, Chris, Alissa, Zhenni. I've learned so much from you all and perhaps most importantly, had a ton of fun together. Thank you all for being amazing colleagues and friends.

Thank you to all the friends and family who have supported me throughout this seemingly endless endeavor. I wished I still lived closer to Jill, Sabrina, Joanna, Elle, Ludovica, Victoria, and Marial. Yet every time we see each other, it's like being transported back to all those years ago when we lived in the same place. Thank you to my second family, the Mullers, who have provided the laughs necessary to sustain morale during an unforgiving PhD. A big hug to my entire family living all over the world, from Barcelona to New York to Shanghai. Thank you for sharing your loving homes with me across the world- our visits were always a highlight during my PhD.

I am extremely grateful to have had all four of my grandparents as a strong presence in my life. I wish I could have lived physically closer to my grandparents in China, but I eagerly awaited our visits and remember with great fondness the rare moments when their serious faces would break into the most deeply loving smiles. I also have to thank Rockefeller for bringing me ten blocks away from Yaya and Avi, allowing us to share the intricacies of our daily lives, in addition to major life events. I looked forward to sharing the *sobretaula* together every weekend, with Avi sharing rich stories and delivering clever jokes with a straight face, and Yaya checking in to make sure the

mosquitoes are ‘behaving’. Our time together has been the highlight of my PhD *i us estimo moltíssim*.

As throughout my entire PhD, I hesitate to disclose here that my parents are scientists themselves. In fact, I may have subconsciously gravitated towards mosquito neurobiology because it is the most extreme opposite of my parents’ expertise. However, when I look back at how my parents showed me the most interesting question is the one for which we cannot predict the answer, I realize it is not a coincidence that I became a scientist. Throughout my PhD, they have been mentors as well as parents. I am so grateful for their love and *extremely* honest feedback that has carried me here today. I would like to think that despite their academic achievements, being parents is their favorite experiment thus far. However, it is only n=1 and we are missing positive and negative controls, so we will never really know.

Finally, thank you Paul. Grad school has been filled with so many ups and downs, but the one constant is that I have been lucky to have you as my partner throughout this entire journey. We’ve shared in so many wonderful memories all over the world, but this chapter is bookended by The Rock. I love you and can’t wait to start the next chapter together. WE OUT (*FINALLY*)! 

x

TABLE OF CONTENTS

LIST OF FIGURES

INTRODUCTION

While generalist species compete with other generalists for a variety of food sources and habitats, specialist species carve out a unique ecological niche by maximizing resources from a particular food source and habitat. These specialist species have evolved remarkable feeding adaptations to flourish in their individual niches. Specialized feeding strategies include exceptional mouthpart morphology, digestive specialization, and resistance to toxins and pathogens. For example, certain butterfly species have mouthparts far longer than their total body length, allowing them to reach deeper stores of floral nectar that are inaccessible to their competitors (Bauder et al., 2011). To digest the toxic eucalyptus plant, koalas have two lineage-specific monophyletic expansions of the cytochrome P450 family to promote liver detoxification (Johnson et al., 2018). Finally, the grasshopper mouse expresses a variant of Nav1.8, which enables the mouse to prey on several venomous creatures including scorpions (Rowe et al., 2013). While adaptation to a particular set of environmental circumstances often makes specialists more susceptible to habitat destruction by humans, certain specialist species like mosquitoes have instead adapted their niche to depend directly on humans and the habitats we have built (McBride, 2016; McBride et al., 2014; Rose et al., 2020; Takken and Verhulst, 2013).

Blood-feeding mosquitoes have adapted extraordinary strategies to obtain large protein meals from vertebrate blood. Female blood-feeding mosquitoes developed a syringe-like stylet that enables them to pierce through skin and pump a blood meal that

effectively doubles their body weight (Duvall et al., 2019; Gordon, 1939; Lee, 1974; Lee and Craig, 1983). Specific vesicle transporter pathways secrete digestive enzymes and proteases into the midgut to efficiently digest this bolus of blood meal proteins (Isoe et al., 2011). To locate a suitable host for this blood meal, certain blood-feeding species like *Ae. aegypti* have evolved a preference for the scent of human victims over that of non-human vertebrates (DeGennaro et al., 2013; McBride, 2016; McBride et al., 2014; Rose et al., 2020; Takken and Verhulst, 2013). This preference for human odor has evolved alongside an ability to breed in human habitats and transmit vector-borne diseases like Zika, dengue, and Yellow fever (McBride, 2016; McBride et al., 2014; Rose et al., 2020; Takken and Verhulst, 2013). Thus, the adaptations to feed on blood from a human are the direct mechanism by which mosquitoes transmit devastating diseases to millions of people across the globe. Despite its relevance for public health, very few studies have directly investigated the female mosquito's ability to recognize and feed on blood (Benton, 2017). Researchers have speculated that exceptional neural coding strategies may facilitate this specialized behavioral program, but mechanistic insight into these strategies has remained elusive (Benton, 2017; Lee, 1974; McBride, 2016).

1.1 Female mosquitoes engage mutually exclusive feeding programs to feed on protein and carbohydrates

Although female *Aedes aegypti* mosquitoes are specialized to obtain protein from blood meals, they also require carbohydrates from nectar meals to survive. Each meal

is linked to a specific nutritional value and food source: nectar carbohydrates are sufficient for energy metabolism in both females and males and blood proteins are necessary for females to develop eggs and successfully reproduce. Mosquitoes take nectar from plant sources like flowers and are likely attracted by olfactory floral cues (Lahondere et al., 2020; Van Handel, 1972). In contrast, a blood meal must be obtained from a human or other vertebrate animal and females integrate sensory cues like carbon dioxide (CO_2), heat, and odor to locate their victim (Dekker et al., 2005; Liu and Vosshall, 2019; McMeniman et al., 2014).

To procure necessary nutrients from these distinct food sources, females employ two behaviorally and anatomically distinct feeding programs: blood feeding and nectar feeding. Each feeding program is linked to a distinct, feeding appendage, meal size, and digestive tract (Gordon, 1939; Trembley, 1952). Nectar is detected by the labium (Sanford et al., 2013). Blood is likely detected by the stylet, which pierces skin and directly contacts blood (Gordon, 1939; Trembley, 1952). The stylet is a needle-like feeding tube and stylet neurons are located on the part of the stylet referred to as the labrum (Lee, 1974). All parts of the stylet, including the labrum, maxillae, mandibles, and hypopharynx pierce the skin and directly contact blood, but the labrum is the only innervated part of the stylet. Females typically take small nectar meals but engorge on blood, consuming a volume that reliably doubles their body weight and provides sufficient protein to allow them to produce 100 – 150 eggs per blood meal. Finally, the nectar meal is routed initially to the crop, whereas ingested blood entirely bypasses the crop and is directed to the midgut, which is specialized to digest protein for egg

(Gordon, 1939; Trembley, 1952). Thus, the mosquito has parallel feeding pathways for blood and nectar from sensory periphery, to visceral organs, to the ultimate metabolic function of the meal. This strict separation in feeding programs may allow the female to maintain a hunger for blood even after taking a nectar meal to sustain her metabolism.

What information does the female evaluate prior to selecting the appropriate feeding program? Classic behavior experiments hinted that initiation of the blood- and nectar-feeding programs is context-dependent and not simply hard-wired to detection of blood or nectar. In the absence of human sensory cues like heat and CO_2, female mosquitoes readily ingest nectar via the nectar-feeding program. In the presence of human sensory cues, females will reliably bite and feed on warm blood delivered in an artificial feeder (Bishop and Gilchrist, 1946; McMeniman et al., 2014). But if the blood meal is replaced with nectar sugars, females reject the meal entirely even though heat and CO_2 are present (Bishop and Gilchrist, 1946). Therefore, the mechanism that distinguishes between blood and nectar must be flexible enough to promote ingestion of nectar only when a mosquito intends to feed on nectar and not when she intends to feed on blood.

Why is it important for the female to draw such a clear distinction between blood and nectar once she engages the blood-feeding program? The standard meal size associated with the blood-feeding program is so large that she needs several hours to days to digest an erroneous meal before the midgut is free for a full blood meal (Duvall et al., 2019; Li et al., 2019). While this may be a worthwhile trade-off for blood - one

meal produces a full clutch of 100 – 150 eggs - engorging on nectar is a grave error because it lacks the protein required for egg production.

From a global health perspective, understanding how the female distinguishes blood from nectar is critical because blood detection is the essential first step in disease transmission. *Ae. aegypti* females acquire flaviviruses like Zika and dengue by ingesting a blood meal from an infected person. If a mosquito could not detect the taste of blood and did not initiate blood feeding, the virus contained in that blood meal would not reach the midgut, where viral replication occurs (Ruckert and Ebel, 2018). However, once a mosquito becomes infected, the taste of blood may not be essential for transmission to the next person. When the female bites the next person, the virus is transmitted through the hypopharynx salivary duct, which is a non-neuronal fascicle bundled with the stylet (Griffiths and Gordon, 1952). Upon piercing, viral transmission through saliva likely occurs, even in the absence of ingesting the meal (Griffiths and Gordon, 1952). Therefore, preventing females from drawing the initial blood meal from an infected person is key to preventing disease transmission.

1.2 The taste of food signals meal quality to animals

How do female mosquitoes recognize blood and distinguish it from nectar? Many animals distinguish between protein- and carbohydrate-rich meals by their savory ("umami") or sweet taste, respectively (Liman et al., 2014; Yarmolinsky et al., 2009). These two taste qualities signal different nutritional values, and animals use diverse

strategies to prioritize ingestion of the food source that best matches their current metabolic requirements. For feeding specialists, discrimination between savory and sweet tastes can be hardwired into the animal's genetic code. Cats are obligate carnivores that have lost the canonical sweet taste receptor but retain a functional umami receptor (Li et al., 2005). Hummingbirds, which are nectar-feeding specialists, have evolved a novel sweet taste receptor from the ancestral umami receptor (Baldwin et al., 2014). For feeding generalists like flies, rodents, and humans, both protein and carbohydrates are useful energy sources, and these animals can detect both savory and sweet tastes. Detection of either taste typically promotes feeding unless an animal becomes deficient in a specific nutrient (Deutsch et al., 1989; Leitao-Goncalves et al., 2017; Liu et al., 2017; Murphy et al., 2018; Ribeiro and Dickson, 2010; Simpson et al., 2015; Steck et al., 2018). After days of protein deprivation, for example, animals can still detect savory and sweet, but savory taste circuit sensitivity is increased to promote a protein-specific appetite (Liu et al., 2017; Steck et al., 2018).

Intrinsic indifference is ideally suited for specialists that utilize only one food source while acute neuromodulation is an effective means for generalists to conditionally prioritize one food source. However, female blood-feeding mosquitoes are specialists with two parallel specific appetites for protein and carbohydrates that each require a different feeding program and fulfill distinct physiological processes. The mechanism that enables mosquitoes to engage mutually exclusive feeding programs for each food source is unknown.

A hint may lie in the fact that independent sensory neuron populations, located in either the stylet or labium, are in direct contact with the meal during the blood- and nectar-feeding programs, respectively. If the preference for blood is hardwired into the sensory appendage involved in blood-feeding, we would expect it to be a specialized blood detector that is either intrinsically insensitive to nectar sugars, or able to detect nectar sugars differently than the sensory neurons involved in nectar feeding. Alternatively, blood-feeding and nectar-feeding neurons do not have to be specialized and could have the capacity to detect both blood and nectar. If so, the presence of a human cues could increase the sensitivity for blood and/or decrease the sensitivity for nectar sugar to selectively promote blood-feeding. To distinguish between these possibilities, a fundamental understanding of blood and nectar detection in *Ae. aegypti* is crucial.

1.3 Detection of blood and nectar is likely mediated by chemosensation

The sensory mechanisms of blood recognition prior to initiating blood-feeding behavior are unknown. However, classic behavioral experiments have demonstrated that the nutritional value of blood as a protein source can be decoupled from blood-feeding behavior. The protein fraction of blood is neither sufficient nor necessary to trigger feeding, but a mixture of key plasma components such as adenosine triphosphate (ATP), sodium chloride (NaCl), and sodium bicarbonate ($NaHCO_3$) reliably induces blood-feeding behavior (Galun et al., 1963; Galun et al., 1984; Hosoi, 1959). Importantly, non-hydrolyzable analogues of ATP in saline are still sufficient to trigger

engorgement, indicating that energy release from ATP hydrolysis is not required (Galun et al., 1985b). Together these results suggest that chemosensory detection of specific blood components is critical for blood recognition.

The stylet is the only sensory appendage that directly contacts blood and is therefore likely the primary structure that evaluates blood prior to initiation of blood-feeding. Electron microscopy studies have revealed the presence of female-specific sensory sensilla at the tip of the stylet (Lee, 1974). Sensilla are specialized insect cuticle structures that house sensory neuron dendrites. Chemical ligands enter chemosensory sensilla through pores to directly contact these dendrites (Stocker, 1994). Extracellular recordings from one stylet sensillum type documented neuronal activity in response to specific plasma components (Werner-Reiss et al., 1999a, b, c). In the two decades since these studies were reported, many questions remain. Do individual stylet sensory neurons respond to whole blood as a mixture or are they are tuned to recognize individual blood components? Blood contains components that are traditionally associated with distinct taste qualities including sodium chloride (salty), protein (umami), glucose (sweet), and CO_2 (sour/carbonation). Is blood recognized as a single taste quality, or are multiple taste qualities integrated to form the perception of blood? Does the taste of blood overlap exclusively with canonical taste qualities, or is recognized by unconventional tastant(s) found exclusively in blood? The stylet's neuroanatomical and molecular organization that could facilitate blood responses also remains completely unexplored.

Unlike blood, the receptors and neural circuits involved in sugar detection have been well characterized in *D. melanogaster,* which has been extensively studied as a model for insect sweet taste processing (Marella et al., 2006; Scott, 2018; Thorne et al., 2004; Yarmolinsky et al., 2009). A subfamily of canonical sugar Gustatory Receptors (GRs), most notably *Dmel_Gr5a* and *Dmel_Gr64f*, are expressed in sweet gustatory neurons that are located on sensory appendages like the labellum and leg (Scott, 2018; Slone et al., 2007; Thorne et al., 2004). Exogenous activation of *Dmel_Gr5a*+ or *Dmel_Gr64f*+ neurons is sufficient to induce sugar-feeding in the absence of real sugar (Klapoetke et al., 2014; Marella et al., 2006). Transcriptomics data of the proboscis and legs indicate that *Ae. aegypti* express orthologs of the sweet taste receptor subfamily (Matthews et al., 2018; Matthews et al., 2016; Sparks et al., 2013). The labium is the mouthpart used in nectar feeding and electrophysiology experiments have demonstrated that labium gustatory neurons can respond to sucrose (Sanford et al., 2013). However, it is unknown if activation of sweet gustatory neurons is sufficient to initiate nectar-feeding in *Ae. aegypti.* Yet the most stimulating question asks how sugar detection is flexible enough to promote ingestion when a mosquito intends to feed on nectar, but prevent ingestion when a mosquito intends to feed on blood.

To prevent errors in selecting the appropriate feeding program, the female should not initiate engorgement when the stylet contacts nectar sugars in the context of blood feeding. Of the sugars found in nectar, glucose is of particular interest since it is the only known redundant cue present in blood and nectar. Other specialists like the cat and hummingbird have eliminated the need for active discrimination by losing the ability to

detect sweet and umami, respectively. However, female mosquitoes must still retain the ability to detect sugars, including glucose, in the context of nectar feeding. One potential way to achieve both goals is to determine segregation by gene expression, rather than genetic mutation. For example, the mosquito could segregate the expression of sweet taste receptors so that they are expressed in the labium, but not the stylet, rendering the stylet nectar-insensitive. If the stylet is nectar-sensitive, however, the presence of human cues associated with the blood-feeding context could modulate sweet taste sensitivity and/or processing. This mechanism would more closely resemble feeding strategies used by generalists like *D. melanogaster* and rodents to temporarily prioritize one food source upon nutrient deprivation. However, these time scales typically occur over several hours to days and therefore could not explain the female's ability to prioritize the blood-feeding program within seconds to minutes of finding a human. If the stylet does express sweet taste receptors, then it must also have a divergent neuromodulatory mechanism that allows for dynamic and rapid changes to glucose sensitivity.

1.4 The neural basis of taste quality recognition

Taste coding has been most extensively characterized in generalist species, including *Drosophila melanogaster* flies*, Mus musculus* mice*, Rattus norvegicus* rats**,** and *Homo sapiens.* These studies have led to the hypothesis that taste is comprised of five canonical taste qualities conserved across insects, rodents, and humans: sweet, sour (CO_2), bitter, salty, and umami (savory) (Liman et al., 2014; Yarmolinsky et al.,

2009). While the molecular receptors for each taste quality are not conserved between insects and mammals, the circuit logic underlying the perception of taste is thought to be conserved across these species (Liman et al., 2014; Yarmolinsky et al., 2009). In the labelled line model of taste coding, each taste quality is detected by unique receptor(s), which are expressed in sensory cells that respond exclusively to that taste quality (Chandrashekar et al., 2009; Liman et al., 2014; Marella et al., 2006; Thorne et al., 2004; Yarmolinsky et al., 2009). Activation of this dedicated sensory cell population activates an anatomically unique region of the taste-processing center in the brain (Barretto et al., 2015; Marella et al., 2006; Thorne et al., 2004). Downstream synaptic partners are also thought to main segregation between taste qualities to ensure that activation of the particular taste-processing circuit is hard-wired to one of two feeding behaviors: ingestion or avoidance of food (Barretto et al., 2015; Chen et al., 2011; Marella et al., 2006; Peng et al., 2015; Zhang et al., 2019). According to this model, sugars should be detected by sweet taste receptors, which are expressed in sweet taste cells, which express to a sweet taste-processing center in the brain, which is hard-wired to ingestion of the sugar meal. This entire sweet taste circuit should never respond to any of the remaining taste qualities and the remaining taste circuits should never respond to sugar. A smaller faction of the field has argued that this model is oversimplified and that some neurons at various nodes in the taste circuit can be more broadly tuned (Jaeger et al., 2018; Ohla et al., 2019; Wu et al., 2015). While technical discrepancies across research groups have yet to be resolved, it has become clear that even these generalist species can detect other qualities of food that are not canonical

taste qualities. For example, fatty acids have been shown to activate a subpopulation of sweet-taste sensory neurons in *D. melanogaster* (Ahn et al., 2017; Tauber et al., 2017).

Do specialists like *Ae. aegypti* rely on canonical taste qualities and segregated circuits to distinguish between blood and nectar? Nectar is composed of sucrose, fructose, and glucose, which are traditionally associated with the sweet taste quality. However, blood is comprised of components that span multiple canonical and non-canonical taste qualities. If multiple blood components and taste qualities are indeed detected, how will they be encoded by blood-sensitive neurons? Will each component activate a unique sensory neuron population that is integrated centrally to form the perception of blood, or is there a single population of blood-sensitive neurons that exclusively represents blood as a novel taste quality in the mosquito? If non-canonical taste qualities are detected, will they be detected by and projected to the same populations and brain regions that detect canonical taste qualities? The strict behavioral separation between blood- and nectar-feeding invites speculation that *Ae. aegypti* may have labelled lines for each feeding program. If so, nectar and blood should be detected by unique receptors and activate mutually exclusive sensory neuron populations, which should in turn project to segregated downstream circuits. Despite decades of taste research in model organisms, the molecular, cellular, and functional rules of mosquito taste coding remain a mystery.

1.5 Final Remarks

Here we show that female *Ae. aegypti* mosquitoes possess sexually dimorphic stylet neurons that are specialized to distinguish blood from nectar. Using pan-neuronal GCaMP calcium imaging, we found that stylet neurons robustly respond to blood and its components but are insensitive to nectar-specific sugars. We defined a mixture of four blood components—ATP, glucose, sodium bicarbonate, and sodium chloride—that reliably trigger blood-feeding behavior and determined that these ligands activate the same population of stylet neurons as blood. By presenting these ligands individually or as mixtures, we show that the taste of blood is combinatorial across multiple taste qualities. We defined functionally distinct subsets of stylet sensory neurons that are selectively tuned to specific blood components. Since the transcriptional profile of stylet neurons was unknown, we performed RNA-seq on the stylet to identify genetic markers that selectively label these neuronal subsets. We identified *Ir7a* and *Ir7f* as female stylet-specific transcripts and generated driver lines for both genes using CRISPR-Cas9 genome editing. We found that each driver line labels a functionally distinct subset of blood-sensitive stylet neurons activated by different components of blood. Finally, we discovered polymodal stylet neurons that respond to physiological levels of blood glucose only in the presence of additional blood components: sodium chloride and sodium bicarbonate. Importantly, all stylet neurons, including these “Integrator” neurons, are not activated by high concentrations of nectar-specific sugars. Since glucose is a redundant cue in blood and nectar, coincident detection of multiple blood components in Integrator neurons confers context-specific information to glucose. These experiments

reveal that upon initial contact with blood, specialized sensory neurons in the mosquito stylet innately encode the distinction between blood and nectar.

CHAPTER 2. STYLET NEURONS ARE THE FIRST TO CONTACT BLOOD PRIOR TO BLOOD FEEDING.

When a female bites a human, she retracts the labium, uncovering the needle-like stylet required to draw blood. During blood feeding, the needle-like stylet pierces the skin to come into direct contact with blood. In contrast, the labium rests on the skin's surface, which prevents it from contacting blood (Figure 2.1A,B) (Gordon, 1939; Griffiths and Gordon, 1952; Ramasubramanian et al., 2008). During nectar feeding, the labium directly contacts the nectar source and the stylet remains recessed and ensheathed within the labium (Figure 2.1C,D). In this configuration the stylet serves as a feeding tube for passing liquids after pumping is initiated. Once pumping begins, all liquids, including nectar, pass over the recessed stylet in both females and males. In this context, the structural function of the stylet likely resembles the labral sensory organ that is best studied in *D. melanogaster* (LeDue et al., 2015; Stocker, 1994). There is a striking difference in the meal volume consumed and how these meals are metabolized by the digestive system after ingestion. The average sugar meal size is 0.87 µL, in stark contrast to the average blood meal size of 3.20 µL (Figure 2.1E,F). Finally, the blood meal is immediately directed to the midgut for blood protein digestion, whereas the sugar meal is first directed to the crop (Figure 2.1G).

Features of each behavioral program can be precisely quantified in the lab using blood- and nectar-feeding assays (Figure 2.1H) (Costa-da-Silva et al., 2013; Liesch et al., 2013). The blood-feeding assay offers females warmed meals in the presence of

CO_2 and heat, which attracts them to the artificial feeder (Liu and Vosshall, 2019; McMeniman et al., 2014). Upon landing, a parafilm membrane separates the female from the meal, forcing her to pierce it with the stylet just as she pierces skin to contact blood (Figure 2.1H, top). In contrast, the nectar-feeding assay offers females room temperature meals on a cotton ball, allowing the labium to directly contact the meal upon landing (Figure 2.1H, bottom).

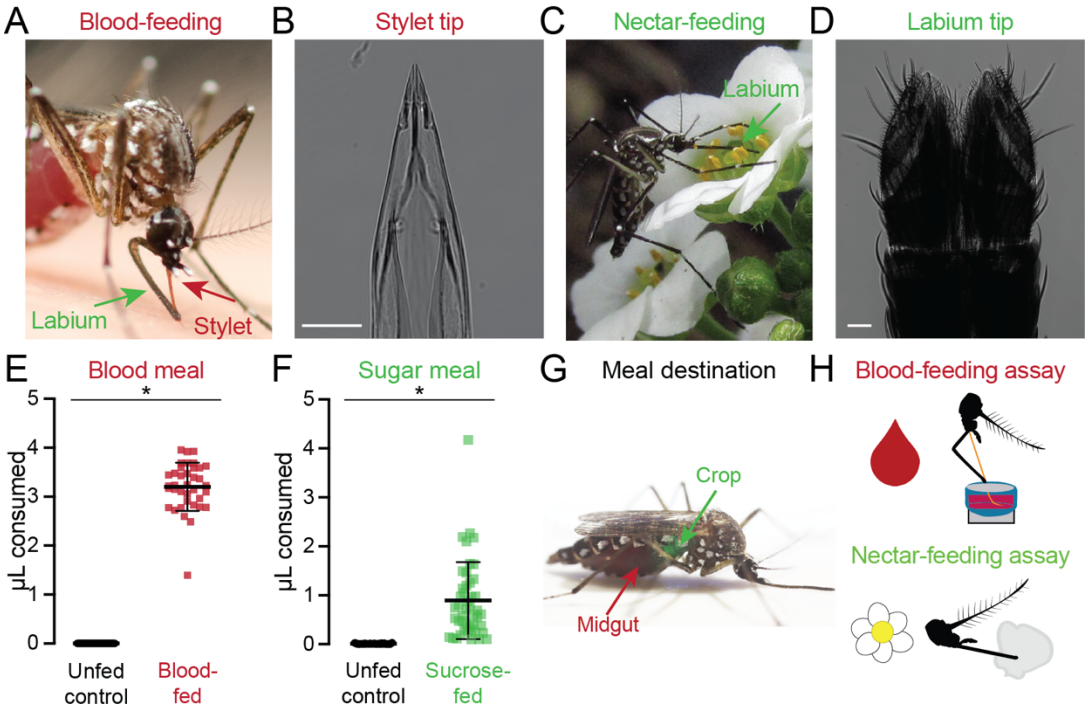

Figure 2.1 Blood- and nectar-feeding are mutually exclusive feeding programs.

(A,C) An *Ae. aegypti* female feeding on human skin (A, Photo: Benjamin Matthews) or flower nectar (C, Photo: Eric Eaton).
(B,D) Transmitted light image of the female stylet (B) or labium (D). Scale bars: 25 µm.
(E,F) Volume of meal consumed after presenting blood (E) or sugar (F). Unfed controls were not given the option to feed and therefore represent the baseline for the assay. Each data point represents 1 female (mean ± SD, N=37-46; * $p < 0.05$ Mann-Whitney test).

(G) *Ae. aegypti* female with a blood meal in the midgut (red) and a 10% sucrose meal in the crop (green). Green food dye added to 10% sucrose to visualize meal location. (H) Schematic of blood- (top) and nectar-feeding (bottom) behavior assay.

Thus, these behavior assays provided data to confirm that blood and nectar feeding are indeed two distinct feeding programs, each segregated by sensory appendage, meal size, and meal destination. Since blood feeding is the most intriguing behavior from both a basic and translational science perspective, we first started with understanding the requirements for blood-feeding. The behavior experiments performed in this chapter were designed to: (1) confirm earlier work that suggested blood-feeding behavior is decoupled from the protein requirement of egg development and (2) test the hypothesis that meal quality is a separate step of sensory evaluation after the female has used volatile sensory cues to locate a host. If meal quality is indeed evaluated prior to engorgement, we hypothesized that the stylet may play a key role because it is the only innervated appendage to directly contact blood. We therefore evaluated the neuroanatomy of the female stylet to identify the sensory neurons poised to detect the taste of blood.

2.1 Female mosquitoes evaluate the taste of blood prior to engorgement

What are the minimal sensory inputs required to initiate blood feeding? When we used the blood-feeding assay to offer females warm sheep blood in the presence of heat and CO_2, they engorged on the meal, roughly doubling their initial body weight (Figure 2.2A-C). To separate meal composition from human cues, we maintained CO_2

and heat delivery and exchanged the warm blood meal for warm sucrose or a saline solution that was isotonic with blood. Females consistently rejected both sucrose and saline in the blood-feeding assay, indicating that engorgement requires a separate step of evaluation after the female encounters a meal in the presence of human cues (Figure 2.2C).

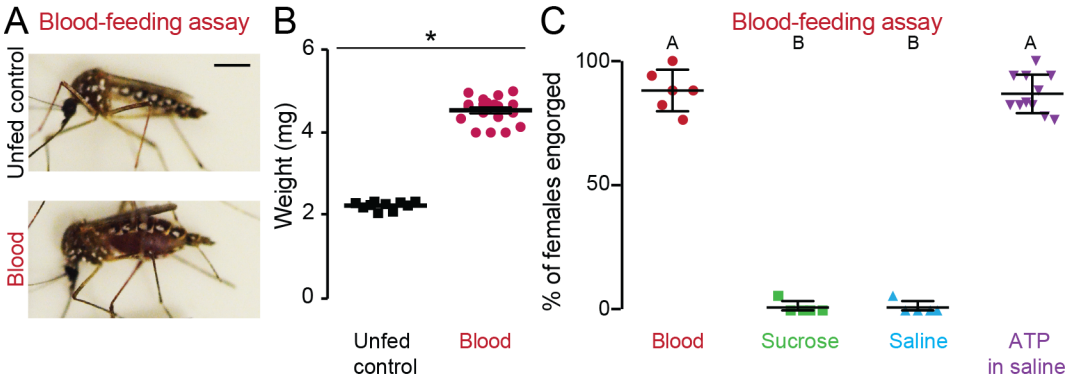

Figure 2.2 Engorgement is a separate step of evaluation after finding a potential host.

(A) Female mosquitoes following 15 min exposure to different meals. Scale bar, 0.1 cm.
(B) Sampled weight measurements from data for engorged females offered blood or unfed controls not offered any meal; N=10-19 weight measurements/meal (mean ± SEM; * $p < 0.05$ unpaired t-test).
(C) Female engorgement on the indicated meal delivered via Glytube. Each data point denotes 1 trial with 15-20 females/trial: N=5-11 trials/meal. Data labeled with different letters are significantly different from each other (mean ± SD; Kruskal-Wallis test with Dunn's multiple comparison, $p < 0.05$).

Classic work from Hosoi and Galun indicated that the nutritional value of blood as a protein source can be uncoupled from blood-feeding behavior. These studies identified ATP as a phagostimulant that could trigger engorgement only when co-presented with additional plasma components like sodium chloride (NaCl) and sodium bicarbonate ($NaHCO_3$) (Galun et al., 1963; Galun et al., 1984). We replicated these experiments in

the Liverpool *Ae. aegypti* laboratory strain and confirmed that an artificial blood meal sufficient for egg production, which consists of blood proteins, NaCl, and $NaHCO_3$ (Kogan, 1990), did not trigger engorgement unless ATP was added (Figure 2.3A,B). As previously reported, a protein-free solution of saline and ATP, or its non-hydrolyzable analogues, is sufficient for engorgement. (Figure 2.3C,D) (Galun et al., 1963; Galun et al., 1985b; Galun et al., 1984). Finally, changing the concentration of ATP altered the probability of initiating engorgement (Figure 2.3E), but did not affect the meal size (Figure 2.3F). These behavioral data confirm classic observations by Galun and Hosoi and suggest that females can accurately recognize specific sensory features of blood and nectar to choose the appropriate feeding response.

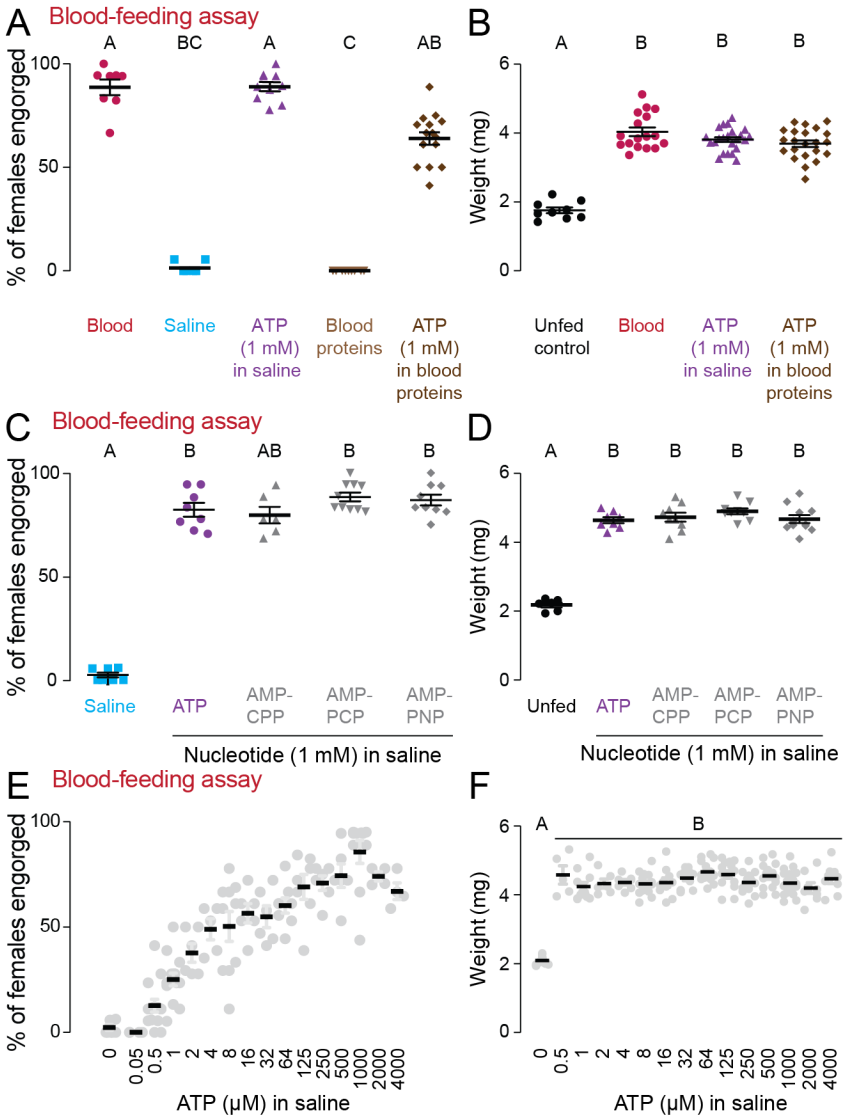

Figure 2.3 Engorgement is decoupled from the protein requirement of egg production.

(A, C) Female engorgement on the indicated meal delivered via Glytube. Each data point denotes 1 trial with 15-20 females/trial: N=6-16 trials/meal**.** Data labeled with different letters are significantly different from each other (Kruskal-Wallis test with Dunn's multiple comparison, $p < 0.05$).
(B, D, F) Sampled weight measurements from engorged females offered the indicated meal or unfed controls not offered any meal from data in (A, C, E), respectively. N=5-25 weight measurements. Data labeled with different letters are significantly different from each other (mean ± SEM; one-way ANOVA with Dunnett's multiple comparisons with a single pooled variance, $p < 0.05$).

(E) Female engorgement on the indicated concentration of ATP delivered in saline via Glytube. Each data point denotes 1 trial with 15-20 females/trial, N=4-14 trials/meal (mean ± SEM).
Ligands: saline = 110 mM NaCl and 20 mM $NaHCO_3$; blood proteins = 15 mg/mL gamma-globulin, 8 mg/mL hemoglobin, 102 mg/mL albumin in 110 mM NaCl and 20 mM $NaHCO_3$ (Duvall et al., 2019; Kogan, 1990); AMP-CPP (α,b-methyleneadenosine 5'-triphosphate lithium salt), AMP-PNP (b,g-imidoadenosine 5'-triphosphate lithium salt hydrate), AMP-PCP (β,γ-methyleneadenosine 5′-triphosphate disodium salt).

2.2 Stylet neurons innervate the distal tip that directly contacts blood

To understand how the taste of blood is recognized prior to blood-feeding, we first examined the stylet because it is the only sensory appendage to directly contact blood. We reasoned that if the stylet is assessing meal composition prior to engorgement, it must directly contact the meal both in situations where the mosquito decides to engorge and those where she does not. The blood-feeding assay gives a sensitive end-point measure of ingestion behavior but does not provide information about how and whether the stylet contacts the meal. To track the stylet of individual females in response to different meals presented with heat and CO_2, we used the biteOscope assay (Hol et al., 2020). The biteOscope consists of a transparent bite substrate mounted in the wall of a cage for high-resolution imaging of freely behaving mosquitoes. Subsequent manual video analysis enables the characterization of landing, piercing, and feeding dynamics at the individual mosquito level.

The biteOscope allowed us to visualize the stylet as it pierces a membrane and to determine whether the female subsequently engorged on warmed meals of water, saline, or ATP in saline (Figure 2.4A). We selected ATP in saline as a proxy for blood

since biteOscope meals must be optically clear to enable stylet video tracking. In all three conditions, the females repeatedly landed on the membrane and pierced it, bringing the stylet into direct contact with the meal, but females engorged only on the meal composed of ATP in saline (Figure 2.4B-E). Once females engorged, they were less likely to return to the membrane, which accounts for a lower number of total landings in the ATP in saline cohort (Figure 2.4B,D). We conclude that human cues like heat and CO_2 are sufficient to cause the female to pierce with her stylet and contact the meal, but additional blood-specific cues from the meal itself are required to trigger and sustain engorgement.

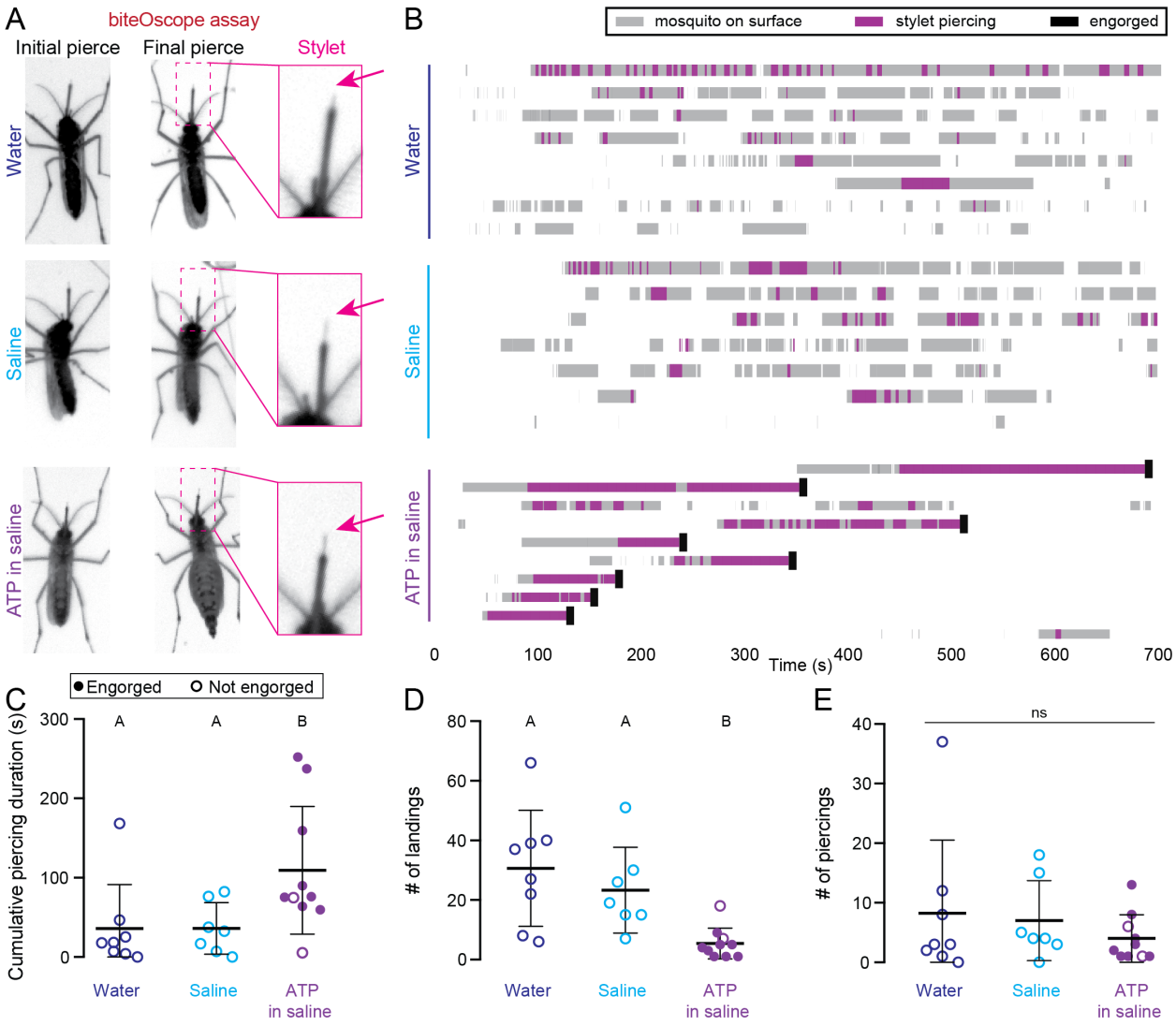

Figure 2.4 The stylet directly contacts the meal prior to engorgement.

(A) Still video frames of female in biteOscope assay when stylet contacted meal for the first (left panel) or last (middle panel) time during the trial. Inset at right is from middle panel.
(B) biteOscope ethogram of landing events (gray boxes), stylet piercing events (purple boxes), and engorgement events (black boxes) for individual females provided water (N=8 females), saline (N=7 females), or 1mM ATP in saline (N=10 females) over 700 sec trial. Each row is an ethogram from 1 female.
(C-E) Summary statistics from individual female ethograms in (B) for cumulative piercing duration during trial (C), # of landings (D), and # of piercings (E) for indicated meal. Each dot denotes 1 female, filled dot represents an engorged female. In C,E, data labeled with different letters are significantly different from each other (mean ± SD; Kruskal-Wallis test with Dunn's multiple comparison, $p < 0.05$). In D, data labeled with

different letters are significantly different from each other (mean ± SD; one-way ANOVA with Tukey's multiple comparisons test).

2.3 The stylet is sexually dimorphic

Since only female mosquitoes feed on blood, we hypothesized that a comparison of the female and male stylet would reveal the specialized sensory neurons involved in blood-feeding. Previous electron microscopy studies showed that females have three bilaterally symmetric sets of sensory sensilla, all of which are likely to directly contact blood underneath the skin (Lee, 1974). The first two sets are putative chemosensory sensilla, located at the distal tip and found only in the female stylet (Figure 2.5A, pink arrows) (Jung et al., 2015; Lee, 1974). The third set comprises mechanosensory sensilla and is found in both the female and male stylet (Figure 2.5A, white arrows) (Jung et al., 2015; Lee, 1974). Beyond this early description of the external morphology of stylet sensilla, there has been limited investigation of its neuroanatomy.

To reveal the organization of the stylet, we used reagents to stain cell nuclei and actin filaments, and visualized dTomato-labeled neurons in a *Brp>dTomato-T2A-GCaMP6s* reporter strain (Figure 2.5B-D) (Zhao et al., 2020). This transgenic line, which we will refer to as pan-neuronal, was generated using the CRISPR-Cas9 system to target the 3' end of the *Brp* locus, which encodes the synaptic protein Brp (Matthews et al., 2018; Zhao et al., 2020). The 3' end was targeted in order to replace the stop codon with the T2A ribosomal skipping sequence upstream of the QF2w transcriptional activator (Kistler et al., 2015; Riabinina et al., 2015; Zhao et al., 2020). Nuclear staining

indicated that there is a concentration of rounded nuclei within the first 300 µm from the distal tip of the stylet, with more proximal nuclei showing a flatter elongated morphology (Figure 2.5B). When we examined dTomato expression in *Brp>dTomato-T2A-GCaMP6s* animals, we found that all stylet neurons are located within the distal region (Figure 2.5C). Finally, super-resolution images of actin staining revealed fine processes innervating the putative chemosensory sensilla at the distal tip (Figure 2.5D,E).

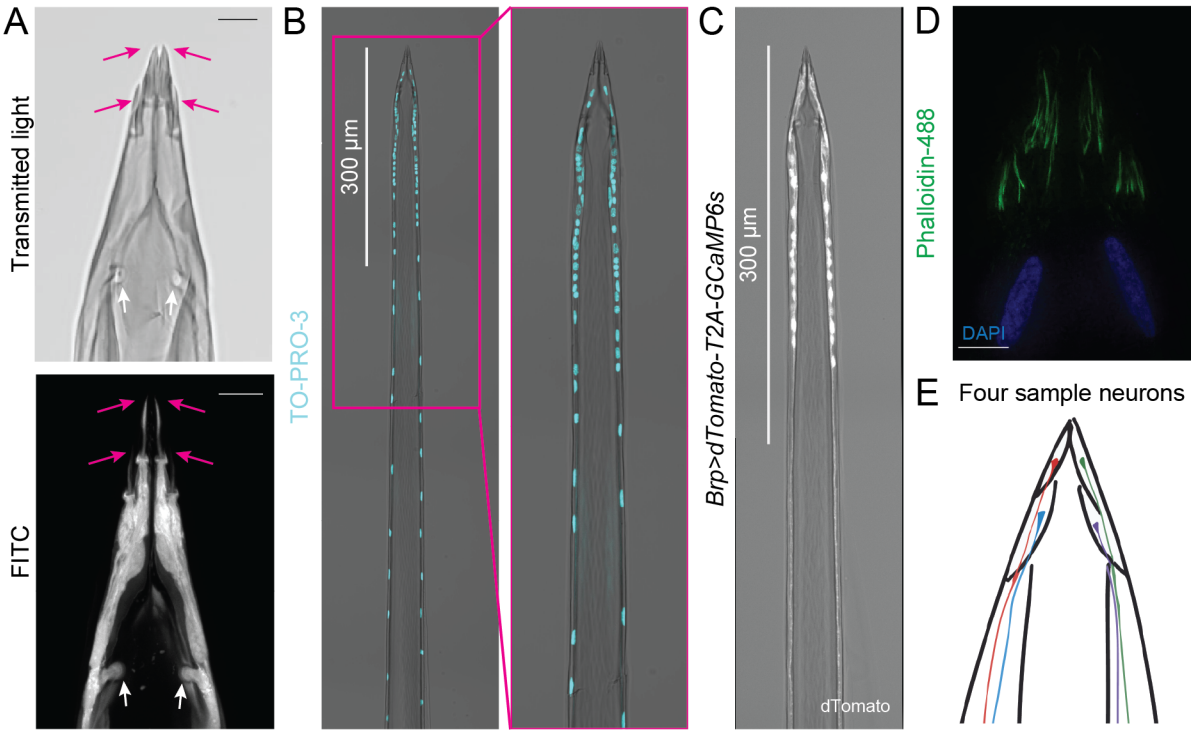

Figure 2.5 Female stylet neurons innervate putative sensory sensilla.

(A) Confocal images of transmitted light (top) and FITC counterstain (bottom) outline the female stylet chemosensory (pink arrows) and mechanosensory (white arrows) sensillar structure. Scale bar: 10 µm.
(B,C) Tiled confocal image with transmitted light overlay of TO-PRO-3 nuclear staining (B, cyan) in a wild-type female stylet and dTomato expression (C, gray) in a *Brp>dTomato-T2A-GCaMP6s* female stylet. Right panel in (B) is an enlargement of the magenta-boxed area in the left panel.
(D) Super-resolution structured illumination image of phalloidin-488 actin stain (green) and DAPI nuclear stain (blue) in the female stylet tip. Scale bar: 5 µm.

(E) Schematic of 4 sample neurons with dendrites, each innervating 1 chemosensory sensillum at the tip of the stylet. The exact number of stylet sensory neurons/sensillum is unknown and this schematic shows only a single neuron/dendrite example per sensillum for clarity.

Moreover, this section of the stylet is dramatically sexually dimorphic. When compared to males, females have a greater number of nuclei (Figure 2.6A,C), neurons (Figure 2.6B,D), and dendritic processes that innervate the distal tip (Figure 2.6E-H). The number of neurons detected in the female stylet correlated with the number of dendrites detected by transmission electron microscopy (Lee, 1974). All females exhibited substantial dendritic innervation of the putative chemosensory pores identified by electron microscopy (Figure 2.6E-G) (Kwon et al., 2006; Lee, 1974). Interestingly, sparse and inconsistent innervation was detected in approximately half the males, despite the fact that previous electron microscopy micrographs did not reveal chemosensory pores in the distal male tip (Figure 2.6E-G) (Kwon et al., 2006; Lee, 1974). To confirm that inconsistent fluorescent expression was not due to variability in transgenic labelling, we co-stained male stylets from *Brp>dTomato-T2A-GCaMP6s* animals with Phalloidin-647. dTomato expression and Phalloidin-647 staining co-localized in male stylets with unilateral distal processes (Figure 2.6H). Finally, we found that sensory dendrites innervated mechanosensory sensilla in both males and females (Figure 2.6E-H). Together these experiments illustrate the distinctive neuroanatomy in the distal female stylet.

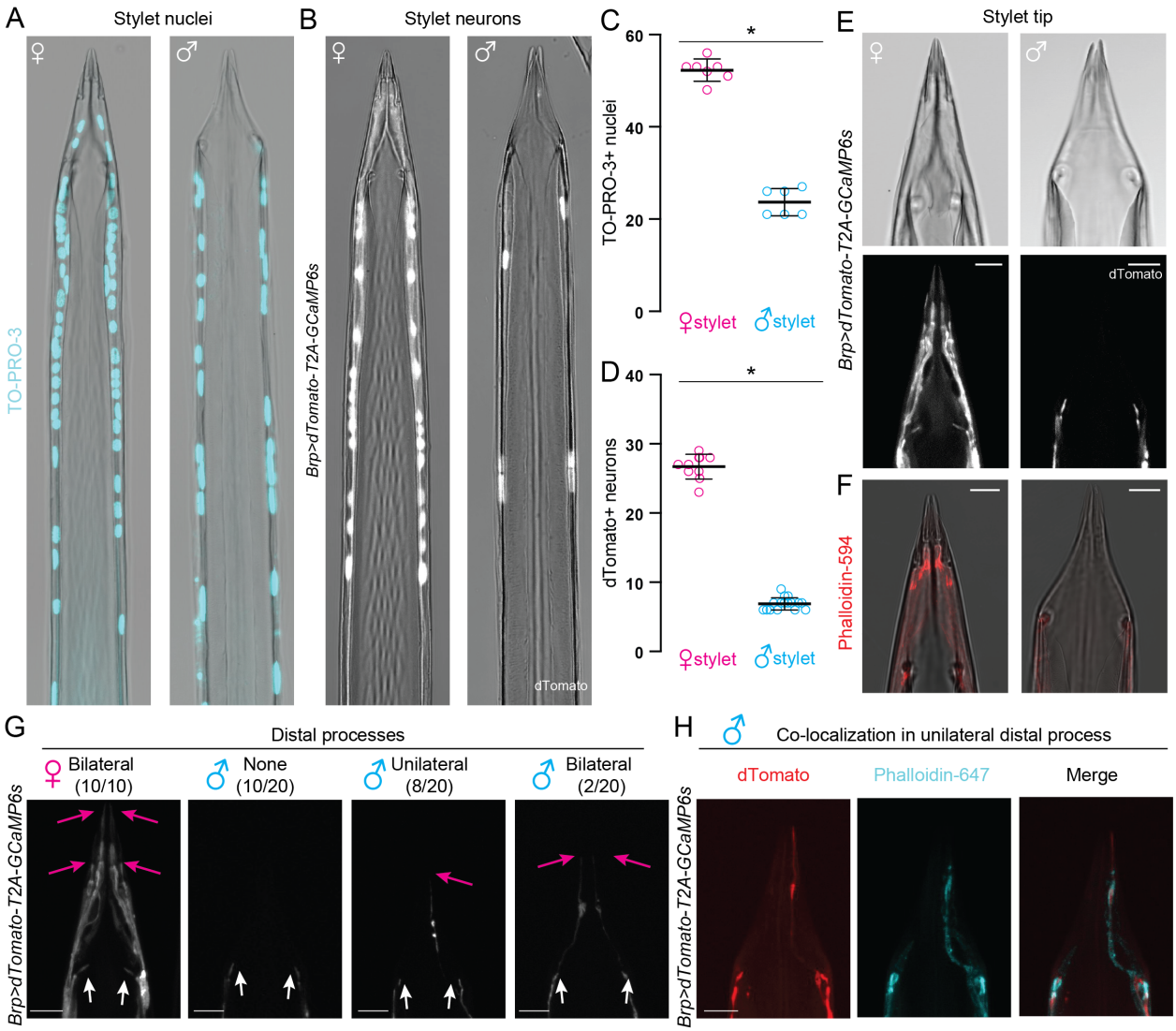

Figure 2.6 The unique neuroanatomy of the female stylet.

(A,B) Confocal image with transmitted light overlay of TO-PRO-3 nuclear staining (cyan) in wild-type female (A, left) and male (A, right) stylets, and dTomato expression (gray) in *Brp>dTomato-T2A-GCaMP6s* female (B, left) and male (B, right) stylets.
(C,D) Average # of TO-PRO-3 nuclei/stylet for most distal 300 µm (C, N=7 females, N=6 males), and dTomato neurons/stylet (D, N=10 females, N=16 males). Each dot denotes 1 animal (mean ± SD, * $p < 0.05$ Mann-Whitney test).
(E) Confocal image of transmitted light (top) and dTomato (gray, bottom) *in Brp>dTomato-T2A-GCaMP6s* female (left) and male (right) stylet tip.
(F) Confocal image with transmitted light overlay of phalloidin-594 (red) staining in wild-type female (left) and male (right) stylets.
(G) Confocal image of dTomato expression in the female (left) and male (remaining 3 panels) stylet tip of *Brp>dTomato-T2A-GCaMP6s* animals. From left to right: 10/10

females examined have extensive bilateral distal processes, 10/20 males examined have no distal processes, 8/20 males examined have sparse unilateral distal processes, and 2/20 males examined have sparse bilateral distal processes.
(H) dTomato expression (left) and phalloidin-647 actin staining (middle) co-localize in the *Brp>dTomato-T2A-GCaMP6s* male stylet. Right panel is a merge of left and middle panel.
Scale bar: 25 μm (A,B,L), 10 μm (E-H).

We next asked where these female stylet neurons project in the mosquito brain. If the stylet detects the taste of blood, we would expect innervation of the subesophageal zone, the putative processing center in the insect taste system (Ito et al., 2014; Scott, 2018). To visualize axon terminals from sensory neurons, we dye-filled severed sensory appendage nerves and subsequently dissected the brains from these animals. We first validated the technique by dye-filling all chemosensory neurons in the proboscis, which includes both the stylet and labium (Figure 2.7A). As expected, proboscis neurons broadly innervated the subesophageal zone (Figure 2.7B,C) (Ignell and Hansson, 2005). We performed dye-fill experiments to label axon terminals from all stylet neurons (Figure 2.7D) and found that stylet innervation was restricted to a discrete anterior and ventral region in the subesophageal zone (Figure 2.7E,F) (Ignell and Hansson, 2005). Another group reported additional innervation of the antennal lobe, the primary olfactory processing center, upon dye-filling the stylet in *Ae. aegypti* (Jung et al., 2015) and *An. gambiae* (Kwon et al., 2006). However, our data obtained from *Ae. aegypti* and data from a third group that specializes in *An. gambiae* did not support these findings in either species (Riabinina et al., 2016).

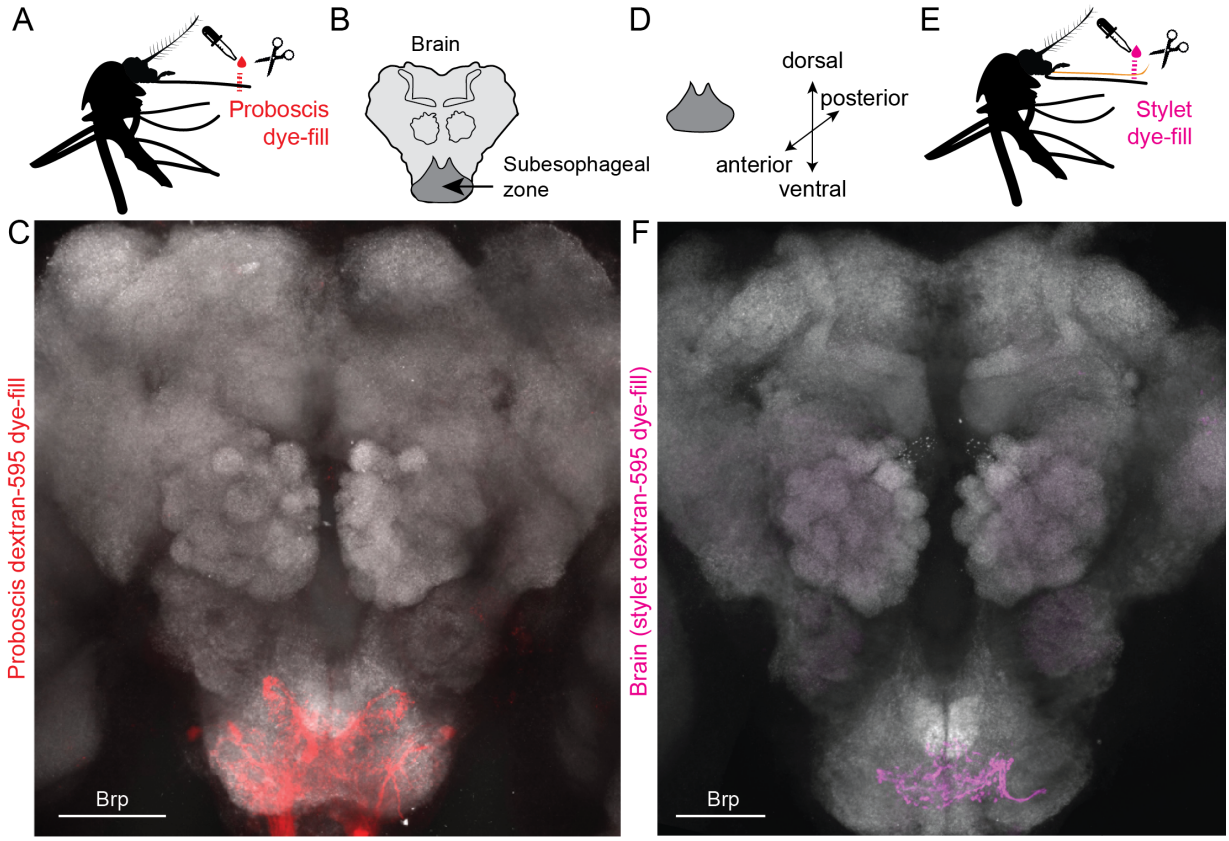

Figure 2.7 Stylet neurons project to the predicted taste-processing center.

(A, E) Schematic of proboscis (A) and stylet (E) dye-fill experiment set-up performed in (C) and (F), respectively.
(B) Schematic of mosquito brain region captured in (C, F).
(C, F) Proboscis (C, red) and stylet (F, magenta) neuron projection pattern revealed by dextran-595 dye-fill. Neuropil stained with anti-*Drosophila* Brp (gray). Scale bar: 50 μm.
(D) Schematic of subesophageal zone anatomy.

Together these results show that initiation of blood feeding behavior is chemosensory driven and independent of satiety and egg development. These controls formally exclude the possibility that blood protein and energy from ATP hydrolysis are required to promote engorgement (Figure 2.2 and Figure 2.3). biteOscope experiments enabled the first high-resolution stylet tracking from individual, freely-behaving *Ae. aegypti* females as they seek out a blood meal. Furthermore, this experimental set up

formally decouples volatile host cues from contact chemosensory cues in the meal, demonstrating that co-presentation of heat and CO_2 specifically results in piercing, but not engorgement. If the taste of blood, or an appropriate mixture of blood components, is not detected, females repeatedly pierce (Figure 2.4).

Furthermore, the stylet is likely to be the initial sensor of meal quality since it is the only sensory appendage in direct contact with the meal. We generated the first neuroanatomical map comparing the entire female and male stylet and confirmed that sexual dimorphism in stylet neuron anatomy mirrors the sexual dimorphism observed in blood-feeding behavior (Figure 2.5 and Figure 2.6). Since the putative chemosensory neurons are significantly enriched in female stylets compared to male stylets, could these neurons be the ones to detect blood?

CHAPTER 3. STYLET NEURONS ENCODE THE MULTIDIMENSIONAL TASTE OF BLOOD.

Blood is a complex mixture that contains a potpourri of ligands belonging to distinct taste qualities. Many key blood components are traditionally associated with the canonical taste qualities described in *Drosophila,* rodents, and humans (Liman et al., 2014; Yarmolinsky et al., 2009). For example, $NaHCO_3$ (the main buffer in blood), NaCl (the predominant electrolyte in blood), amino acids (found both as free amino acids and in blood protein), and glucose (the only blood sugar), each contribute to our perception of carbonation, salty, umami, and sweet, respectively. This raises an interesting number of possibilities for how the female perceives the taste of blood as she bites. Which components of blood are detected by the female and do all females recognize the same components? Since multiple blood components are required for engorgement, is blood detected as a mixture by a dedicated population of neurons tuned to multiple blood components? Or is the taste of blood distributed across distinct subpopulations, each tuned to specific blood components or taste qualities?

Early electrophysiology experiments by Galun and colleagues provided exciting clues for how the taste of blood may be encoded, but were limited to examining responses from four putative neurons in one sensillar type and presentations of deconstructed components of blood such as ATP or $NaHCO_3$ (Werner-Reiss et al., 1999a, b, c). If every stylet sensillum contains the same, stereotyped neuron population, similar to every labellar sensillum in *D. melanogaster* (Scott, 2018), this sampling could

be representative of the entire chemosensory population. Yet functional organization of stylet neurons remains completely unexplored. Furthermore, whole blood delivery is critically different from deconstructed blood components. It was not clear if phagostimulants like ATP and $NaHCO_3$ and activate the same neurons as whole blood, or if they act through an orthogonal circuit to promote the same engorgement phenotype.

Based on our neuroanatomical data, we reasoned two key technological innovations were necessary to fully unravel the complexity of blood taste coding: (1) a pan-neuronal driver and imaging preparation that enabled simultaneously recordings from the entire stylet neuron population, which is located in the first ~300 μm of the stylet and (2) a novel whole blood delivery system that restricted blood to a ~25 μm zone at the stylet's tip so that blood contacted chemosensory pores, but did not obscure fluorescence measurements from the cell bodies. In this chapter we creatively solved these tremendous technical challenges to reveal how the stylet encodes the taste of blood.

3.1 Stylet Neurons Detect Blood

Our behavioral and anatomical results strongly suggest that stylet neurons can directly detect blood. We tested this by developing an *ex vivo* calcium imaging preparation with the pan-neuronal *Brp>dTomato-T2A-GCaMP6s* mosquito, which expresses both a dTomato marker and the genetically-encoded calcium indicator GCaMP6s (Chen et al., 2013) in all stylet neurons (Figure 3.1A,B). Because all stylet

neurons are located in one plane, we were able to image responses from all neurons simultaneously. When we applied 500 mM potassium chloride (KCl) as a depolarizing stimulus, we observed strong responses in all stylet neurons (Figure 3.1C). Since whole blood is opaque, it was necessary to restrict blood to the stylet tip so that it did not interfere with GCaMP6s signal in the cell bodies. To solve this problem, we used the BioPen microfluidic device to deliver blood to the chemosensory pores that are innervated by sexually dimorphic distal processes (Figure 3.1D).

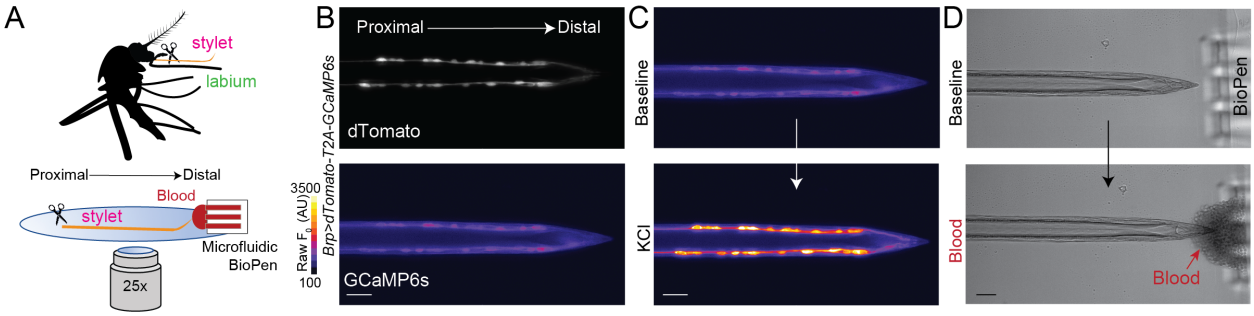

Figure 3.1 Stylet imaging preparation to measure blood responses.

(A) Schematic of *ex vivo* stylet imaging preparation.
(B) Wide-field image of dTomato (top) and baseline GCaMP6s (bottom, scale: arbitrary units) for a representative stylet, oriented proximal to distal.
(C) Representative image of GCaMP6s fluorescence increase to bulk neuronal depolarization with 500 mM KCl (bottom) compared to baseline (top).
(D) Representative bright-field image before (top) and during (bottom) delivery of sheep blood to the stylet tip via the BioPen.
(B-D) Scale bar: 25 μm.

We next developed an analysis pipeline to calculate and visualize peak $\Delta F/F_0$ responses to individual ligands for each stylet neuron (Figure 3.2). For each neuron in a given stylet, raw fluorescence traces were recorded in response to a stimulus train of ligands (Figure 3.2A). The ligands were presented in a shuffled order and each ligand

was delivered once per movie (Figure 3.2A). Three movies, and therefore three replicate measurements, were measured for each ligand (Figure 3.2A). For each ligand, the peak $\Delta F/F_0$ was calculated per neuron for each of the three movies (Figure 3.2B) and the average peak $\Delta F/F_0$ per neuron is calculated by averaging peak $\Delta F/F_0$ from each movie (Figure 3.2C,D). When spatial information was required, the average peak $\Delta F/F_0$ to a given ligand was represented as one square per neuron in a heatmap, where neurons are ordered from proximal to distal along the stylet's length (Figure 3.2C). When it was necessary to directly compare each neuron's average peak $\Delta F/F_0$ response to various ligands, average peak $\Delta F/F_0$ was represented as one dot per neuron in a dot plot (Figure 3.2D).

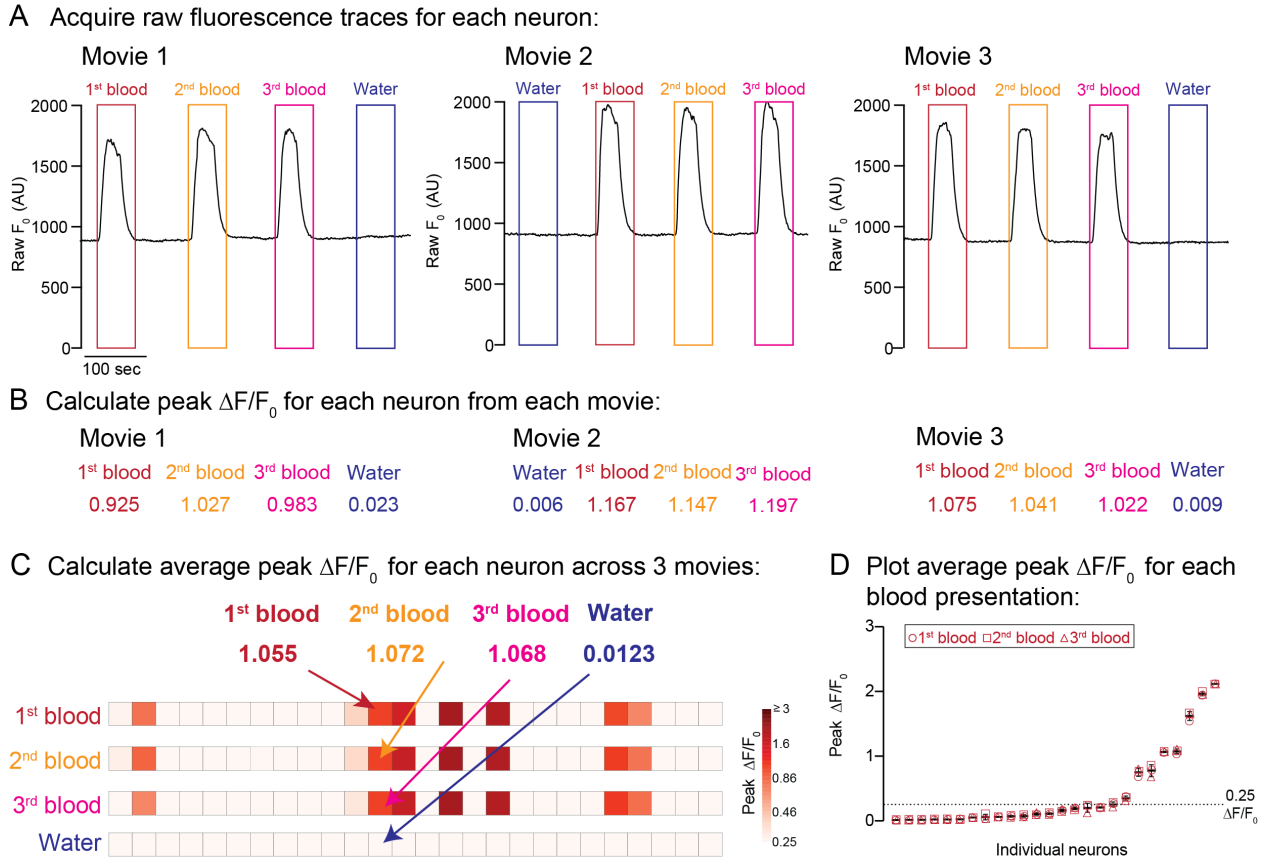

Figure 3.2 Analysis pipeline for stylet neuron responses.

(A-D) These panels provide more information on how the average peak $\Delta F/F_0$ values were calculated by showing measurements acquired from 1 individual female in Figure 3.3. (A) Raw fluorescence traces in response to indicated ligand recorded from 1 neuron for 3 replicate movies; each ligand (water, 1st blood, 2nd blood, 3rd blood) is delivered once per movie. (B) For each ligand, the peak $\Delta F/F_0$ is calculated per neuron for each of the 3 movies. (C) Next, the average peak $\Delta F/F_0$ per neuron is calculated by averaging peak $\Delta F/F_0$ from each movie in (B). The average peak $\Delta F/F_0$ to a given ligand is represented as 1 square per neuron in the heatmap. Each column represents 1 neuron and each row represents the response to the indicated ligand for all neurons from 1 individual female. Neurons are ordered from proximal to distal. (D) For each neuron in (C), the average peak $\Delta F/F_0$ to 1st, 2nd, and 3rd blood is represented as a circle, square, and triangle respectively. Data points (mean ± SD) are sorted by peak $\Delta F/F_0$.

Stylet neurons consistently responded to three presentations of blood (denoted as 1st, 2nd, and 3rd blood) separated by 60 sec intervals, and not to water (Figure 3.3A-C). Within a given female, the peak ΔF/F response to multiple presentations of blood was stable, but the exact number and position of blood-sensitive neurons was not stereotyped across individuals (Figure 3.3C-F). Across individuals approximately 50% of stylet neurons responded to blood (Figure 3.3D). Different neurons within an individual had unique GCaMP6s response waveforms that were stable across every blood presentation for a given neuron (Figure 3.3E,F). These results demonstrate that a large population of stylet chemosensory neurons responds directly to whole blood.

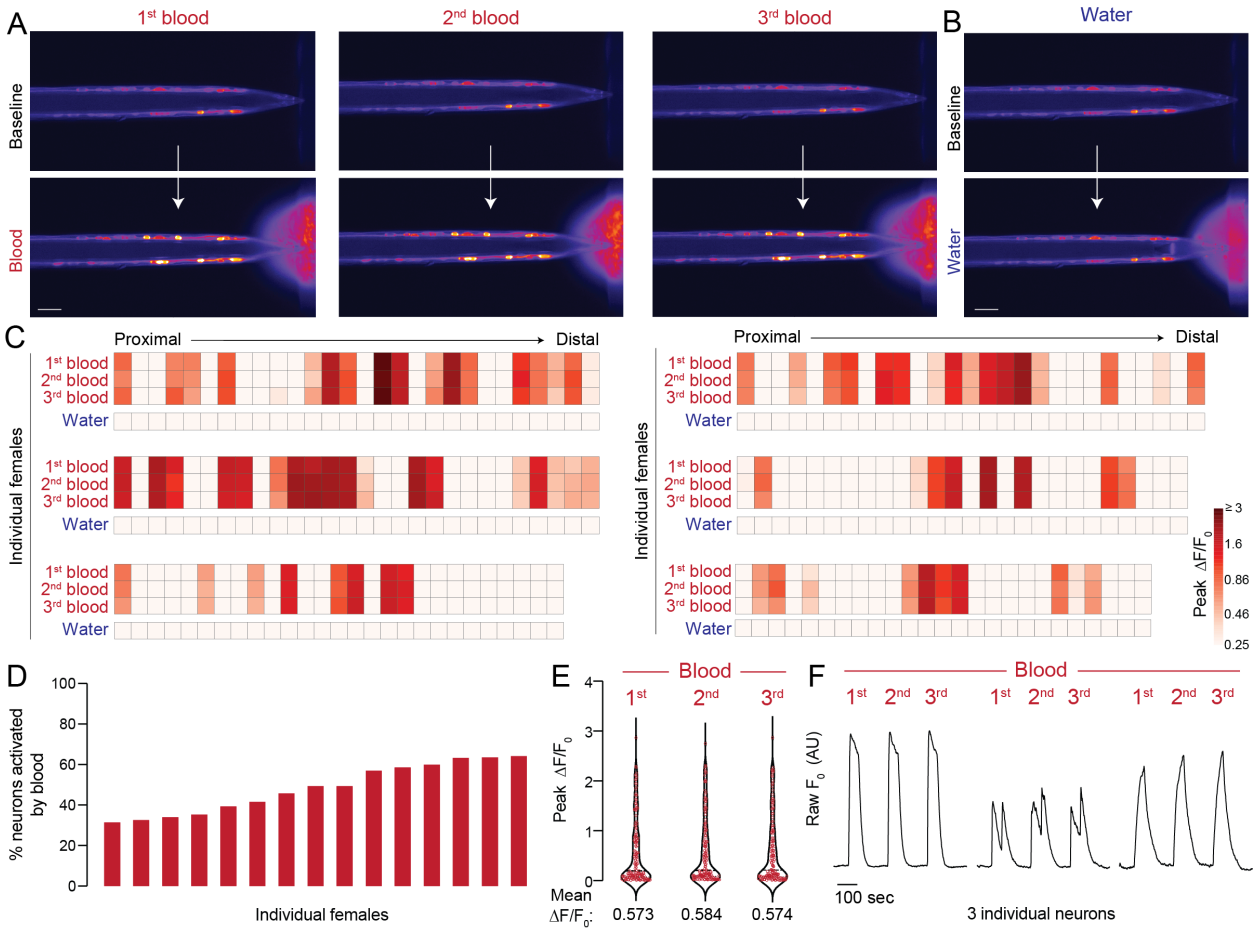

Figure 3.3 Stylet neurons respond consistently to consecutive blood presentations.

(A,B) Representative image of GCaMP6s fluorescence increase to indicated blood presentation (bottom, A) or water control (bottom, B), compared to baseline (top). Scale bar: 25 μm. 0.0002% fluorescein was added to blood and water stimuli to visualize ligand delivery zone.
(C) Heat maps of peak $\Delta F/F_0$ response to the indicated ligand. Each square is the average of the peak $\Delta F/F_0$ measured in 3 separate trials. Each column represents 1 neuron and each row represents the response to indicated ligand for all neurons from 1 individual female, with neurons ordered from proximal to distal. N=6 individual females.
(D) Summary of % neurons with ≥ 0.25 peak $\Delta F/F_0$ to blood for all females in (C), Figure 3.4, and Figure 3.5, (N=15 females). Each column represents 1 female and columns are sorted by % neurons activated by blood (average across all samples = 49.05%).
(E) Summary of peak $\Delta F/F_0$ data for all neurons from the 6 females in (C), (N=161 neurons). Data is shown as median with range (1st blood vs 2nd blood, p = 0.05; 1st blood vs 3rd blood, p > 0.99; Friedman's test with Dunn's multiple comparisons).
(F) A subset of traces for 3 neurons from 1 individual in (C), y axis scale: arbitrary units of raw fluorescence.

3.2 Blood Detection is Combinatorial Across Taste Qualities

How is blood, a complex mixture of cells, proteins, lipids, metabolites, and salts, represented by stylet neurons? We used a reductionist approach to understand how the taste of blood is encoded in stylet neurons. We selected 4 blood components [adenosine triphosphate (ATP), glucose, sodium bicarbonate ($NaHCO_3$), and sodium chloride (NaCl)] that have been individually shown to increase the probability of engorgement (Galun et al., 1984; Gonzales et al., 2018). ATP and unbuffered $NaHCO_3$ (pH = 8 - 9) are not associated with canonical taste qualities, but glucose and sodium chloride are traditionally associated with sweet and salty, respectively. We selected concentrations of glucose, $NaHCO_3$, and NaCl within range of standard blood values for vertebrate species. For ATP, it is difficult to determine the exact *in vivo* concentration present when the female bites a human because ATP is derived from multiple sources and is rapidly hydrolyzed. Micromolar- to millimolar-range ATP can be released from the deformation and lysis of red blood cells, or from epithelial cells lining the blood vessel as a damage response to the stylet piercing (Born and Kratzer, 1984; Forsyth et al., 2011). At steady-state, free ATP in plasma is present in the nanomolar-range (Gorman et al., 2007). We selected 1 mM because it resulted in the most robust responses in the behavioral dose response curve (Figure 2.3E). Using the blood-feeding behavior assay, we found that the combination of these 4 ligands (hereafter referred to as Mix+ATP) was sufficient to trigger engorgement (Figure 3.4A,B).

Since both blood and Mix+ATP trigger engorgement we asked if there are differences in how stylet neurons respond to these taste stimuli. When we delivered blood or Mix+ATP to *Brp>dTomato-T2A-GCaMP6s* animals, we found that blood and Mix+ATP activated the same population of stylet neurons (Figure 3.4C-F). Although the magnitude of response can vary within a given neuron (Figure 3.4D,F), Mix+ATP-responsive neurons track with blood-responsive neurons across individuals, irrespective of variability in the position of the neuronal cell body along the proximal-distal axis of the stylet (Figure 3.4D,E).

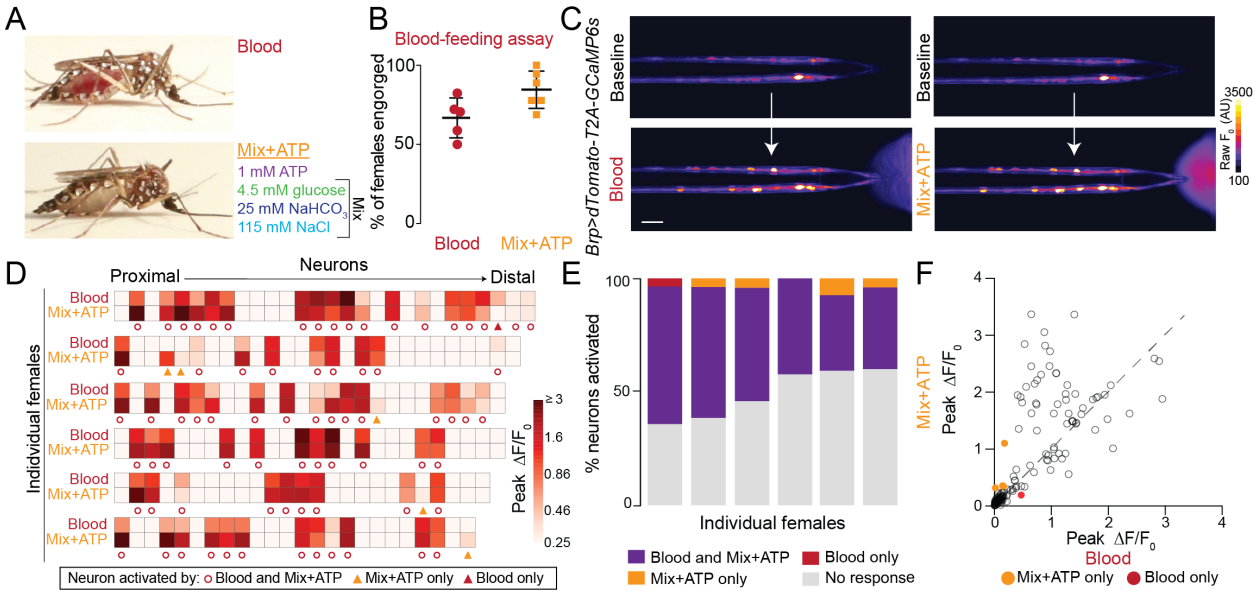

Figure 3.4 Blood and Mix+ATP activate the same subset of stylet neurons.

(A) Representative engorged *Ae. aegypti* female following 15-min exposure to blood (top) or Mix+ATP (bottom) via Glytube assay.
(B) Female engorgement on blood (N=5 trials) and Mix+ATP (N=6 trials) delivered via Glytube (lines denote mean ± SD, 15–20 females/trial, p = 0.0714, Mann-Whitney test).
(C) Representative image of GCaMP6s fluorescence increase (scale: arbitrary units) to blood (bottom, left) or Mix+ATP (bottom, right), compared to baseline (top). Scale bar: 25 μm.
(D) Heat maps of peak $\Delta F/F_0$ response to the indicated ligand. Each square is the average of 3 ligand exposures and each column represents one neuron. Each row

represents the response to indicated ligand for all neurons from 1 individual female, with neurons ordered from proximal to distal. N=6 individual females.
(E) Summary of % neurons with ≥ 0.25 peak $\Delta F/F_0$ to the indicated ligand from (D), each column represents 1 female.
(F) Scatter plot comparing peak $\Delta F/F_0$ in response to Mix+ATP (y-axis) and blood (x-axis) summarized across N=6 females from (D,E). Each dot represents 1 neuron, dots that fall on the dashed line have the same peak $\Delta F/F_0$ in response to blood and Mix+ATP. Dots that fall above the line respond more to Mix+ATP than to blood and dots that fall below the line respond more to blood than to Mix+ATP.
In (A-F) and all subsequent experiments “Mix” is 4.5 mM glucose, 25 mM $NaHCO_3$, 115 mM NaCl and “Mix+ATP” is Mix supplemented with 1 mM ATP. To visualize ligand delivery zone, 0.0002% and 0.00002% fluorescein was added to blood and Mix+ATP, respectively, in BioPen experiments.

To understand how blood components contribute to the perception of whole blood, we used Mix+ATP as a chemically-defined mixture that activates blood-responsive neurons. When we presented each component of Mix+ATP individually, we found that blood-sensitive neurons are a heterogenous population and that different neuronal subsets within each female can respond to distinct blood components (Figure 3.5). Moreover, all components except 4.5 mM glucose reliably activated subpopulations of stylet neurons when presented individually (Figure 3.5).

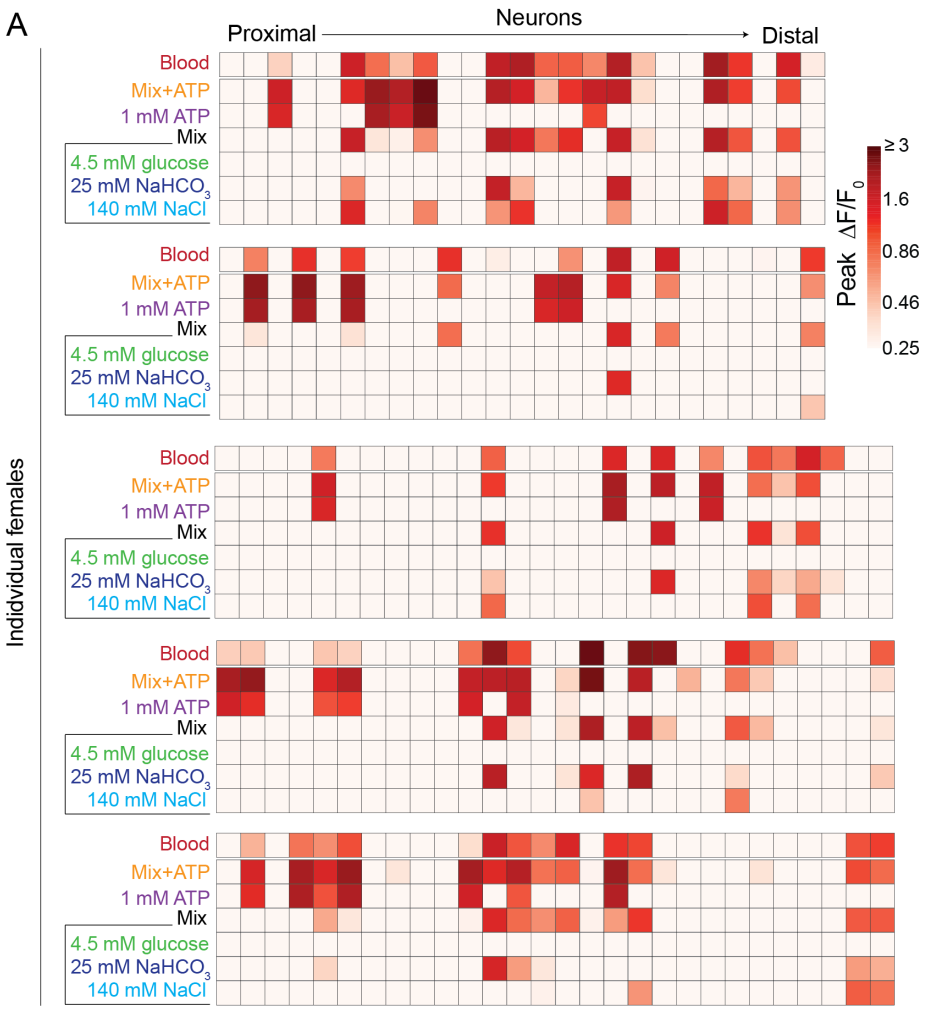

Figure 3.5 Stylet neurons are functionally heterogenous.

(A) Heat maps of peak $\Delta F/F_0$ response to the indicated ligand for individual females prior to clustering in Figure 3.6. Each square is the average of 3 ligand exposures. Each column represents one neuron and each row represents the response to the indicated ligand for all neurons from 1 individual female. Neurons are ordered from proximal to distal. N=5 individual females.

The 134 individual neurons from the five females in Figure 3.5 were pooled and subjected to hierarchical clustering using Euclidean distance with complete linkage, based on each neuron's response profile to seven ligands indicated in Figure 3.5: blood, mix+ATP, mix, ATP, NaCl, $NaHCO_3$, glucose. Unsupervised hierarchical clustering of

this dataset grouped neurons into five functionally distinct clusters (Figure 3.6A). For each neuron in a cluster, we calculated a ratio of peak $\Delta F/F_0$ response to Mix+ATP compared to the peak $\Delta F/F_0$ response to any individual ligand (Figure 3.6B). The first three clusters represent neurons activated by an individual component: ATP, $NaHCO_3$, and NaCl, respectively (Figure 3.6B). Although Cluster IV was not reliably activated by any individual ligand, it was activated by a mixture of $NaHCO_3$, NaCl, and glucose (hereafter referred to as “Mix”) (Figure 3.6C). We define these as “Integrator” neurons and explore their function in subsequent experiments. Cluster V neurons were non-responsive or showed weak responses (Figure 3.6C). Neurons from the five clusters were found across different females, but the exact number of neurons per cluster was not stereotyped across individual females (Figure 3.6D).

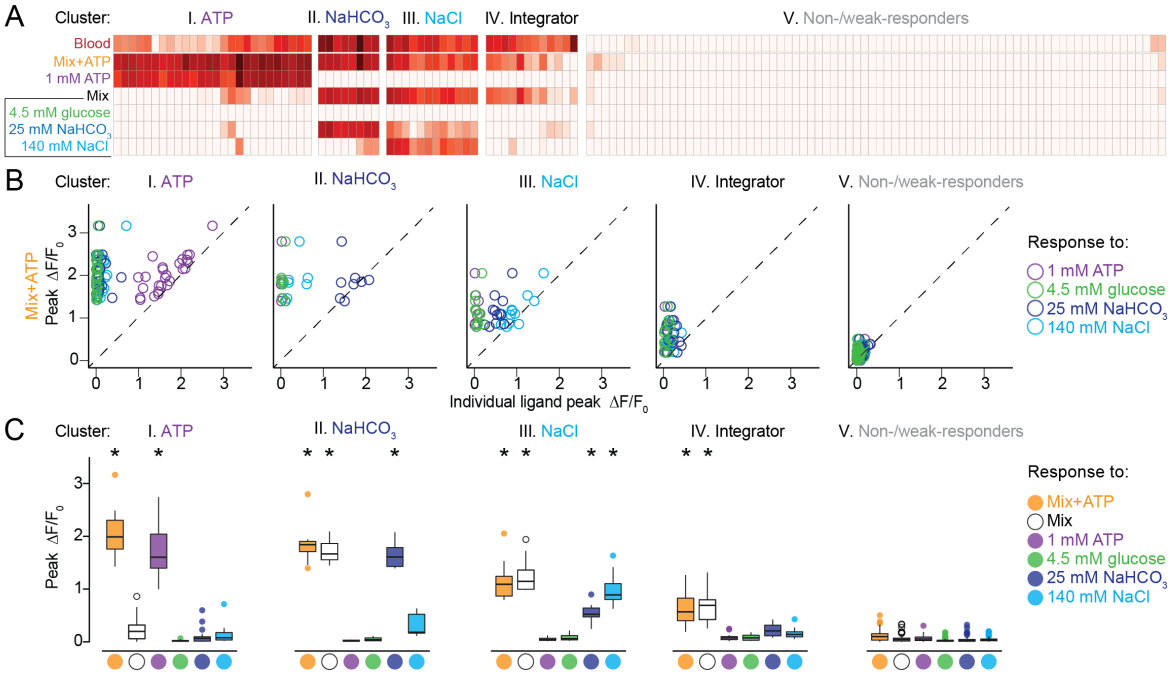

Figure 3.6 The taste of blood is composed of multiple taste qualities.

(A) Unsupervised hierarchical clustering of data in Figure 3.5, as determined by peak $\Delta F/F_0$ responses to the indicated ligands indicated. Clustering removes proximal-distal ordering and female identity from Figure 3.5, N=5 females.
(B) Scatter plot comparing peak $\Delta F/F_0$ responses within each cluster to Mix+ATP (y-axis) and the indicated individual ligands (x-axis). Individual ligands are distinguished by colored open circles (legend, far right); circles that fall on the dashed line have the same peak $\Delta F/F_0$ in response to Mix+ATP and the indicated individual ligand.
(C) Box plots comparing peak $\Delta F/F_0$ responses to the indicated ligand within each cluster. Median indicated by black line, bounds of box represent first and third quartile, whiskers are 1.5 times the inter-quartile range. Outliers are denoted by a dot without whisker. (* $p < 0.05$, one-sample Wilcoxon signed-rank test).

We then performed control analyses on these data to assess prep quality and assay reliability. If the prep quality decreased over time, we would expect the peak ΔF/F to significantly decrease from the 1st to 2nd to 3rd movie. However, when we examined the peak ΔF/F responses from all neurons in Figure 3.5, we found that peak ΔF/F is stable across all three movies (Figure 3.7A). We next asked if variability in the number of blood-sensitive neurons is due to neurons dying throughout the experiments or poor image acquisition of GCaMP signal in specific neurons. To test this, we performed a bulk depolarization with a positive control of KCl after the ligand presentations. All neurons examined showed robust responses to KCl (Figure 3.7B) and the percent of blood-sensitive neurons falls within the range observed across several experiments (Figure 3.7C). Together these experiments demonstrate that subsets of blood-sensitive neurons are selectively tuned to specific blood components that span multiple canonical and noncanonical taste qualities.

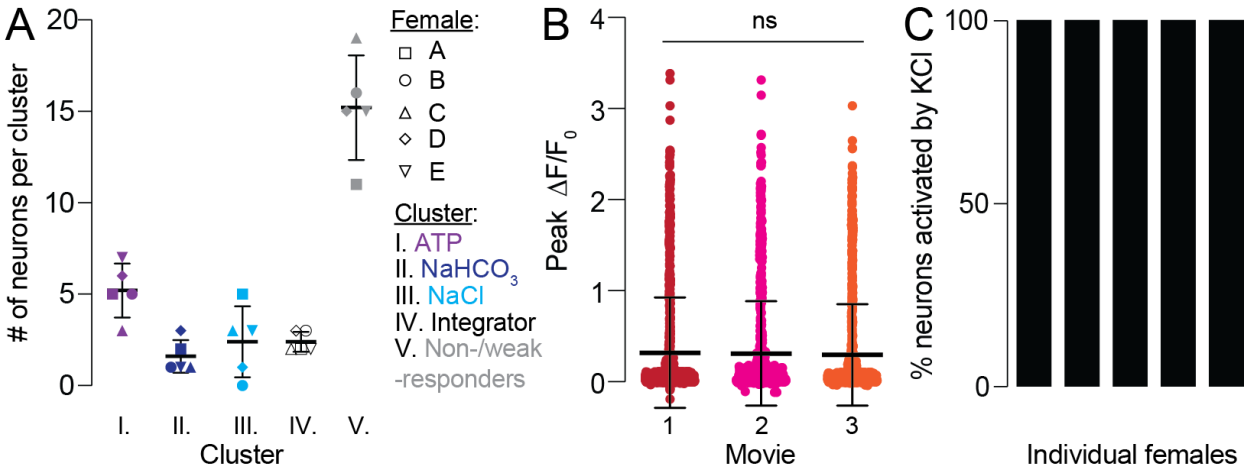

Figure 3.7 The stylet imaging preparation is stable and viable.

(A) Number of neurons per cluster in Figure 3.6. All females have neurons in every cluster with the exception of Female D, which has neurons in all clusters except for the NaCl cluster.
(B) For all neurons in Figure 3.6, peak $\Delta F/F_0$ to every perfusion ligand tested in movie 1 (red dots), compared to movie 2 (pink dots) and movie 3 (orange dots). Each data point denotes the response from 1 neuron to 1 ligand, 6 ligands were presented to N=161 neurons (ns: not significant, $p > 0.05$, Friedman test with Dunn's multiple comparisons).
(C) For all females in Figure 3.6, summary of % neurons with ≥ 0.25 peak $\Delta F/F_0$ to the positive control, KCl. Each column represents 1 female, N=5 females.

Finally, we performed several analyses to validate this clustering method. Suitability of the normalized response measurements to clustering was assessed by the Hopkins statistic (h) (Lawson and Jurs, 1990). The derived Hopkins statistic of 0.9046932 (p-value = 4.0126e-39) showed the dataset contains suitable information for clustering (Figure 3.8A). In datasets which are not amenable to clustering, the distances between neighboring closest points will be close to the random dataset and the Hopkins statistic will approach 0. In a dataset with clusters present, the distances between neighboring closest points will be low compared to the random dataset and the Hopkins statistic will approach 1 (Lawson and Jurs, 1990). The optimal number of clusters to be drawn for the data was established by the Silhouette method (Rousseeuw, 1987) with potential

cluster numbers in the range of 2 to 10. Five was the optimal cluster number with the highest mean silhouette value 0.769 across clusters (Figure 3.8B). One single neuron in Cluster IV can be considered mis-clustered with a silhouette width less than 0 (Figure 3.8B, indicated by *). To evaluate the stability of the five clusters, we assessed the bootstrap distribution of the Jaccard coefficient of resampled versus original data (Hennig, 2007, 2008). Clusters showing a Jaccard bootstrap mean of less than 0.5 can be considered unstable and unreliable, and an average Jaccard bootstrap mean across clusters above 0.85 shows a highly stable clustering (Hennig, 2007). All clusters identified had Jaccard bootstrap mean values above 0.7, indicating a set of stable of clusters, and an average Jaccard bootstrap mean across clusters of 0.8727142 (Figure 3.8C). Finally, the hierarchical clustering approach used in this study is agnostic to female identity and therefore was assessed to ensure no biases in clustering are associated with specific individuals. Principal component analysis (PCA) was applied to neuronal responses to visualize the contribution of female or cluster to derived principal components. Comparison of PCA plots demonstrates that the differing clusters are well distributed and defined by the major principal components in the data (Figure 3.8D), whereas the animals are distributed throughout principal components (Figure 3.8E). Cluster membership can be seen to highly significantly correlated with all principal components, but female showed low correlation and no significant association with any principal components (Figure 3.8F). Collectively these analyses demonstrate that the dataset is highly clusterable (Hopkins statistic, Figure 3.8A), the optimal number of clusters is five (Silhouette analysis, Figure 3.8B), cluster identity is stable (Jaccard

bootstrap mean, Figure 3.8C), and that cluster membership is not correlated with female identity (PCA analysis, Figure 3.8D-F).

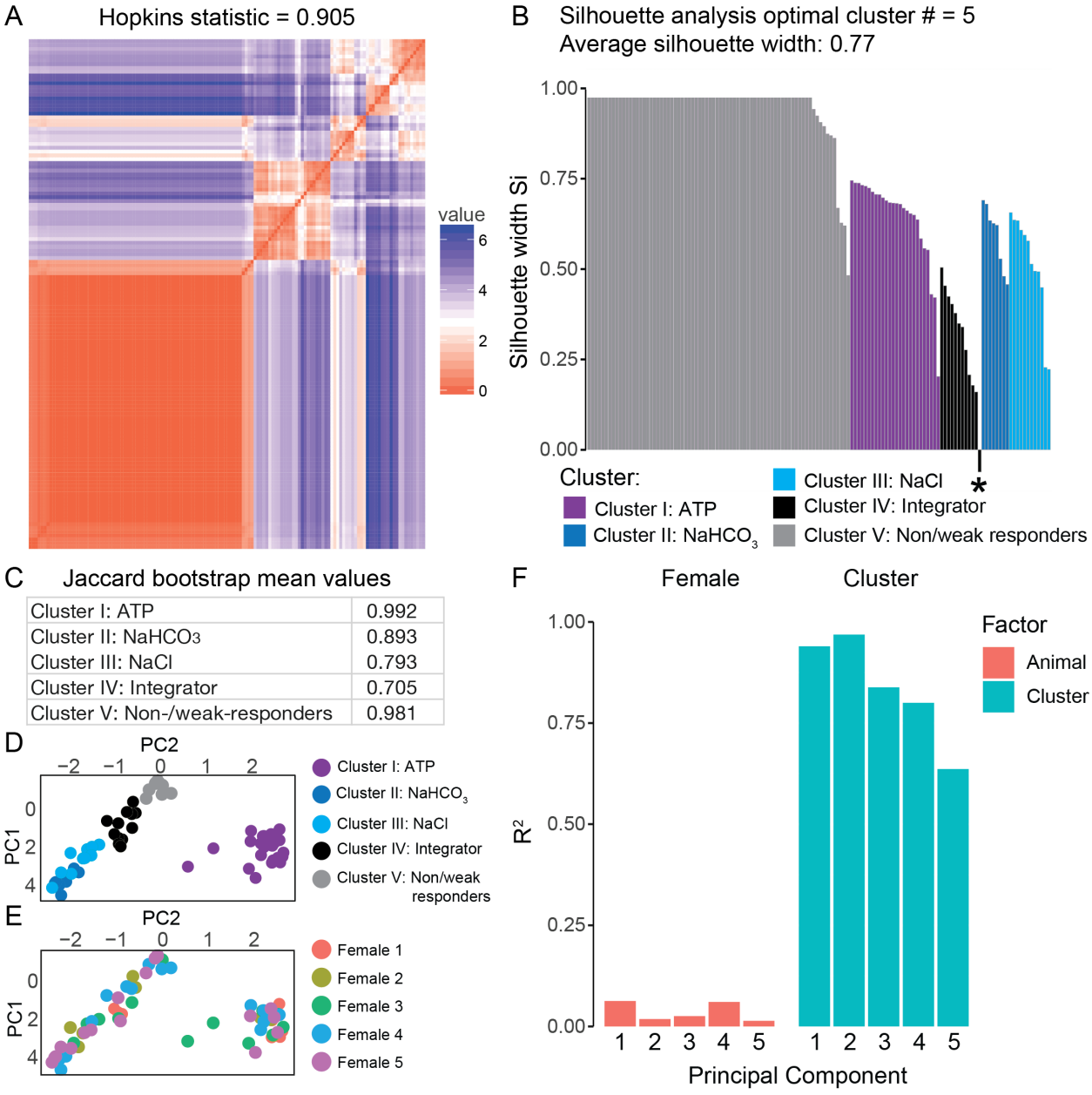

Figure 3.8 Statistical analysis of neuronal hierarchical clustering method.

(A) Clustering tendency in neuronal responses was assessed by calculating the Hopkins statistic using the factoextra R package (https://CRAN.R-project.org/package=factoextra). In the ordered dissimilarity matrix the color level is proportional to the value of dissimilarity between observations and objects belonging to the same cluster are displayed in consecutive order.

(B) The optimal number of clusters was assessed by performing Silhouette analysis (Rousseeuw, 1987) using the NbClust R package (Charrad et al., 2014) with potential cluster numbers in the range of 2 to 10. 5 was selected based on the highest mean silhouette value across clusters (* indicates that 1 neuron in Cluster IV: “Integrator” can be considered mis-clustered with a silhouette width less than 0).
(C) Cluster stability was evaluated by assessing the bootstrap distribution of the Jaccard coefficient of resampled versus original data (Hennig, 2007, 2008). The Jaccard bootstrap mean for each cluster and average across clusters was calculated using the fpc R package’s clusterboot function (https://CRAN.R-project.org/package=fpc) with 100 bootstraps.
(D,E) Principal component analysis for individual neurons colored by cluster membership (D) or female (E).
(F) Correlation between each principal component and female identity (orange, left) or cluster membership (cyan, right) was assessed in FactoMineR (Lê et al., 2008).

Here we show that despite the complexity of whole blood, the entire blood-sensitive population in the stylet can be activated by co-presentation of the four blood components in Mix+ATP (Figure 3.4). The stylet recognizes the taste of blood through four functionally distinct classes of neurons, each tuned to specific blood components associated with diverse taste qualities (Figure 3.5 and Figure 3.6). In contrast to stereotyped organization of sensilla in *D. melanogaster*, blood-sensitive neuron subtypes are distributed along the proximal-distal axis of the stylet and vary in their number and position (Figure 3.5). Therefore blood-sensitive neuron subtypes were reliably identified across females by signature functional profiles instead of anatomical position (Figure 3.7 and Figure 3.8).

Furthermore, co-presentation of these four blood components was required to activate all blood-sensitive stylet neurons (Figure 3.5), mirroring the requirement of multiple blood components to promote engorgement (Figure 2.2C). While mixtures did not increase responses in ATP-, $NaHCO_3$-, and NaCl-sensitive populations, Integrator

neurons were not reliably activated by an individual component, and instead responded to a mixture of glucose, NaCl, and $NaHCO_3$ (Figure 3.5 and Figure 3.6). Together, these data suggest that the various subsets of blood-sensitive neurons collectively contribute to blood-feeding behavior. We speculate that coincident detection of multiple blood components may decrease the false positive rate for engorging on a meal other than blood.

CHAPTER 4. FEMALE STYLET-SPECIFIC TRANSCRIPTS MARK FUNCTIONALLY DISTINCT BLOOD-SENSITIVE NEURONAL SUBSETS.

We next asked if these functionally distinct blood-sensitive subsets are transcriptionally-defined populations. If so, how can we gain genetic access to each subset to study its anatomical and functional properties? Prior to our study, there were no candidate molecular markers for blood-sensitive neurons because gene expression in the stylet had not been profiled, and model organisms like *D. melanogaster* do not have a directly comparable structure for orthologue identification. We hypothesized that to specify its unique functional properties, the female stylet has a distinct gene expression profile compared to other sensory appendages not involved in blood-feeding behavior. If so, among the transcripts expressed selectively in the female stylet as compared to non-blood-feeding tissues would be likely candidates for molecular markers of blood-sensitive neurons. Our objective in this chapter was to generate the first unbiased molecular profile of the female and male stylet and search for transcripts expressed only in the female stylet and nowhere else in adult females and males. In parallel, methods to generate cell-type specific reporters rapidly advanced (Kistler et al., 2015; Matthews et al., 2019), facilitating our ability to make driver lines for the new candidate markers. With these two key advances, we set out to define the molecular landscape of blood-sensitive neurons.

4.1 Identification of female-stylet specific transcripts

We hypothesized that transcripts that are uniquely expressed in the female stylet compared to non-blood-feeding tissues are more likely to be expressed in blood-sensitive neurons. To this end we performed an RNA-seq experiment and generated the first untargeted molecular profile of the stylet. We first developed a novel method for extracting low-input RNA because the chitinous and needle-like nature of the tissue made it very difficult to release RNA from a sparse population of neurons while maintaining RNA integrity. Unfortunately, this method required an exceptionally pure population of tissue samples, forcing the doctoral candidate to meticulously dissect stylets for several hours every day for many months despite the significant pain that resulted from these dissections. Once sufficient samples were dissected to generate cDNA libraries, we profiled transcript abundance in the female stylet using RNA-seq and compared it to two control tissues that are not involved in blood-feeding behavior: the male stylet and the female labium. We hypothesized that transcripts enriched in the female stylet over the male stylet should be more likely to be involved in chemosensation, since the female stylet has a significant enrichment in chemosensory processes (Figure 2.6E-H). Furthermore, transcripts enriched in the female stylet over the female labium should be more likely to be involved in blood chemosensation, since the labium is believed to detect nectar (Sanford et al., 2013). Since these tissues have not been previously profiled, we first performed a set of quality control analyses (Figure 4.1). Using PCA analysis, we confirmed that replicates from one tissue are more similar to each other than replicates from different tissues (Figure 4.1A). We then confirmed

expression of *Brp* and an additional neuronal marker, *nSyb*, in all three tissues (Figure 4.2).

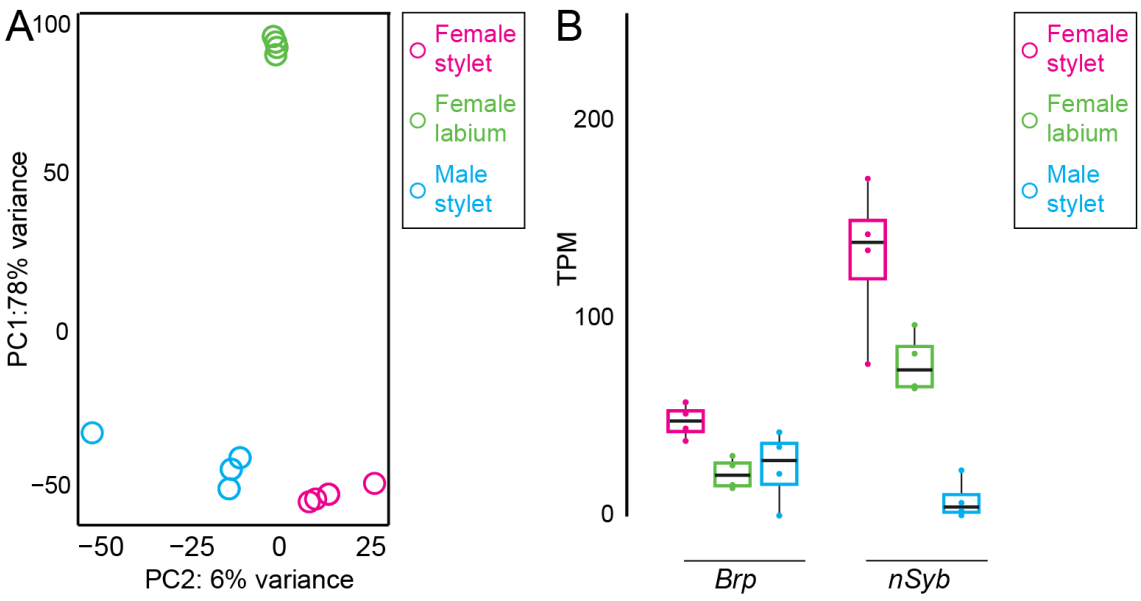

Figure 4.1 Validation of RNA-seq data set.

(A,B) RNA-seq data set comparing the female stylet (pink), female labium (green), and male stylet (blue). N = 4 replicates/tissue.
(A) Principal component analysis of transcriptome-wide expression profiles of indicated tissues.
(B) Transcripts per million (TPM) data represented as box plots for selected neuronal markers. Median indicated by black line, bounds of box represent first and third quartile, whiskers are 1.5 times the inter-quartile range, and dots represent TPM value from each biological replicate.

When we compared the intersection of genes significantly enriched in the female stylet compared to both the female labium and the male stylet, we identified 53 transcripts enriched in the female stylet (Figure 4.2A,B, fuchsia data points). We further filtered the data to select transcripts that were expressed at very low levels (< 0.5 transcripts per million, TPM) in a comprehensive transcriptome dataset that included

other sensory appendages, brain, and ovary (Figure 4.2C) (Matthews et al., 2018; Matthews et al., 2016). Of the four transcripts that met these criteria for female stylet-specific expression, two were members of the ionotropic receptor (IR) superfamily, *Ir7a* and *Ir7f* (Figure 4.2C,D). Since IRs have been shown to play roles in chemo-, thermo-, and mechano-reception (Benton et al., 2009; Rytz et al., 2013), we reasoned that *Ir7a* and *Ir7f* were likely to be expressed in sensory neurons. Interestingly, both transcripts belong to the same *Ir7* sub-clade of IRs (Matthews et al., 2018). The *Ir7* subclade has been greatly expanded in *Ae. aegypti* and *An. gambiae* mosquitoes in comparison to *D. melanogaster* and it has been suggested that this expansion may underlie mosquito-specific adaptations (Croset et al., 2010; Matthews et al., 2018). Furthermore, multiple IRs are thought to be co-expressed in one neuron whereby putative ligand-specific IRs can pair with putative co-receptor IRs (*Ir25a, Ir76b*, and *Ir8a*) to form functional multimeric ion channel complexes (Rytz et al., 2013; Sanchez-Alcaniz et al., 2018). If the stylet contains functional IR complexes, we would predict expression of the co-receptors *Ir25a* and *Ir76b*, which are thought to be broadly expressed across chemosensory tissues (Matthews et al., 2018; Matthews et al., 2016; Rytz et al., 2013; Sanchez-Alcaniz et al., 2018). Indeed, we observed expression of *Ir25a* and *Ir76b* in the female stylet (Figure 4.2E). Finally, we confirmed that *Ir8a*, which is believed to be the antennal-specific IR co-receptor (Matthews et al., 2018; Matthews et al., 2016), is not expressed in the female stylet (Figure 4.2E).

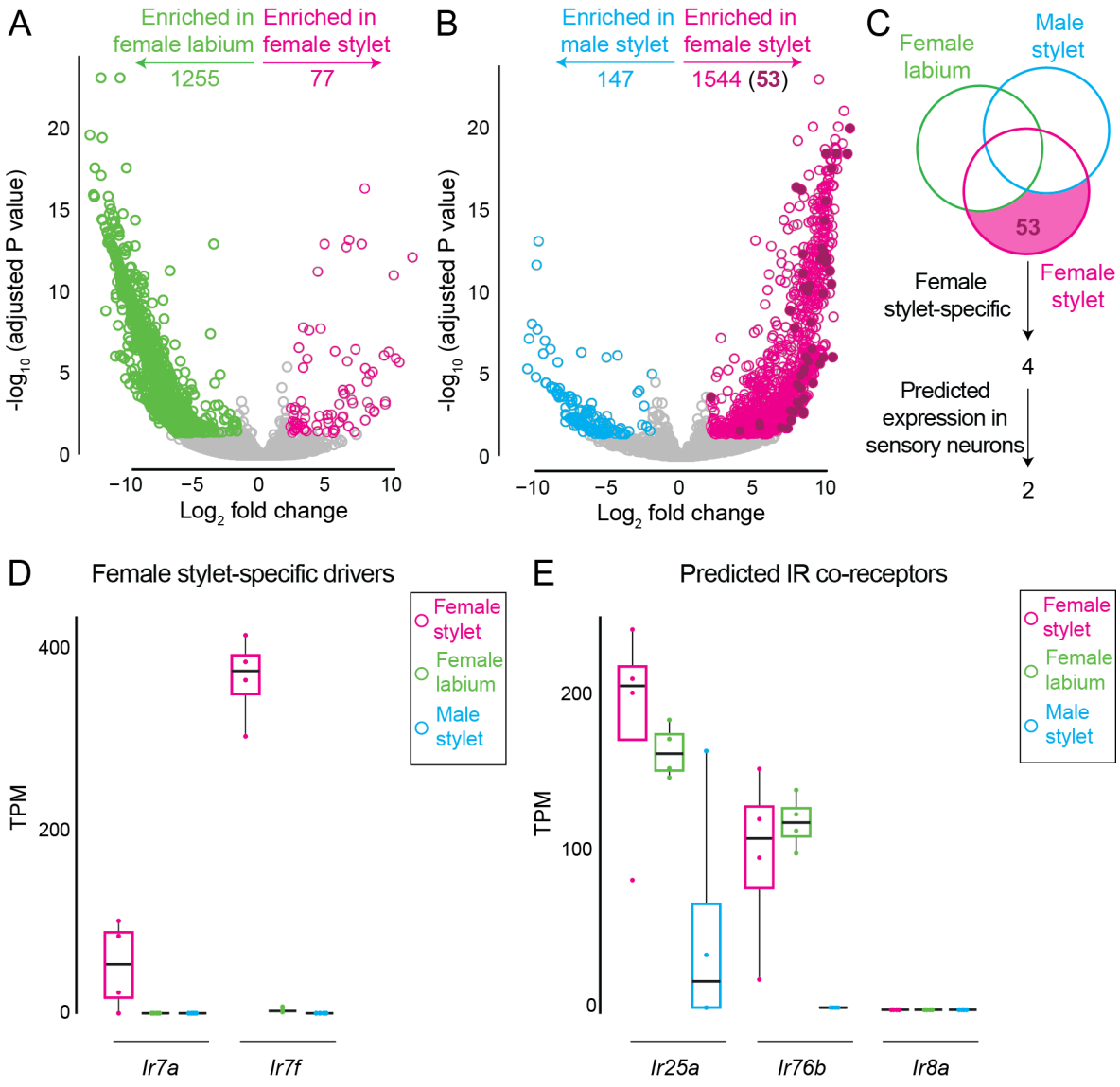

Figure 4.2 Identification of female stylet-specific transcripts.

(A-E) RNA-seq dataset comparing the female stylet (pink), female labium (green), and male stylet (blue). N=4 replicates/tissue.
(A,B) Volcano plot of transcripts enriched in the female stylet (pink) or female labium (green) in (A), and female stylet (pink) or male stylet (blue) in (B). 53 transcripts (fuchsia) were enriched in the female stylet compared to both female labium and male stylet. Transcripts were identified as significantly enriched in indicated tissue if Log_2 fold change > 2 and adjusted p value < 0.05, as determined by DESeq2 differential expression analysis.
(C) Venn diagram schematizing filters for identifying female stylet-specific transcripts.
(D,E) Transcripts per million (TPM) data represented as box plots for putative female stylet-specific transcripts selected as driver lines in (D) and predicted Ionotropic

Receptor (IR) co-receptors in (E). Median indicated by black line, bounds of box represent first and third quartile, whiskers are 1.5 times the inter-quartile range, and dots represent TPM value from each biological replicate. In (E) the outlier is denoted by a dot without whisker.

A previous study reported *orco*, *Or8*, and *Or49* expression in the female stylet (Jung et al., 2015), but we found no strong evidence for *orco* and *Or8* transcripts in our stylet RNA-seq data (Figure 4.3A). We did not examine *Or49* because it was annotated as a predicted pseudogene (Matthews et al., 2018). *orco* expression was not detected in preliminary RNA *in-situ* hybridization experiments in the female stylet (Figure 4.3B), although we confirmed the same *orco* probe co-localized with anti-*orco* staining in the antenna (Figure 4.3C).

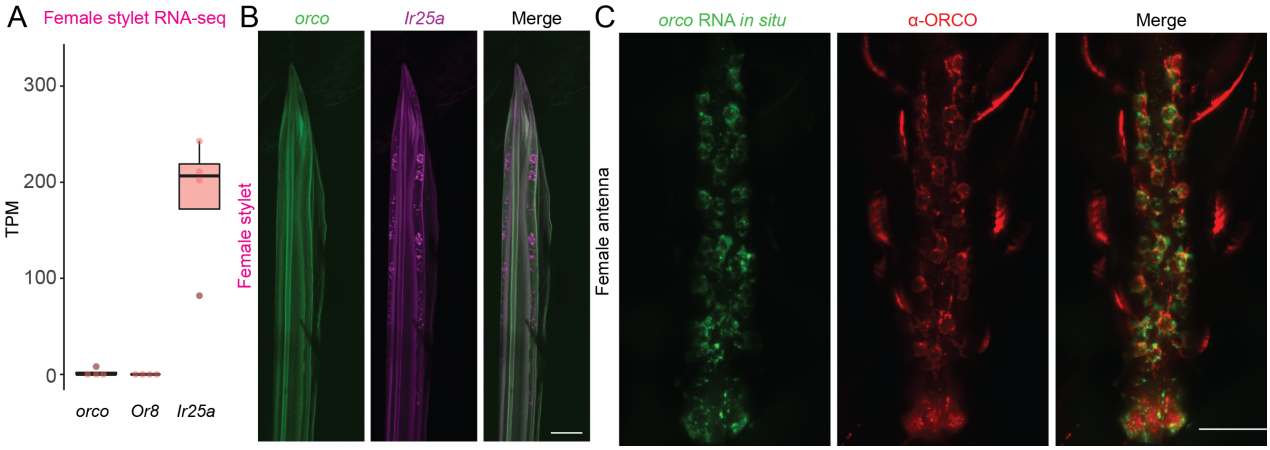

Figure 4.3 *orco* expression in the female stylet cannot be confirmed.

(A) *orco*, *Or8*, and *Ir25a* expression from RNA-seq analysis of the female stylet, N=4 replicates. Median indicated by black line, bounds of box represent first and third quartile, whiskers are 1.5 times the inter-quartile range, and dots represent TPM value from each biological replicate. Outliers are denoted by a dot without whisker.
(B) Confocal image of RNA *in situ* hybridization for *orco* (green, left), *Ir25a* (magenta, middle), and merge (right) in the female stylet. There is no detectable expression of *orco* RNA in the stylet. Unpublished data provided by Nipun Basrur.
(C) Control experiments show robust expression of *orco* RNA and ORCO protein in the antenna. Confocal image of RNA *in situ* hybridization for *orco* (green, left), antibody

staining for ORCO (red, middle), and merge (right) in the female antenna. RNA *in situ* hybridization was carried out as described (Choi et al., 2018), with modifications specific for this tissue. Unpublished data provided by Margaret Herre.
(B,C) Scale bar: 25 μm.

We did detect *orco* in the female labium RNA-seq dataset (Figure 4.4), which is in agreement with previous experiments that detected *orco* in the labium of *An. gambiae* (Kwon et al., 2006; Riabinina et al., 2016). Importantly, we did not pursue further experiments related to odorant receptor (*OR*) expression in the female stylet since the presence or absence of *OR*s does not affect the interpretation of the data presented here.

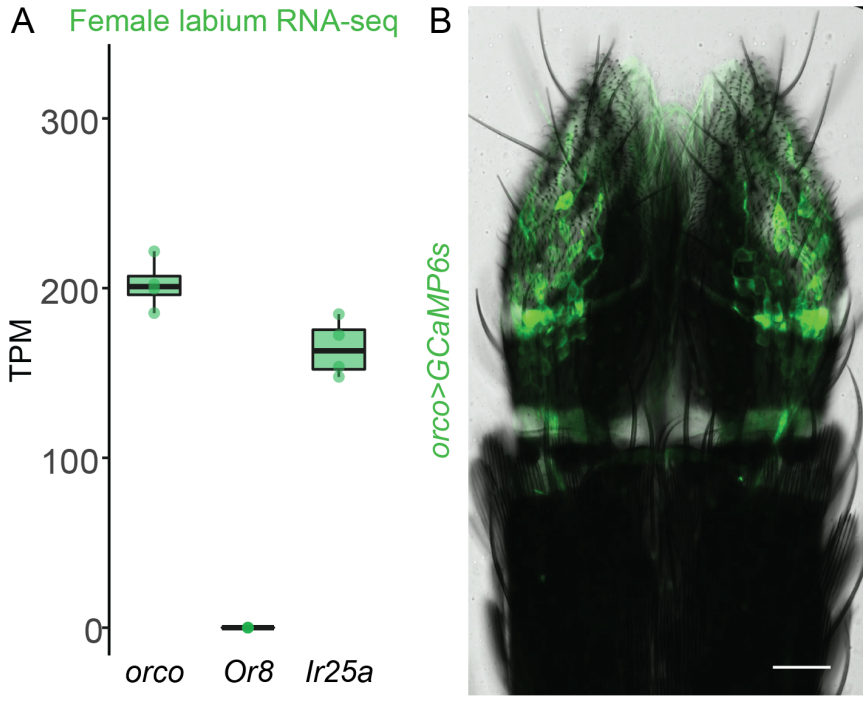

Figure 4.4 *orco* is expressed in the female labium.

(A) *orco*, *Or8*, and *Ir25a* expression from RNA-seq analysis of the female labium, N=4 replicates. Median indicated by black line, bounds of box represent first and third

quartile, whiskers are 1.5 times the inter-quartile range, and dots represent TPM value from each biological replicate.
(B) Confocal image with transmitted light overlay of GCaMP6s expression in the female labium of *orco>GCaMP6s* animals. Scale bar: 25 μm.

4.2 *Ir7a* and *Ir7f* mark functionally distinct populations of blood-sensitive neurons

To gain selective genetic access to *Ir7a*- and *Ir7f*-expressing cells, we used CRISPR-Cas9 homology-directed repair to generate QF2 driver lines for each transcript (Kistler et al., 2015; Matthews et al., 2019). We then crossed these drivers to reporter lines to examine the expression pattern of *Ir7a* and *Ir7f*. These experiments revealed sparse expression in subsets of chemosensory neurons in the female stylet (Figure 4.5A,B). *Ir7a* and *Ir7f* are expressed in approximately 1 - 2 neurons and 3 - 4 neurons, respectively. No expression of either gene was detected in male stylets. The sparse nature of these drivers revealed dendritic innervation of the bilaterally symmetric set of two chemosensory sensilla at the stylet tip (Figure 4.5A,B). Both populations of neurons innervate the same ventral subesophageal zone region identified in our stylet dye-fills (Figure 4.5C-F). Importantly, no regions in the male brain or additional regions in the female brain were labeled in these strains, highlighting the exquisite selectivity of *Ir7a* and *Ir7f* gene expression to the female stylet.

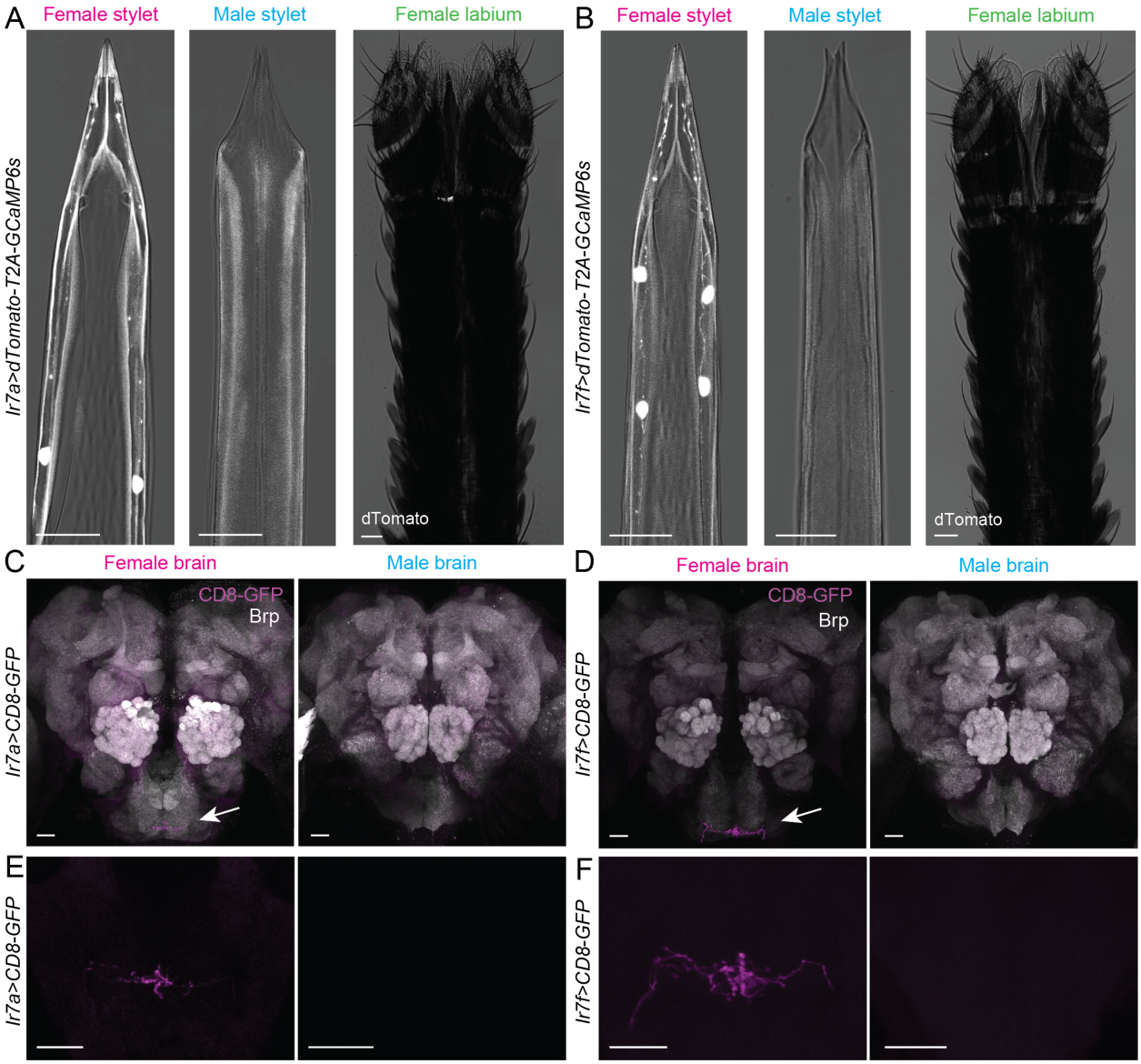

Figure 4.5 *Ir7a* and *Ir7f* are expressed exclusively in the female stylet

(A,B) Confocal image with transmitted light overlay of dTomato expression (gray) in the female stylet (left panel), male stylet (middle panel), and female labium (right panel) of *Ir7a>dTomato-T2A-GCaMP6s* (A) and *Ir7f>dTomato-T2A-GCaMP6s* (B) animals. *Ir7a* expression: 10/13 females = 2 neurons, 2/13 females = 1 neuron, 1/13 females = 0 neurons. *Ir7f* expression: 6/11 females = 4 neurons, 5/11 females = 3 neurons. (C-F) mCD8:GFP expression (magenta, white arrow) of *Ir7a>mCD8:GFP* (C,E) and *Ir7f>mCD8:GFP* (D,F) in female (left) and male (right) brain (top) and subesophageal zone (bottom). Neuropil in C and D is labeled with anti-*Drosophila* Brp (gray). The brain and subesophageal zone images in C-F were acquired from different individuals.

(A-F) Scale bar: 25 μm.

To determine the functional properties of *Ir7a* and *Ir7f* neurons, we performed cell-type specific calcium imaging experiments and found that almost all *Ir7a* neurons and a subpopulation of *Ir7f* neurons responded to blood (Figure 4.6A,B). The blood-sensitive neuronal subset from both genotypes responded robustly to Mix [glucose, $NaHCO_3$, and NaCl] (Figure 4.6A,B). *Ir7a*-expressing blood-sensitive neurons were robustly activated by 25 mM $NaHCO_3$ (Figure 4.6C,D), sharing a profile with $NaHCO_3$-sensitive neurons identified in Cluster II (Figure 3.6). In contrast, *Ir7f*-expressing blood-sensitive neurons were consistently activated by Mix and had variable responses to 140 mM NaCl and/or 25 mM $NaHCO_3$ (Figure 4.6E,F), sharing a profile most similar to Integrator neurons in Cluster IV (Figure 3.6). Thus, these two female stylet-specific driver lines define the molecular and functional identity of two non-overlapping blood-sensitive neuron populations in the female stylet.

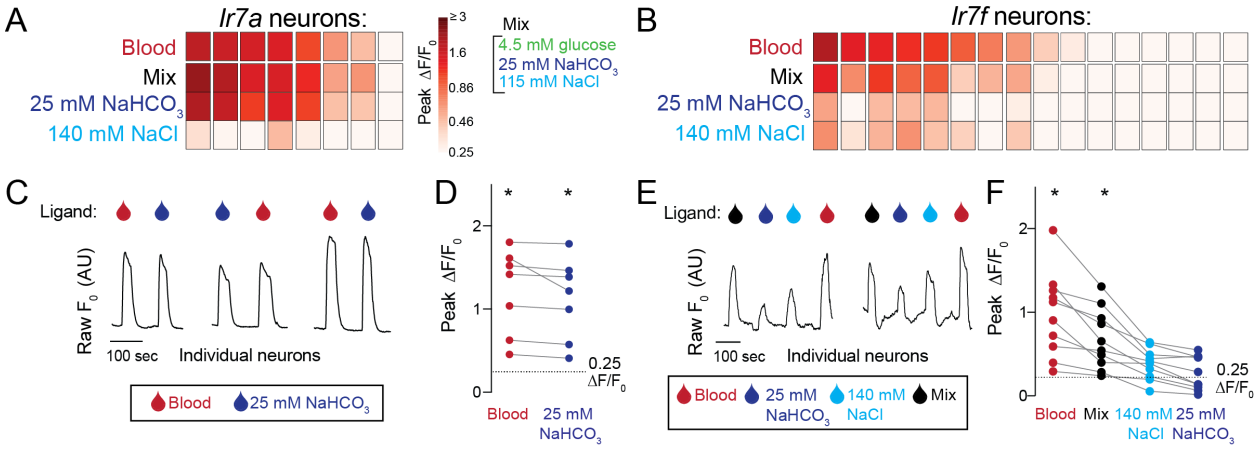

Figure 4.6 *Ir7a* and *Ir7f* mark mutually exclusive subsets of blood-sensitive neurons.

(A,B) Heat maps of peak $\Delta F/F_0$ response to the indicated ligand in *Ir7a>dTomato-T2A-GCaMP6s* (A) and *Ir7f>dTomato-T2A-GCaMP6s* (B) neurons across N=5 females. Each square is the average of 3 ligand exposures and each column represents one neuron. Columns are sorted by largest to smallest peak $\Delta F/F_0$ in response to blood.
(C,E) Raw F_0 traces from individual neurons in response to indicated ligand.
(D,F) For blood-sensitive neurons, peak $\Delta F/F_0$ to indicated ligand. Each data point denotes the response from 1 neuron and responses from the same neuron are connected by a line (* $p < 0.05$, one-sample Wilcoxon signed-rank test).
(A-F) 0.0002% fluorescein was added to blood and 140 mM NaCl, and 0.00002% was added to Mix and 25 mM $NaHCO_3$ in the BioPen to visualize ligand delivery zone.

Importantly, we conclude that *Ir7a*- and *Ir7f*-expressing neurons share a profile most similar to the clusters established using pan-neuronal imaging in Figure 3.6. To definitively place *Ir7a*- and *Ir7f*-expressing neurons into a cluster, two orthogonal binary expression systems (ie Gal4-UAS and Q-system) would be required to concomitantly drive *Brp > GCaMP6s* and *Ir7f > dTomato* or *Brp > GCaMP6s* and *Ir7a > dTomato*. This method would allow all neurons to be clustered based on functional imaging experiments performed in *Brp > GCaMP6s* animals, and subsequently determine if *Ir7a*- and *Ir7f*-expressing neurons always cluster in the $NaHCO_3$ and Integrator clusters, respectively. Since the Gal4-UAS system is inconsistent in *Ae. aegypti* (Zhao et al., 2020), orthogonal binary expression systems are an active area of investigation in the field.

To confirm that preparation viability and stability does not explain the lack of ATP responses, we directly compared the peak $\Delta F/F_0$ response to ATP and the positive control, KCl. Although none of the *Ir7a*- and *Ir7f*-expressing neurons responded to ATP, all neurons responded to KCl (Figure 4.7).

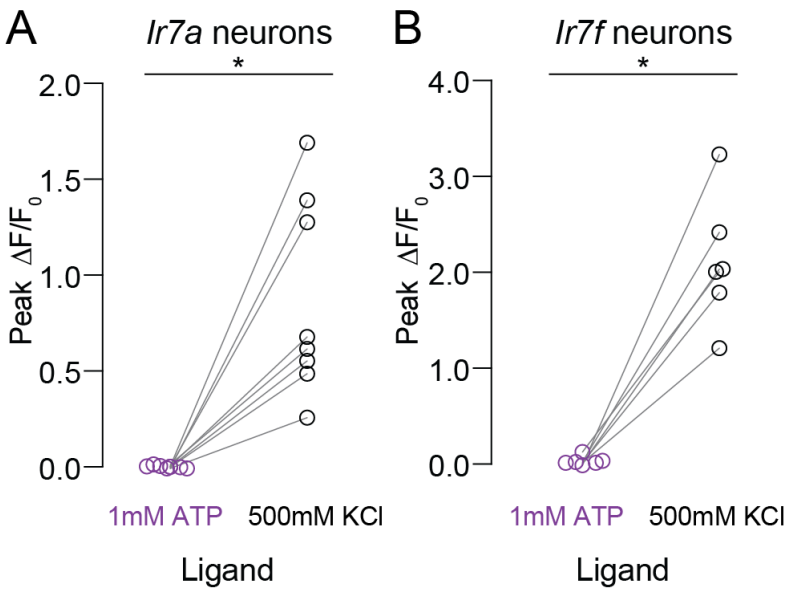

Figure 4.7 *Ir7a*- and *Ir7f*-expressing neurons do not respond to ATP.

(A,B) Peak $\Delta F/F_0$ in response to 1mM ATP (purple) or positive control (500 mM KCl, black) for *Ir7a*- (A, N=8) and *Ir7f*-expressing (B, N=6) neurons. Each data point denotes the response from 1 neuron and responses from the same neuron are connected by a line (* $p < 0.05$, Wilcoxon matched-pairs signed rank test).

4.3 The search for the receptors that detect blood components

To determine if expression of *Ir7a* or *Ir7f* is required for engorgement on blood or ATP in saline, we used the CRISPR-Cas9 system to generate knockouts for each gene (Kistler et al., 2015). In generating stable homozygous mutant strains, we confirmed that both $Ir7a^{-/-}$ and $Ir7f^{-/-}$ females reliably engorged on blood and produced eggs. Since whole blood may contain redundant cues, we simplified blood to the minimal physiological meal sufficient to promote engorgement: 1mM ATP in 110 mM NaCl and 25 mM $NaHCO_3$ (referred to as ATP in saline). When we measured engorgement on ATP in saline, we found no significant difference between $Ir7a^{-/-}$ females and $Ir7f^{-/-}$

females compared to their respective heterozygote sibling controls (Figure 4.8A,B). These negative data do not distinguish between whether (1) *Ir7a* and *Ir7f* are not required to detect $NaHCO_3$ and components of Mix, respectively, or (2) there are redundant neuronal populations for detecting $NaHCO_3$ and components of Mix. Both outcomes are plausible since (1) multiple chemosensory receptor transcripts can be expressed in a given sensory neuron (Sanchez-Alcaniz et al., 2018) and (2) redundancy at the neuronal and molecular level is unsurprising for a chemosensory cue as important as blood.

It is also important to note that addition of $NaHCO_3$ to ATP in NaCl is necessary in the minimal physiological meal because ATP is rapidly hydrolyzed, as measured by an immediate drop in pH, when added to an unbuffered solution like water or NaCl alone (Figure 4.8C). Nonetheless, $NaHCO_3$ itself is not absolutely required because 1 mM ATP in phosphate-buffered saline (PBS) is sufficient to promote engorgement (Galun et al., 1984; Hol et al., 2020). Thus, it is unclear from these behavior experiments if detection of a base is required, or if its role is simply to buffer ATP. Classic behavioral experiments by Galun and colleagues suggest that mosquitoes prefer $NaHCO_3$ as the ideal buffer for ATP, but further experiments are required to understand the mechanism underlying this preference (Galun et al., 1984).

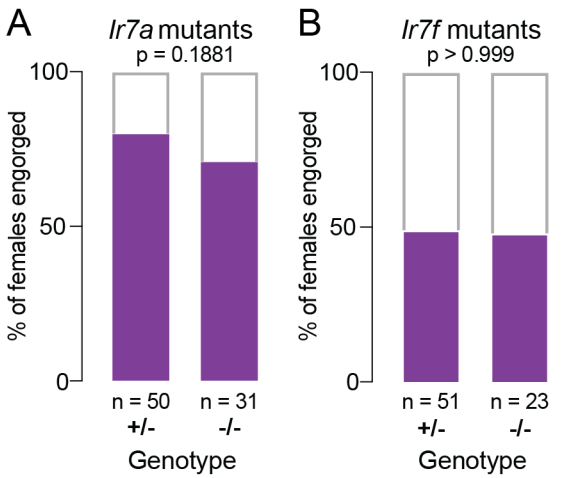

C Empirical pH measurements:

Solution	Baseline pH	+ 1mM ATP
Water	7.4	3.5
120 mM $NaHCO_3$	8.7	8.7
120 mM NaCl	6.9	3.3
110 mM NaCl, 20 mM $NaHCO_3$	8.2	7.9

Figure 4.8 Expression of *Ir7a* and *Ir7f* is not required for engorgement on ATP and saline.

(A,B) *Ir7a*$^{-/-}$ (A) and *Ir7f*$^{-/-}$ (B) female engorgement on 1 mM ATP in 110 mM NaCl and 20 mM $NaHCO_3$ delivered via Glytube (statistical significance determined using Fisher's exact test).
(C) pH of the indicated solution immediately before and after the addition of 1 mM ATP.

The stylet RNA-seq dataset provided the first insight into the molecular identity of blood-sensitive neurons and led to the identification of *Ir7a* and *Ir7f* as female stylet-specific transcripts that mark blood-sensitive neurons (Figure 4.2 and Figure 4.5). Together these results delineate two independent blood-sensitive stylet neuron subtypes, each tuned to specific blood components (Figure 4.5 and Figure 4.6). The *Ir7a* and *Ir7f* driver lines and mutants generated in this study will facilitate future experiments to understand how these receptors respectively contribute to the functional properties of the $NaHCO_3$ and Integrator neuronal subsets. As the first unbiased molecular profile of the stylet in any mosquito species, the RNA-seq dataset will inform

future screens for: (1) drivers that label the remaining blood-sensitive neurons and (2) receptors that directly detect blood components.

While these results reveal how the stylet detects the taste of blood, it remains unclear how blood is differentiated from nectar to ensure the female only engorges on blood. Does the stylet's neuronal architecture innately distinguish between these two appetizing food sources? Or is valence assigned through downstream integration with additional context-specific sensory information associated with blood feeding? To distinguish between these two possibilities, it is first necessary to understand how the stylet responds to nectar sugars.

CHAPTER 5. SPECIALIZATION IN STYLET NEURONS ENABLES DISCRIMINATION BETWEEN BLOOD AND NECTAR

Sugars present an interesting discrimination challenge for mosquito taste coding because a female wants to recognize nectar as appetizing when she intends to feed on nectar, but not when she intends to feed on blood. To further complicate matters for the mosquito, glucose is a redundant cue in blood and nectar (Figure 5.1).

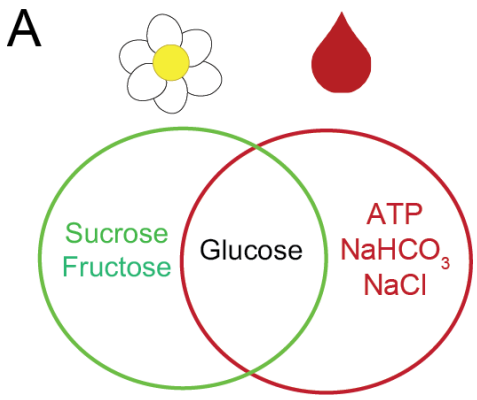

Figure 5.1 Glucose is a redundant cue between blood and nectar.
(A) Venn diagram schematizing the principal sugars in nectar (left circle) and the blood components sufficient recapitulate whole blood behavioral and neuronal responses (right circle).

To avoid confusion between the blood-feeding and nectar-feeding feeding programs, it is important that a female not trigger engorgement when the stylet contacts nectar sugars during blood feeding. How is this discrimination achieved? Since stylet neurons are the only sensory neurons that directly contact the meal during blood feeding, do they have a specialized taste coding strategy to selectively distinguish blood

components from nectar components? One way to achieve this discrimination is to exclude the expression of sweet taste receptors from the stylet. Alternatively, stylet neurons could express the same sweet taste receptors that mediate nectar detection for nectar-feeding behavior, but sweet taste sensitivity and/or processing could be rapidly modulated during blood-feeding by the presence of human cues like CO_2 and heat. If the stylet has a canonical sweet taste pathway, we would expect the stylet to express sweet gustatory receptors and respond to sucrose, fructose, and glucose, which are the principal components of nectar (Liman et al., 2014; Yarmolinsky et al., 2009). To address this question, we investigated expression of sweet taste receptors in the stylet, in addition to the stylet's behavioral and neuronal responses to nectar sugars.

5.1 The stylet lacks canonical sweet taste receptor expression

We first provided the same 298 mM sugars in the context of the nectar- or blood-feeding assay and compared the behavioral responses. 298 mM was selected because it is approximately equivalent to the female's normal sugar meal that is sufficient for energy metabolism (Van Handel, 1972, 1984). Females readily ingested all three sugars when the labium directly contacted the meal in the nectar-feeding assay, where no host cues are present (Figure 5.2A,C). In contrast, they rejected these same sugars in the blood-feeding assay when the stylet directly contacted the meal in the presence of heat and CO_2 (Figure 5.2B,D). In control experiments we showed that blood stimulated robust consumption in the blood-feeding assay (Figure 5.2B,D). Therefore, the behavioral response to the principal components of nectar is context dependent.

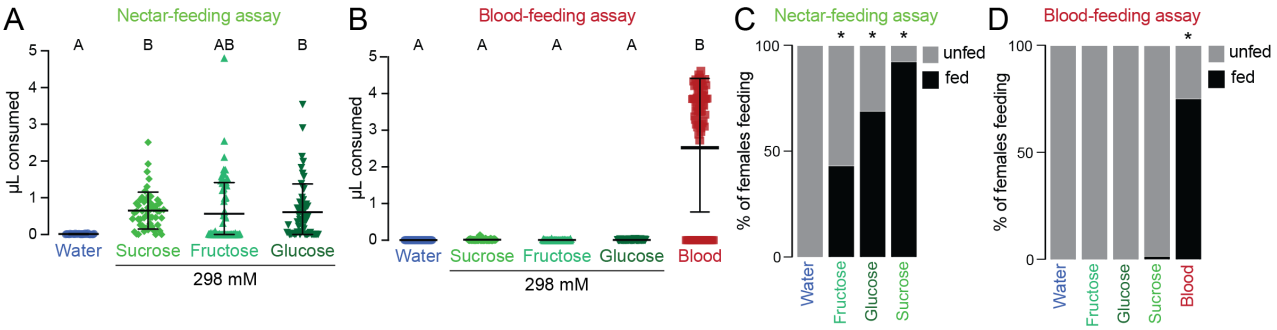

Figure 5.2 The behavior response to nectar sugars is context-dependent.

(A,B) Volume of indicated meal consumed in the nectar-feeding (A) and blood-feeding (B) assay. Each data point represents 1 female: water N=36-40; sucrose N=53–60; fructose N=40-74; glucose N=55-59. Blood in (B) is a positive control for blood-feeding assay, N=76 females. Data labeled with different letters are significantly different from each other (mean ± SD; Kruskal-Wallis test with Dunn's multiple comparison, $p < 0.05$). (C,D) % of females feeding on the indicated meal offered in the nectar-feeding (C) and blood-feeding (D) assay, based on µL consumed measurements in (A) and (B), respectively. Unfed and fed females consumed ≤0.05 µL and >0.05 µL, respectively. Groups labeled with * are significantly different from water ($p < 0.001$, Fisher's exact test with Bonferroni correction).

These results lead to the question of whether stylet neurons can detect these nectar sugars at all. Orthologues of the sweet taste Gustatory Receptor (GR) genes first described in *D. melanogaster* (Clyne et al., 2000; Scott, 2018; Slone et al., 2007; Thorne et al., 2004) are thought to play a conserved role in *Ae. aegypti* mosquitoes (Kent and Robertson, 2009). Recent phylogenetic analyses predict that the *Ae. aegypti* genome encodes 7 full-length orthologues (*Gr4, Gr5, Gr6, Gr7, Gr9, Gr10,* and *Gr11*) of the sweet taste subfamily (Matthews et al., 2018). While the female labium expresses all predicted orthologues (Figure 5.3, green), none were detected in the female or male stylet (Figure 5.3, pink and blue).

Figure 5.3 The labium, but not the stylet, expresses canonical sweet taste receptors.

(A) Canonical sweet taste receptor expression from RNA-seq analysis of the indicated tissues. N=4 replicates/tissue. Median indicated by black line, bounds of box represent first and third quartile, whiskers are 1.5 times the inter-quartile range, and dots represent TPM value from each biological replicate. The outlier is denoted by a dot without whisker.

To validate this finding using an orthogonal method, we used CRISPR-Cas9 homology-directed repair to insert the QF2 transcriptional activator at the endogenous *Gr4* locus (Kistler et al., 2015; Matthews et al., 2019; Potter et al., 2010; Riabinina et al., 2016). *Ae. aegypti Gr4* is the closest orthologue of both *D. melanogaster Gr5a* and *Gr64f*, which are the driver lines most commonly used to target sweet taste neurons in *D. melanogaster* (Kent and Robertson, 2009; Matthews et al., 2018). The *Gr4* reporter line showed no expression in the female and male stylet but was expressed in a large group of labial neurons (Figure 5.4A). Furthermore, the axons of *Gr4*-expressing

neurons projected to the posterior region of the subesophageal zone (Figure 5.4B,C), but not to the anterior, ventral region occupied by stylet neuron projections (Figure 2.7B). Of note, we detected labelling in the subesophageal zone of both females and males (Figure 5.4B,C), consistent with sweet taste and nectar-feeding being common to both sexes. Together these results demonstrate that stylet neurons do not express canonical sweet taste gustatory receptors. Furthermore, segregation of canonical sweet taste receptor expression intimates that the stylet and labium may have divergent roles in food source detection.

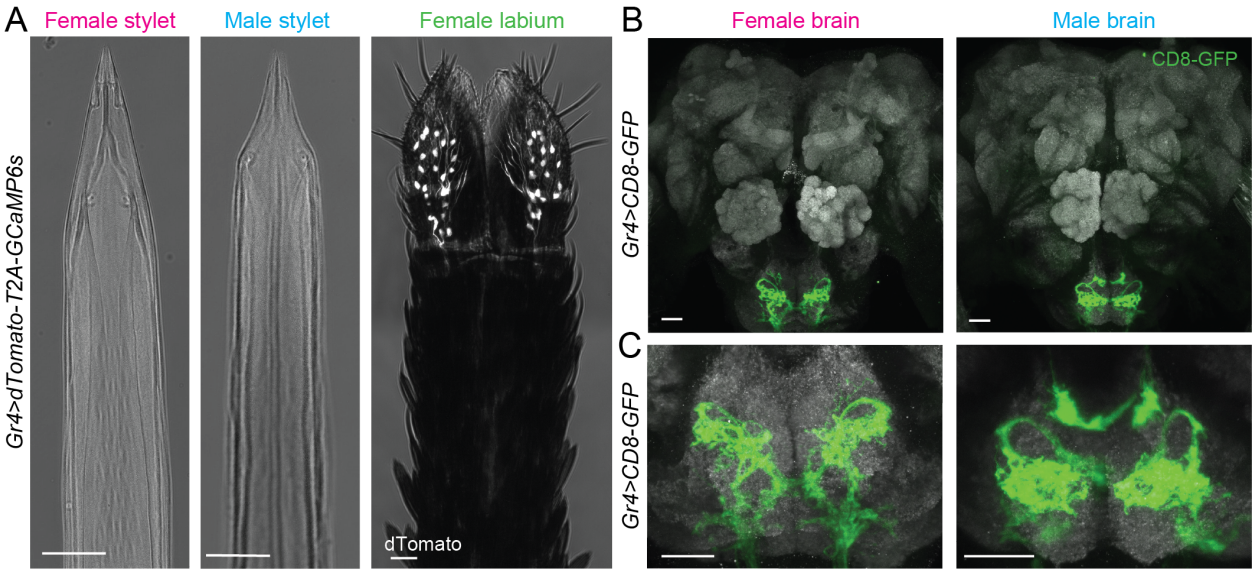

Figure 5.4 The predicted sweet taste co-receptor is expressed in the labium.

(A) Confocal image with transmitted light overlay of dTomato expression (gray) in the female stylet (left panel), male stylet (middle panel), and female labium (right panel) of *Gr4>dTomato-T2A-GCaMP6s* animals.
(B,C) mCD8:GFP expression (green) of *Gr4>mCD8:GFP* in female (left) and male (right) brain (B) and subesophageal zone (C). Neuropil labeled with anti-*Drosophila* Brp (gray). Brain and subesophageal zone images were acquired from two different individuals.
(A-C) Scale bar: 25 μm.

5.2 Stylet neurons are insensitive to nectar-specific sugars

Although stylet neurons lack a canonical sweet taste pathway, it is formally possible that stylet neurons are still sensitive to nectar sugars through an alternate receptor mechanism. To determine if stylet neurons are activated by nectar sugars, we performed calcium imaging experiments in stylets from *Brp>dTomato-T2A-GCaMP6s* animals and examined stylet neuron responses. If stylet neurons lack a canonical sweet taste pathway, we expect no responses to sucrose, fructose, and glucose. Indeed, no stylet neurons responded to 298 mM of the nectar-specific sugars sucrose and fructose (Figure 5.5) (Werner-Reiss et al., 1999b). In half of the females, we observed occasional responses to 298 mM glucose, which is the only sugar found in both blood and nectar (Figure 5.5). In positive control experiments, we observed that all stylet neurons responded to KCl (Figure 5.5).

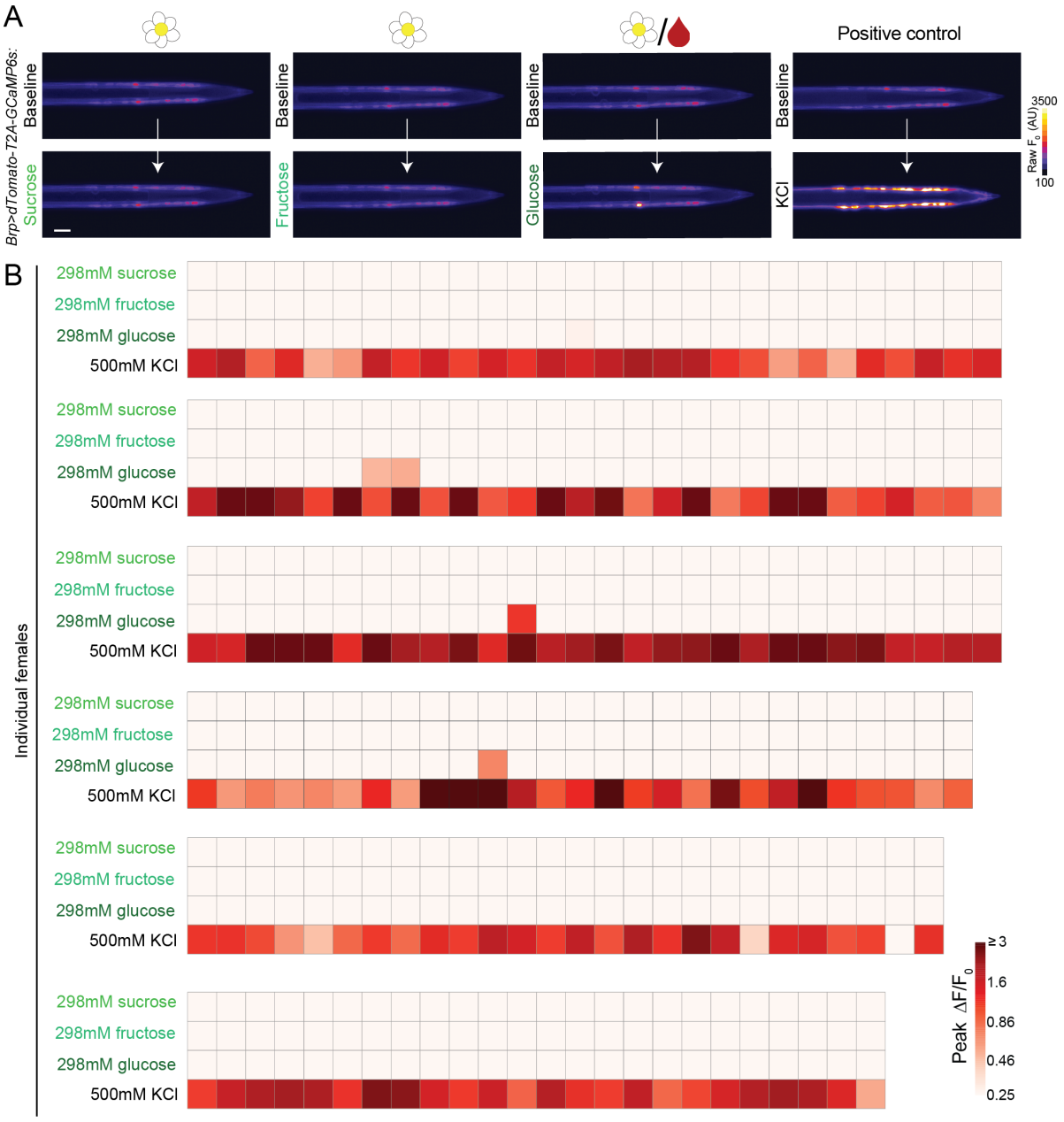

Figure 5.5 Stylet neurons are not activated by nectar-specific sugars.

(A) Representative image of GCaMP6s fluorescence increase to indicated 298 mM sugar presentation (bottom) compared to baseline (top). Flower/blood symbol (3rd from left) indicates that sugar is found in nectar and blood. Scale bar: 25 μm.
(B) Heat maps of peak $\Delta F/F_0$ response to the indicated ligand for individual females. Each square is the average of 3 ligand exposures. Each column represents one neuron and each row represents the response to the indicated ligand for all neurons from 1 individual female. Neurons are ordered from proximal to distal. N=6 individual females.

5.3 Polymodal stylet neurons assign context-specific information to glucose

Although responses to 298 mM glucose were rare (Figure 5.6A), peak $\Delta F/F_0$ responses were reliably above the 0.25 threshold for activation (Figure 5.6B, dotted line). We next asked if 298 mM glucose-sensitive stylet neurons intersected with the previously identified subset of blood-sensitive stylet neurons, or if they are an independent subset. All 298 mM glucose-sensitive neurons were activated by blood and there was a trend for peak responses to be greater to blood than to 298 mM glucose (Figure 5.6B).

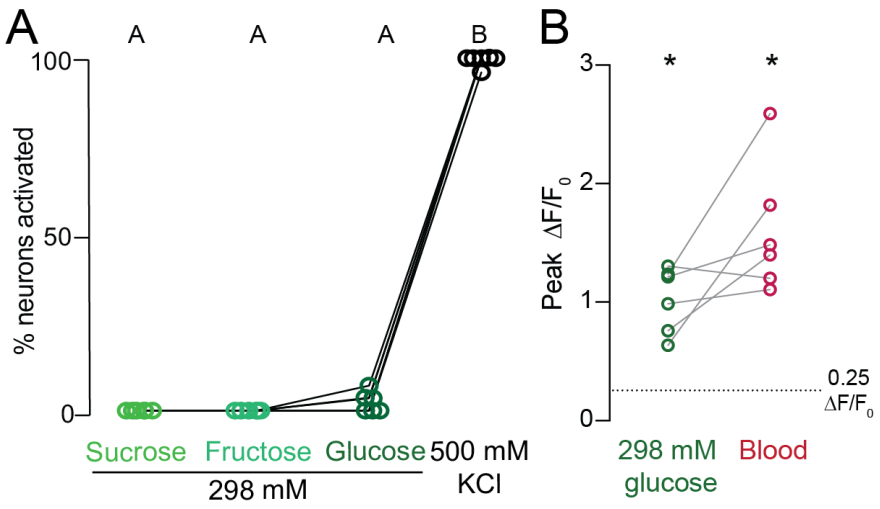

Figure 5.6 298 mM-sensitive neurons intersect with Integrator neurons.

(A) Quantification of % neurons with ≥ 0.25 peak $\Delta F/F_0$ to the indicated ligand from the females analyzed in Figure 5.5, each data point denotes the response from 1 female, responses from the same female are connected by a line, N=6 females. Data labeled with different letters are significantly different from each other (mean ± SD; Kruskal-Wallis test with Dunn's multiple comparison, $p < 0.05$).
(B) For 298 mM-sensitive neurons (response to 298 mM glucose ≥ 0.25 peak $\Delta F/F_0$), peak $\Delta F/F_0$ to 298 mM glucose, compared to blood. Each data point denotes the response from 1 neuron and responses from the same neuron are connected by a line (N=6 neurons, mean ± SD, * indicates $p < 0.05$, one-sample Wilcoxon signed rank test).

Further functional experiments revealed that 298 mM-sensitive neurons primarily intersected with the Integrator neuron cluster of blood-sensitive neurons (Figure 5.7A), which are responsive to the Mix of 4.5 mM glucose, 115 mM NaCl, and 25 mM $NaHCO_3$ (Figure 3.6). Intriguingly, Integrator neurons consistently responded more robustly to Mix, which contains physiological levels of blood glucose (4.5 mM), than to glucose concentrations relevant for nectar-feeding behavior (298 mM) (Figure 5.7B). Furthermore, no stylet neurons, including Integrator neurons, respond to presentation of 4.5 mM glucose alone (Figure 3.6 and Figure 5.7C). Together these results demonstrate that Integrator neurons are not exclusively tuned to glucose detection.

We therefore asked if physiological levels of blood glucose directly contribute to Mix responses observed in Integrator neurons. Since Integrator neurons are not reliably activated by an individual component of Mix (Figure 3.6), we tested if the addition of 4.5 mM glucose to other Mix components increased the total neuronal response. Integrator neurons responded to 4.5 mM glucose when co-presented with NaCl or $NaHCO_3$, and by co-presentation of all three components of Mix (Figure 5.7D). Therefore, individual sensory neurons can directly integrate multiple blood components that belong to disparate taste qualities: glucose (sweet), NaCl (salty), and $NaHCO_3$. Taken together, our results demonstrate that the stylet is specialized to detect blood over nectar.

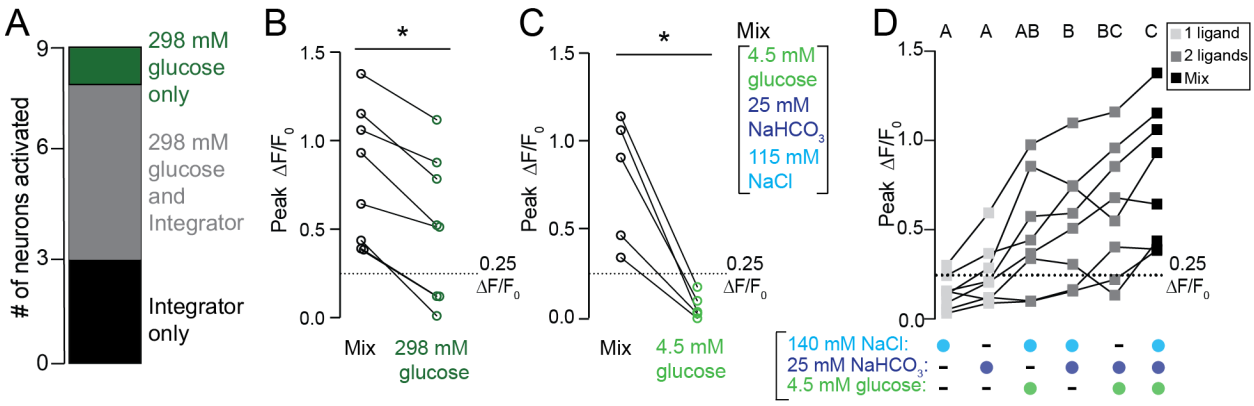

Figure 5.7 Integrator neurons detect blood glucose in the presence of other blood components.

(A) A dataset from N=6 females was filtered for all 298 mM-sensitive neurons and Integrator neurons to compare the intersection of 298 mM-sensitive neurons and Integrator neurons (N=9 neurons; 1/9 = 298 mM glucose only, 5/9 = 298 mM glucose and Integrator, 3/9 = Integrator only).
(B,C) For Integrator neurons, peak $\Delta F/F_0$ to 298 mM glucose (B, N=8 neurons) and 4.5 mM glucose (C, N=5 neurons). Each dot represents 1 neuron (mean ± SD, * $p < 0.05$ Mann-Whitney test).
(D) For Integrator neurons, peak $\Delta F/F_0$ to indicated ligand(s). Each data point denotes the response from 1 neuron, N=8 neurons. Data labeled with different letters are significantly different from each other (one-way repeated measures ANOVA, with the Geisser-Greenhouse correction and Tukey's multiple comparisons test, $p < 0.05$).
(B-D) responses from the same neuron are connected by a line.

While nectar-specific sugars are not detected by stylet neurons, glucose detection depends on the presence of additional blood components. Stylet neurons lack canonical sweet taste receptor expression (Figure 5.3 and Figure 5.4) and do not respond to the concentrations of nectar-specific sugars that are sufficient to promote nectar-feeding behavior (Figure 5.5). Thus, the molecular and functional properties of stylet neurons mirror the lack of behavioral response to nectar-specific sugars in the blood-feeding assay (Figure 5.2).

In contrast to sucrose and fructose, glucose is the only known redundant cue shared between blood and nectar (Figure 5.1). Yet females are not confused by this conflicting signal- glucose is consistently consumed in the nectar-feeding assay and reliably rejected in the blood-feeding assay (Figure 5.2). The most parsimonious explanation is that the stylet does not detect glucose, in addition to sucrose and fructose, since stylet neurons lack a canonical sweet taste pathway (Figure 5.3 and Figure 5.4) and are not reliably activated by 4.5 mM glucose (Figure 3.6 and Figure 5.7C). To our surprise, however, we found that Integrator neurons can detect 4.5 mM glucose but require co-presentation of either NaCl or $NaHCO_3$ to cause reliable activation (Figure 5.7D). We propose that glucose integration assigns context-specific information to physiological levels of blood glucose. Taken together, our results demonstrate that the stylet is specialized to detect blood over nectar.

CHAPTER 6. ARE THERE SPECIALIZED CIRCUITS FOR BLOOD- AND NECTAR-FEEDING BEHAVIORS?

To what extent are blood- and nectar-feeding behaviors segregated in their chemosensory coding, central processing, and descending motor control? To answer this question, it is imperative to decouple these features from the structural role of the stylet and labium during feeding. When a mosquito feeds on sugars from a plant or in the nectar-feeding assay, the labium directly contacts the meal, and the stylet is recessed within the gutter-like folds of the labium (Figure 6.1A). In this context, the stylet functions as a feeding tube, similar to the labral sense organ of *D. melanogaster* (LeDue et al., 2015; Stocker, 1994). Liquids only contact the stylet after pumping is initiated, but once ingestion has been initiated, all liquids flow over the recessed stylet in both sexes. The experiments presented thus far have demonstrated that the stylet is specialized to detect blood over nectar, but do not reveal if chemosensory input from the stylet is dispensable for nectar-feeding behavior. Entomologists in the mid-1900s tried to decouple the stylet's chemosensory role from its structural role by force-feeding liquids to immobilized mosquitoes with amputated feeding appendages (Owen, 1963; Pappas, 1978). However, these experiments are difficult to interpret because the stylet's function as a feeding tube necessitates that nectar pass through the stylet as it is consumed.

During blood feeding, the stylet pierces through skin to contact blood while the labium remains on the skin's surface (Figure 6.1B,C) (Gordon, 1939; Kong and Wu,

2010). By definition, chemosensory detection of blood by the labium is not a requirement for blood-feeding behavior since the labium does not contact blood. Yet the labium provides lateral support on the skin that is required for piercing, an essential prerequisite for blood feeding on a live animal or in the blood-feeding assay (Figure 6.1B,C) (Ramasubramanian et al., 2008). Furthermore, the skin is a rich chemosensory environment that directly contacts labium sensory neurons during blood feeding. Although previous studies have hinted that this chemosensory input is not required, many groups have traditionally used animal skin or a skin mimic to separate the blood meal (Galun et al., 1985b; Gordon, 1939; Griffiths and Gordon, 1952; Ramasubramanian et al., 2008). In this chapter we extended our genetic and behavioral toolkit to finally decouple each sensory appendage's chemosensory role from its structural role in blood- and nectar-feeding behavior. These experiments lay the foundation for determining the degree of specialization in the downstream circuits controlling blood- and nectar-feeding programs.

Figure 6.1 The stylet and labium change positions between blood and nectar feeding.

(A) When the female is at rest (pictured) or feeding on nectar, only the labium is visible. The stylet is recessed within the labium and does not contact the external environment.

(B) Once the female lands on a host and begins to bite, the labium is retracted as the stylet's tip pierces through skin to contact blood.
(C) During blood feeding, the labium is fully retracted, forming a loop that rests on the skin's surface. Only the stylet is in direct contact with blood.
Images by Alex Wild.

6.1 Chemosensory input from the stylet is dispensable for nectar-feeding behavior

First, we investigated the molecular identity of the sensory neurons that mediate nectar-feeding behavior. We hypothesized that orthologues of *D. melanogaster* sweet taste Gustatory Receptor (GR) genes (Clyne et al., 2000; Scott, 2018; Slone et al., 2007; Thorne et al., 2004) may have a conserved role in *Ae. aegypti.* With the goal of labeling and manipulating neurons that express *Gr4*, we generated an effector QUAS line to express both the dTomato fluorescent reporter and the rat cation channel TRPV1 in *Gr4*-expressing neurons (Tobin et al., 2002). In *Gr4>dTomato-T2A-TRPV1* mosquitoes, we detected dTomato expression in the labium and legs, the two major taste appendages of insects (Figure 6.2A,B). In our nectar-feeding assay, both the labium and leg can directly contact the meal during feeding, but the labium is the mouthpart used when feeding. Ectopic expression of dTomato was not detected in the labium of driver- (*Gr4*) and effector- (TRPV1) only transgenic strain controls (Figure 6.2C,D).

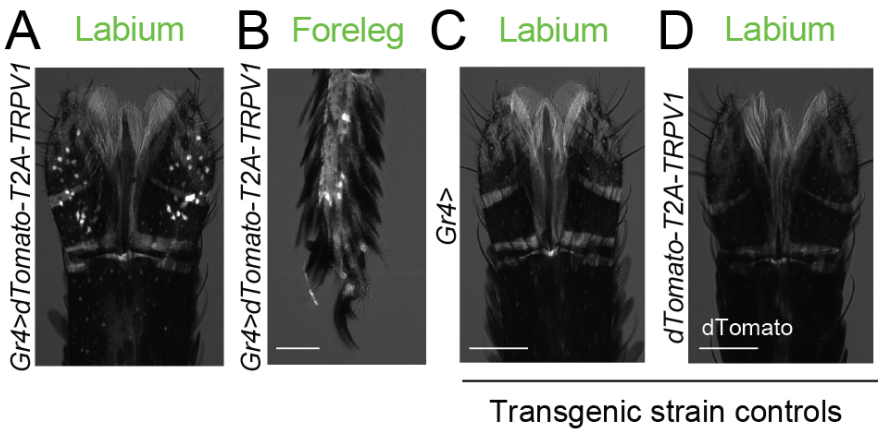

Figure 6.2 Generation of chemogenetic tools in *Ae. aegypti.*

(A-D) Confocal image of dTomato expression with transmitted light overlay in *Gr4>dTomato-T2A-TRPV1* labium (A), *Gr4>dTomato-T2A-TRPV1* foreleg (B), *Gr4* driver-only control labium (C), and *dTomato-T2A-TRPV1* effector-only control labium (D).
Scale bar: 50 μm.

To ask whether activation of *Gr4* neurons is sufficient to initiate nectar-feeding behavior, we performed chemogenetic experiments that used capsaicin, the active ingredient in chili peppers, to activate TRPV1. Capsaicin should not affect feeding behavior of wild-type animals because capsaicin-sensitive TRP channels have not been described in invertebrates (Lima and Miesenbock, 2005; Marella et al., 2006; Matthews et al., 2018; Tobin et al., 2002). In control experiments, we confirmed that capsaicin did not alter ingestion of water or sucrose by wild-type animals in the nectar-feeding assay (Figure 6.3A). Furthermore, we did not detect significant difference between the amount of 10% sucrose or water ingested by *Gr4>dTomato-T2A-TRPV1* females compared to the driver- (*Gr4*) and effector- (TRPV1) only transgenic strain controls (Figure 6.3B, left and middle). Similar to previous observations in *D. melanogaster* (Marella et al., 2006),

addition of 50 µM capsaicin to water promoted ingestion of the otherwise inert water meal only in animals expressing TRPV1 in *Gr4* neurons (Figure 6.3B, right). Thus, nectar-feeding can be initiated by activation of sensory neurons that express sweet taste receptors. Since *Gr4* is not expressed in the stylet (Figure 5.3 and Figure 5.4), chemosensory stylet neurons were not activated by capsaicin addition, demonstrating that activity in these neurons is not required to promote nectar-feeding behavior.

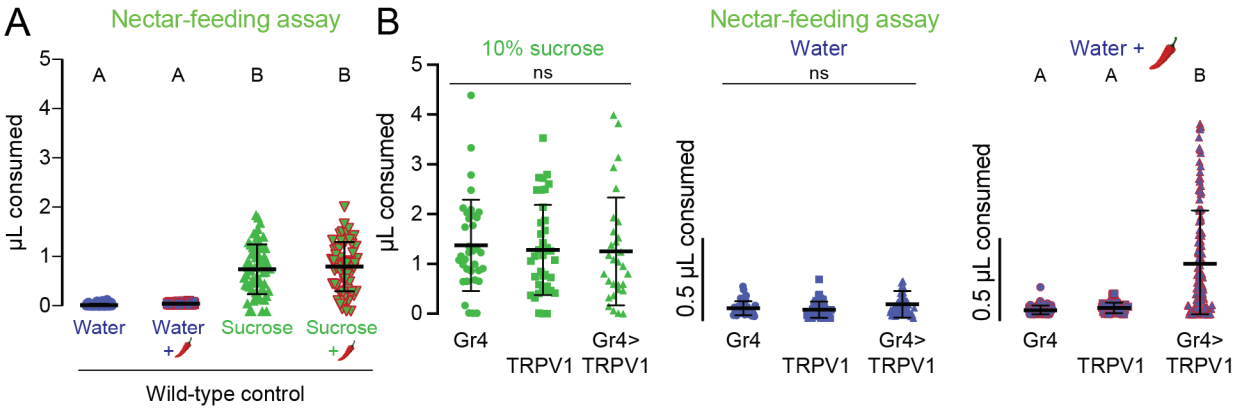

Figure 6.3 Activation of *Gr4*-expressing neurons is sufficient to promote nectar feeding.

(A) Volume of meal consumed by wild-type mosquitoes. Chili pepper cartoon indicates addition of 50 µM capsaicin. Each data point represents 1 female: N=58-60 females/meal.
(B) Volume of meal consumed by the indicated genotypes. Each data point represents 1 female: 10% sucrose N=30-40 females/genotype; water N=41-60 females/genotype; water + 50 µM capsaicin (red chili pepper): *Gr4* N=61, *TRPV1* N=62, *Gr4>TRPV1* N=124 females.
(A,B) Data labeled with different letters are significantly different from each other (mean ± SD; Kruskal-Wallis test with Dunn's multiple comparison, $p < 0.05$).

These genetic manipulations establish that chemosensory input from an intact stylet is not required to initiate nectar-feeding behavior. It should be noted that *Gr4>dTomato-T2A-TRPV1* females consistently consumed a larger volume of 10% sucrose than water

+ 50 μM capsaicin (Figure 6.3). Increasing capsaicin concentration in pilot experiments did not significantly increase the meal volume consumed. Multiple explanations, none of which are mutually exclusive, may explain the reduced volume: (1) *Gr4* does not capture all neurons that detect real nectar, (2) TRPV1 activation by capsaicin does not faithfully mimic the endogenous activity patterns, and (3) mechanosensory detection of sugar osmolarity by the stylet can enhance nectar feeding. Future work will refine the requirements to initiate nectar-feeding behavior.

Furthermore, no one has systematically tested whether the labium can respond to blood components like ATP and $NaHCO_3$ that are associated with non-canonical taste qualities. Sanford and colleagues recorded from medium-sized sensillar hairs on the labium and detected responses to 10 – 1000 mM NaCl, but not to ATP (Sanford et al., 2013). These results suggest that ATP does not activate labium neurons, but further work is needed to comprehensively characterize labium neuron responses to the blood components tested in our study.

6.2 Chemosensory input from the labium is dispensable for blood-feeding behavior

In classic experiments, researchers observed mouthpart behavior as *Ae. aegypti* mosquitoes fed on the thin webbing of frog (Gordon, 1939) and the skin of a mouse ear (Griffiths and Gordon, 1952). With proper transillumination, the authors were able to observe the stylet penetrating the skin as the labellar lobes of the labium remained on

the surface of the frog-web or mouse skin. A modern version of the mouse ear experiment was repeated using intravital video microscopy to record *An. gambiae* blood feeding on a piece of mouse skin (Choumet et al., 2012). These movies elegantly demonstrate that only the stylet is endowed with the ability to pierce through blood capillaries to swiftly pump blood. Furthermore, *Ae. aegypti* blood-feeding behavior was filmed at 2000 fps for high magnification observation of mosquito bite mechanics to develop models for hypodermic needles (Ramasubramanian et al., 2008). The authors found that only the stylet penetrates the skin and that the labium remains on the surface of the skin to provide lateral support as the stylet is injected into the skin (Ramasubramanian et al., 2008).

Although the labium is not in direct contact with blood in these live animal assays, it is in direct contact with the rich chemosensory palate of skin. To completely remove input from human chemosensory cues to the labium, we replaced skin with an inert piece of parafilm in all of our biteOscope and blood-feeding assay experiments. Individual stylet tracking in biteOscope experiments confirm that the presence of volatile CO_2 and heat is sufficient to promote piercing, in the absence of skin and blood detection by the labium and stylet, respectively (Figure 2.4). Therefore, chemosensory input from the labium is not required to initiate biting or to promote blood-feeding behavior.

While these experiments definitively establish that chemosensory input labium is dispensable for blood-feeding behavior, the data do not prove that chemosensory input

from the stylet is sufficient to promote blood-feeding behavior. Since females require multiple meal components (at minimum, ATP, NaCl, and $NaHCO_3$) to initiate engorgement, the ideal genetic driver for this experiment would label the entire blood-sensitive neuron population in the female stylet and no other neurons in the entire nervous system. However, it remains unknown if there are regulatory elements that could achieve this goal and if so, what their identity may be.

Although *Ir7a* and *Ir7f* are exclusively expressed in the female stylet, neither is the ideal driver line because we found each labels a specific subset of blood-sensitive neurons, as opposed to tiling the entire population. Thus, experiments that exogenously activate either population are only informative if activation is sufficient to promote blood-feeding behavior. Nevertheless, we performed chemogenetic experiments by crossing *Ir7a* and *Ir7f* driver lines to the TRPV1 effector strain and adding capsaicin to sub-optimal meals. We found that addition of capsaicin did not promote engorgement in either genotype (Figure 6.4). These results are unsurprising given that even the minimal ATP in saline meal activates multiple subsets of stylet neurons, in addition to *Ir7a*- and *Ir7f*-expressing neurons.

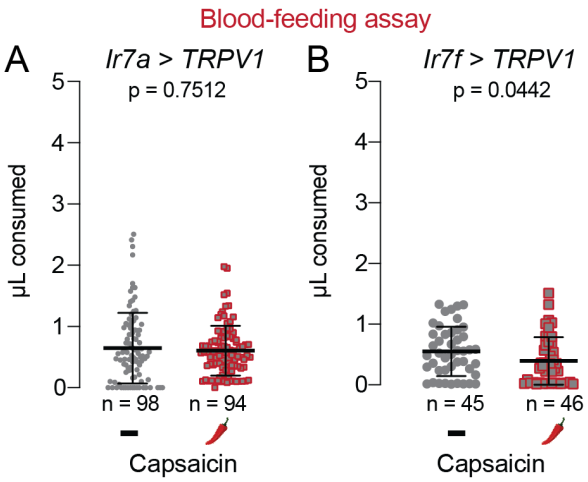

Figure 6.4 Activation of *Ir7a*- and *Ir7f*-expressing neurons is not sufficient to promote blood feeding.

(A,B) Volume of sub-optimal meal consumed by the indicated genotypes. Sub-optimal meal consists of 1 mM ATP in 20 mM $NaHCO_3$, with addition of DMSO vehicle (gray) or 50 µM of capsaicin (gray with red outline). Each data point represents 1 female: *Ir7a>TRPV1* N = 94- 98, *Ir7f>TRPV1* N = 45-46 females/meal (mean ± SD, p values calculated using Mann-Whitney test).

Finally, we looked to take advantage of the fact that capsaicin can be spatially restricted to the meal to exclude activation of many external chemosensory tissues, including the antenna, labium, and legs. However, capsaicin in the meal can still contact neurons in internal mouthparts like the cibarium (Kirti et al., 2015; Lee, 1974), in addition to stylet neurons, as the meal is ingested. To this end we searched for a driver that captured a larger population of blood-sensitive stylet neurons while sparing internal mouthparts. None of the existing driver lines examined in *Ae. aegypti*, including *Brp* and *Ir25a*, permitted selective manipulation of stylet neurons independently of internal mouthpart neurons. Therefore, the neurons sufficient to promote blood feeding remain unknown.

6.3 Sensory input from stylet and labium neurons are segregated at the first synapse

To ask how female stylet neuron projections in the subesophageal zone relate to projections from female labium neurons, we performed a dual dye-fill experiment in which we labelled stylet and labium neurons with different dye colors in the same animal (Figure 6.5A). Female stylet neurons project to the ventral region of the subesophageal zone, anterior to projections from female labium neurons (Figure 6.5B-E). To observe a clear sagittal view of labium and stylet neuron projection patterns, we performed a unilateral labium dye fill in parallel with a bilateral stylet dye fill (Figure 6.5D,E). We did not observe overlapping projection patterns from the two appendages (Figure 6.5C,E). Thus, inputs from the stylet and labium are segregated at the first synapse in the subesophageal zone. In *D. melanogaster*, axons from different sensory appendages like the labellum and internal mouthparts also project to distinct regions in the subesophageal zone (Scott, 2018). It will be interesting to trace the post-synaptic partners of each population to understand how sensory information is relayed to higher brain areas and the extent of segregation between these information streams.

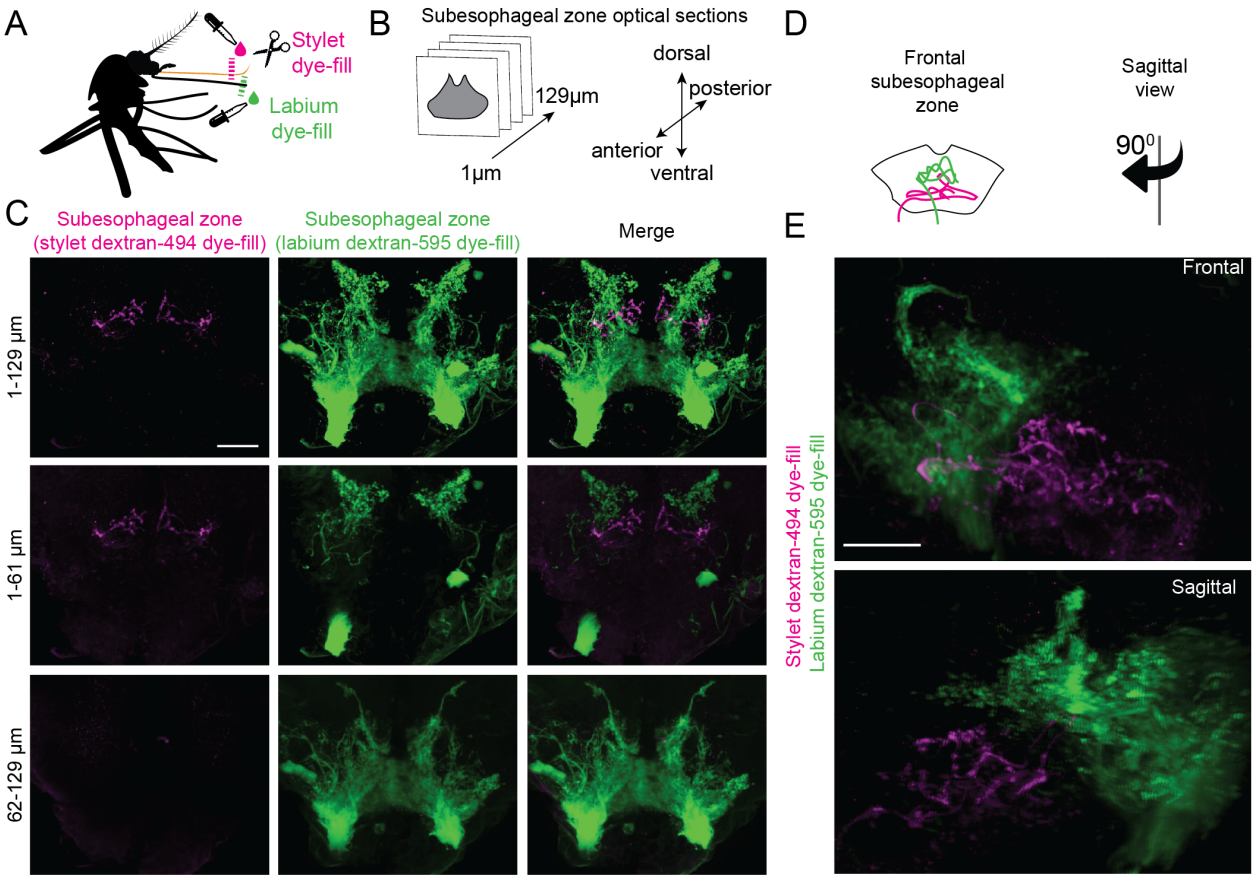

Figure 6.5 Sensory neurons from the stylet and labium project to non-overlapping regions in the subesophageal zone.

(A) Schematic of double dye-fill experiment set-up performed in (C) and (E). (C) and (E) are images collected from independent experiments.
(B) Schematic of subesophageal zone optical sections captured in (C).
(C) Optical subesophageal zone sections from most anterior (top row) to most posterior (bottom row) of stylet (left, magenta) and labium (middle, green) projection pattern revealed by dual dextran-494 and dextran-595 dye-fill.
(D,E) Subesophageal zone after dual dye-fill with bilateral stylet dextran-494 (magenta) and unilateral labium dextran-595 (green). Bottom panel is a 90^{o} optical rotation from the sagittal perspective, as cartooned in (D).
(C,E) Scale bar: 25 µm.

By disentangling structure from chemosensation, we confirmed that an intact stylet and labium is structurally necessary for both feeding programs. Conversely, sensory neurons in the stylet and labium have distinct molecular and functional properties that are specific to their role in blood- and nectar-feeding behavior, respectively. Do these sensory neurons synapse onto parallel downstream circuits that are specialized for all features of either the blood- or nectar-feeding program? At one extreme, activation of stylet or labium neurons could be hard-wired to downstream activation of the circuits that specify meal size and digestive tract destination. An alternate possibility is that activation of the stylet or labium both promote pumping, and subsequent evaluation(s) of meal quality occur downstream to specify how long pumping should last and where the contents are directed. As always, a multitude of intermediate possibilities exist between these two extreme models. The first model is the most parsimonious and aligns best with the current labelled line model described in *D. melanogaster* and rodents. In these model organisms, elegant anatomical and functional studies have shown that circuits mediating recognition of distinct taste qualities remain segregated from sensory input to motor output (Barretto et al., 2015; Harris et al., 2015; Marella et al., 2006; Peng et al., 2015; Thorne et al., 2004; Wang et al., 2004; Zhang et al., 2019). Future studies will uncover how well this model captures mosquito feeding behavior.

It is important to note that model organisms are faced with a choice to feed (ie sweet, appetitive) or not to feed (ie sour or bitter, aversive) (Marella et al., 2006; Peng et al., 2015; Zhang et al., 2019). The mosquito, on the other hand, must choose between two different context-dependent modes of feeding: nectar feeding for metabolic energy

and blood feeding for egg development. Perhaps unsurprisingly, behavior experiments from the mid-1900s suggest the mosquito may be more complicated. There are discrepancies across different papers, but the results hint that altering the ratio of blood and nectar sugars can confuse the female, causing her to misdirect the meal (Bishop and Gilchrist, 1946; Day, 1954; Hosoi, 1959). Since we now know that the stylet cannot detect these nectar sugars, these data implicate a downstream site of evaluation. It will be of great interest to unravel the mechanism that enables the female to maintain two parallel feeding programs.

CHAPTER 7. DISCUSSION

Together the experiments presented in this thesis demonstrate that sexually dimorphic stylet neurons are the first sensory neurons to detect blood as an *Ae. aegypti* female draws a blood meal. Using pan-neuronal calcium imaging, we show that stylet neurons taste multiple blood components to form the percept of blood. We discovered that stylet neurons are specialized to detect blood over nectar, facilitating peripheral discrimination between these two appetizing food sources during blood-feeding.

7.1 Anatomical, Molecular, and Functional Properties of the Stylet

The female stylet is an unconventional sensory organ whose functional properties are poorly understood. The microneedle-like biophysical properties needed to efficiently pierce skin (Choumet et al., 2012; Ramasubramanian et al., 2008) may influence its unique anatomical organization into two single-file rows of cells along each side. Consistent with its role in female-specific blood-feeding behavior, we identified dramatic sexual dimorphism in neuron number and innervation of chemosensory sensilla. The sparse, stylet-specific *Ir7a* and *Ir7f* driver lines allowed us to show that individual neurons send ipsilateral dendrites into one of the two chemosensory sensilla found on each side of the stylet tip. Interestingly, we observed inter-individual differences in blood-sensitive neuron number and cell body position. This variability is in stark contrast to the high degree of stereotypy observed in *D. melanogaster* taste neurons (Scott, 2018; Stocker, 1994). We do not yet understand the mechanism of developmental

patterning that produces variable cell body position along the proximal-distal axis of the stylet. Variability in the exact distance of the cell to the stylet tip may be tolerated because all stylet neuron dendrites terminate at the tip, irrespective of cell body position.

By generating two female stylet-specific driver lines, we identified non-overlapping blood-sensitive neurons belonging to two functionally distinct subsets: *Ir7f* blood mixture-sensitive neurons and *Ir7a* $NaHCO_3$-sensitive neurons. Together, these driver lines mark approximately one quarter of total stylet neurons. Future work will allow us to determine if *Ir7a* and *Ir7f*, along with additional putative chemosensory receptors identified in our stylet RNA-seq dataset, directly contribute to blood ligand detection. This dataset is also an important resource to help identify genetic markers for NaCl- and ATP-sensitive subsets and to resolve the complete molecular landscape of stylet neurons.

A major finding of this work is that four ligands previously shown to increase the probability of initiating blood-feeding behavior do indeed directly activate the stylet. When presented as a mixture, these four blood components—ATP, glucose, $NaHCO_3$, and NaCl—are sufficient to activate the same neurons as blood and initiate blood-feeding behavior. It is surprising that females will so readily engorge on Mix+ATP because it does not contain the proteins required for egg development. Proteins may not serve as an ideal substrate for blood recognition because their amino acid sequences and structures can evolve over time and across species. In contrast, the

chemical structures of ATP, glucose, $NaHCO_3$, and NaCl are invariant across evolutionary time and species.

Our functional imaging shows that roughly half of the 40 stylet neurons can be activated by blood. The remaining stylet neurons may respond to a variety of different ligands, including ligands found only when the stylet contacts an intact capillary microenvironment. For example, once blood is drawn, the concentration of certain volatile or unstable blood components is likely to decrease. There may also be ligands specific to human blood, or circulating factors released from surrounding cells as a damage response to the piercing stylet. These unidentified ligands may be detected in an *in vivo* context, but none appear to be required for blood-feeding behavior or egg development. Another possibility is at least some of the remaining stylet neurons respond to additional taste qualities observed in other feeding appendages. For example, responses to osmolarity, high salt, CO_2, and bitters have been in observed in labellar neurons in *D. melanogaster* (Liman et al., 2014; Yarmolinsky et al., 2009). Bitters are of particular interest because specific bitters added to blood prevent feeding (Dennis et al., 2019). Finally, the stylet could be capable of thermosensation or mechanosensation related to sensing blood flow or tissue penetration. The pan-neuronal stylet imaging preparation we have developed will facilitate future systematic analyses of stylet responses to diverse sensory stimuli.

7.2 Stylet Neurons Integrate Across Taste Qualities to Detect Blood

Our work shows that the taste of blood is multidimensional and that blood-sensitive neurons can be divided into functionally distinct subtypes, each activated by a behaviorally-relevant concentration of a ligand, or mix of ligands, found in blood. Glucose and NaCl are associated with the distinct taste qualities of sweet and salty, but it is unclear if $NaHCO_3$ or ATP overlap with a canonical taste quality. In blood, $NaHCO_3$ is buffered at pH 7.4 and predominately present as HCO_3-, with 10% or less present as CO_2 (Centor, 1990). While CO_2 contributes to sour taste and encodes the taste of carbonation (Chandrashekar et al., 2009; Fischler et al., 2007; Sanchez-Alcaniz et al., 2018), HCO_3- has not yet been assigned to a defined taste quality. Similarly, there is no description of the taste of ATP. The closest comparison to ATP detection is in mammals, where specific 5'-monophosphate nucleotides potentiate umami perception (Yamaguchi, 1967) and in *D. melanogaster* larvae, where certain ribonucleosides directly activate *Dmel_Gr28*-expressing taste neurons (Mishra et al., 2018).

These distinct taste qualities, both canonical and noncanonical, are integrated across subsets of blood-sensitive neurons and for the particular subset of Integrator neurons, within individual neurons. In the Integrator subset, neurons are maximally activated by co-presentation of glucose, NaCl, and $NaHCO_3$. Simultaneous detection of sweet, salty, and $NaHCO_3$ in one neuron is unexpected because distinct taste qualities are thought to activate non-overlapping sensory neuron populations in both mammals and insects (Yarmolinsky et al., 2009). Yet here we only detect responses to

physiological levels of blood glucose (4.5 mM) in the presence of NaCl or $NaHCO_3$. We speculate that polymodal Integrator neurons act as coincidence detectors and that 4.5 mM glucose alone produces subthreshold responses without the co-presentation of NaCl and/or $NaHCO_3$. Since glucose is a redundant cue in blood and nectar, this unconventional taste coding mechanism confers an important distinction between glucose present in blood versus nectar.

Does taste quality integration occur downstream of distinct blood-sensitive neuronal subsets to form the neural representation of blood? We found that behaviorally-relevant concentrations of ATP, $NaHCO_3$, and NaCl were individually sufficient to activate a subset of stylet neurons. However, any individual component was unable to trigger blood-feeding behavior or activate all blood-sensitive stylet neurons. Consistent with these observations, we found that activation of either *Ir7a*- and *Ir7f*-expressing subpopulations alone using the TRPV1 chemogenetic system did not promote engorgement. We speculate that activation of multiple neuronal subtypes in response to whole blood may be required to promote blood-feeding behavior, similar to how detection of multiple host cues is required to promote host-seeking behavior (Liu and Vosshall, 2019; McMeniman et al., 2014). We propose that activation of multiple stylet neuron subsets is required to initiate blood feeding to decrease the possibility that a female accidentally engorges on nectar instead of blood. For instance, 298 mM glucose occasionally activated blood-sensitive neurons, but females still rejected this meal in the blood-feeding assay.

Prior to tasting blood, females must seek out a host. A previous study showed integration across sensory modalities like olfaction and thermosensation is critical to attract females to a blood source (McMeniman et al., 2014). Our biteOscope experiments further clarify that co-presentation of heat and CO_2 specifically results in piercing, but not engorgement (Hol et al., 2020). Taken together, these results demonstrate that *Ae. aegypti* employ multimodal integration across various scales: within individual neurons, across taste qualities, and across sensory modalities. We speculate that integration increases flexibility and specificity in the complex task of locating a suitable blood meal.

7.3 The Stylet is Specialized to Detect Blood Over Nectar

The needle-like anatomy of the stylet is ideally adapted for blood feeding (Choumet et al., 2012; Ramasubramanian et al., 2008) and we discovered that its molecular and functional properties directly encode a distinction between blood and nectar. Stylet neurons are insensitive to nectar-specific sugars and only respond to glucose in the presence of additional blood components. We propose that specialization of peripheral sensory neurons in the stylet may explain why sugars do not promote nectar feeding in the context of blood feeding. This mechanism is distinct from previously described examples of food source valence changes upon nutrient deprivation or mating in *D. melanogaster*, which typically involve a state-change that modulates the sensitivity of sensory neurons, and/or their downstream processing, to a given ligand (Devineni et al., 2019; Inagaki et al., 2012; Steck et al., 2018; Walker et al., 2015). One key difference

between *D. melanogaster* and *Ae. aegypti* feeding is that *Ae. aegypti* have two distinct feeding appendages. We speculate that feeding appendage segregation and specialization is a mechanism to ensure that the female ingests blood and not nectar in the context of blood feeding.

7.4 Future Directions

Which receptors and neurons mediate blood-feeding behavior?

A natural extension of our work is to determine whether activation of blood-sensitive neurons in the stylet is sufficient and necessary to trigger blood-feeding behavior. While stylet neurons are the first and only external sensory neuron population to directly contact blood, they may not be the only sensory neurons capable of detecting blood. Since activation of external sweet taste neurons was sufficient to promote nectar-feeding behavior, it is plausible that activation of all blood-sensitive stylet neurons will be sufficient to promote blood-feeding behavior. Necessity, however, is a trickier question. If the extensive taste research in *D. melanogaster* is an instructive model, multiple internal sensory neuron populations may detect blood after pumping is initiated. In *D. melanogaster,* internal pharyngeal sweet gustatory neurons can sustain sugar ingestion in *poxn* mutants that lack all external sweet taste sensation from labellar taste bristles (LeDue et al., 2015). Although the external labellar neurons are not required for sweet taste, they are the first mouthpart sensory neurons to directly contact the meal prior to ingestion and are integral to understanding natural feeding behavior in *D.*

melanogaster. A complete understanding of blood detection will require identification of all sensory neuron populations that detect blood and regulate blood-feeding behavior in *Ae. aegypti*. Future studies will determine if blood detection by stylet neurons is necessary and sufficient for blood-feeding behavior.

The receptors that directly detect blood ligands remain unknown. We identified two members of the *IR* sensory receptor family, *Ir7a* and *Ir7f,* that are expressed in blood-sensitive neurons. It is tempting to speculate that *Ir7a* is involved in $NaHCO_3$ detection because all *Ir7a*-expressing neurons responded to $NaHCO_3$, and the number of *Ir7a*-expressing neurons correlates with the number of $NaHCO_3$-responsive neurons identified in our pan-neuronal imaging experiments. The driver lines and mutants needed to test this hypothesis were generated throughout the course of our study and will facilitate an exciting future direction. A parallel set of reagents exists for *Ir7f,* but the role of *Ir7f* is less clear because only a subset of *Ir7f*-expressing neurons shared a functional profile with Integrator neurons.

What is the molecular mechanism of glucose detection and integration in polymodal stylet neurons, given that no canonical sweet taste receptors are detected in the stylet? It remains unknown if one receptor can directly integrate the chemically distinct ligands of sodium bicarbonate, glucose, and sodium chloride, or if the neuron integrates activity from multiple independent receptors. Although we found no canonical sweet gustatory receptor expression in the stylet, the stylet does express *Gr34*, an orthologue of *D. melanogaster Gr43a* (Matthews et al., 2018). *D. melanogaster Gr43a* does not share

sequence homology with the sweet taste subfamily and is the only gustatory receptor also expressed in the brain, where it acts as a metabolic sensor of circulating fructose (Miyamoto et al., 2012). *Gr34* may be repurposed as a glucose receptor in the stylet or there may be an unconventional receptor for glucose in these neurons. Since *Ir7f*-expressing neurons intersect with the Integrator neuron subset, their molecular profile may help uncover this mechanism of taste quality integration.

For decades researchers have pursued the receptor(s) that enable *Ae. aegypti* to detect ATP (Burnstock and Verkhratsky, 2009; Galun, 1987). In addition to the entomologists who are fascinated by ATP's potent phagostimulatory effect when it is co-presented with additional plasma components (Galun, 1987), evolutionary biologists have long queried why purinergic signaling is notably absent from key phyla like arthropods (Burnstock and Verkhratsky, 2009; Fountain, 2013). Using bioinformatics and BLAST, we were not able to find any clear orthologues to P2X receptors in the *Ae. aegypti* genome (Matthews et al., 2018). Although P2X receptors have been identified in diverse species such as algae, ticks, and vertebrates (Bavan et al., 2011; Fountain, 2013), clear orthologs are notably absent in *D. melanogaster* and *C. elegans* (Burnstock and Verkhratsky, 2009; Lima and Miesenbock, 2005) (Appendix A). Therefore, the receptor used by *Ae. aegypti* mosquitoes to detect ATP remains to be identified.

How does blood detection trigger blood-feeding behavior?

How is information from the network of blood-sensitive neurons integrated to form the perception of blood? Experiments in *D. melanogaster* and mice found that

information from each of the canonical taste qualities remains segregated as each population projects to discrete regions in central taste-processing centers and activate different higher order neuronal populations (Barretto et al., 2015; Harris et al., 2015; Marella et al., 2006; Peng et al., 2015; Thorne et al., 2004; Wang et al., 2004; Zhang et al., 2019). Based on this model, one would expect information from $NaHCO_3$, ATP, NaCl, and Integrator stylet neuron subsets to be processed by more than one labelled line since these blood components are associated with multiple taste qualities. However, another possibility is that information from blood-related cues is channeled into one cohesive labelled line that represents blood as a unified taste quality. Future work will shed light on this question through anatomical comparisons of projections from individual stylet subsets and functional analysis of the downstream synaptic partners. It will be interesting to see if and when signals from blood-sensitive subpopulations converge, and if the one or multiple blood-processing streams are segregated from other subpopulations of stylet sensory neurons that do not respond to blood. Finally, if there are additional blood-sensitive populations in the internal mouthparts, does input from these neurons also converge on the same region?

Once ingestion begins, which neuronal mechanisms determine the meal size and destination associated with each feeding program? In *D. melanogaster*, sensory information is relayed to various higher order neuronal populations inside and outside of the subesophageal zone (Scott, 2018). The populations identified thus far are taste quality-specific and are thought to ultimately communicate with subesophageal zone motor neuron populations that control pumping and ingestion (McKellar, 2016; Scott,

2018; Yapici et al., 2016). Here we show that sensory neurons from the stylet and labium project to distinct subesophageal zone regions. Does sensory input from the stylet and labium remain segregated as specialized blood-feeding and nectar-feeding circuits? Detection of blood by the stylet could be hardwired to dedicated sensory processing pathways, motor neurons, and muscles that control blood meal size and destination. Information about blood and nectar could also eventually converge onto overlapping neurons and activate motor neurons that initiate pumping. In this case, additional downstream input would be required to specify the appropriate meal size and digestive organ destination. The ability to implement circuit tracing techniques (Fosque et al., 2015; Matthews et al., 2019; Ruta et al., 2010; Talay et al., 2017) in *Ae. aegypti* will enable future studies of downstream central and peripheral circuits.

Is blood recognition conserved across blood-feeding mosquitoes?

Blood detection is an important step for *Ae. aegypti* mosquitoes to transmit diseases like Zika and dengue because they acquire these flaviviruses by ingesting a blood meal from an infected person (Ruckert and Ebel, 2018). However, *Ae. aegypti* and the *Aedes* genus are one of many mosquito species and genera that feed on blood to obtain protein. *Anopheles* and *Culex* also rely on blood for egg development and have evolved an ability to transmit diseases like malaria and West Nile virus, respectively. Therefore, a global understanding of how multiple mosquito species detect blood to initiate blood-feeding behavior is critical for describing the basis of mosquito-borne disease transmission.

Galun and colleagues pioneered research to determine the behavioral requirements to initiate blood-feeding behavior and found variation across species belonging to each genus (Galun, 1987; Galun et al., 1963; Galun et al., 1988; Galun et al., 1985a; Galun et al., 1985b; Galun et al., 1984). While a mixture of ATP, NaCl, and $NaHCO_3$ is sufficient to promote engorgement in *Ae. aegypti*, there is a sharp decrease in engorgement rates if ATP is substituted for ADP or AMP (Galun et al., 1985b). For *Culex pipiens*, however, ATP, ADP, and AMP are all sufficient for engorgement when co-presented with NaCl and $NaHCO_3$ (Galun et al., 1988). Yet *An. gambiae* only require a solution of NaCl to initiate engorgement, and addition of ATP does not increase the percentage of females engorging on the meal (Galun et al., 1985a). Although mosquito species differ in the minimum blood components required to initiate blood feeding (Galun, 1987), blood detection via stylet neurons may be a conserved mechanism across blood-feeding mosquito species. An exhaustive electron microscopy analysis across 40 mosquito species belonging to 15 genera revealed that sexual dimorphism in stylet sensilla is conserved across blood-feeding species (Lee and Craig, 1983). All males examined lack the chemosensory sensilla that we found to be innervated by blood-sensitive neurons. Furthermore, these female-specific chemosensory sensilla are absent in non-blood-feeding *Toxorhynchites* species (Lee and Craig, 1983). These results intimate a close association between the presence of stylet chemosensory sensilla and blood-feeding behavior.

These classic experiments open up several interesting lines of questioning regarding the neural mechanisms that underly the difference in behavioral requirements. For example, which mechanisms underly the difference in behavioral requirements? Have *Ae. aegypti* and *Cx. pipiens* evolved independent molecular mechanisms to detect adenine nucleotides? It is unclear if *An. gambiae* simply cannot detect additional blood components, or if multiple blood components can be detected but are not required to promote blood-feeding behavior. If all blood-feeding females utilize chemosensory stylet neurons to evaluate blood prior to blood-feeding behavior, is the tuning of functionally distinct stylet neuron subsets across taste qualities conserved at the functional level? Even if stylet neuron subsets are tuned to the same taste qualities as *Ae. aegypti*, unique molecular markers or receptors may have evolved to define the subset and/or detect the same ligand.

If blood detection is not distributed across functionally distinct subtypes, how would these differences in stylet neuron tuning alter downstream processing to produce the perception of blood? It is surprising that *An. gambiae* does not require coincident detection of multiple blood components to initiate blood-feeding. Could less stringent evaluation of meal quality imply that *An. gambiae* is more discerning when evaluating volatile cues from the host? Or does *An. gambiae* have less specific metabolic requirements that reduce the need to evaluate blood meal quality? Finally, it remains unknown if other species have evolved distinctive mechanisms to discriminate between blood and nectar. Segregation of sweet taste receptor expression may be conserved across blood-feeding mosquitoes, but polymodal taste quality integration may be

irrelevant to a species like *An. gambiae* if blood glucose is not detected by blood-sensitive neurons.

We have developed immunofluorescence, molecular, functional imaging, and behavior techniques that provide a foundation to study the stylet and blood-feeding behavior across mosquito species. Extending the genetic toolkit and transgenic methods we established to other species will also facilitate additional comparative analyses. Ultimately, an understanding of blood detection is fundamental to prevent mosquito blood-feeding behavior, which is responsible for transmission of vector-borne diseases to hundreds of millions of people world-wide each year.

Does polymodal integration contribute to sensory perception?

The discovery of polymodal integrator neurons in the taste system was unexpected because individual taste qualities are thought to be detected by non-overlapping populations of sensory neurons (Liman et al., 2014; Yarmolinsky et al., 2009). It is important to note that Integrator neurons are not the first example of an individual sensory neuron class detecting multiple ligands. In *C. elegans*, for example, ASH sensory neurons respond to tactile stimuli, osmotic strength, and volatile chemosensory ligands to promote avoidance behavior (Bargmann and Kaplan, 1998; Kaplan and Horvitz, 1993). Polymodal C-fiber nociceptors, which can respond to diverse thermal, mechanical, and chemical noxious stimuli, have also been described in mammalian systems (Julius and Basbaum, 2001; Patapoutian et al., 2009).

However, one key difference between these examples and stylet Integrator neurons is found in how these neurons respond to individual ligands. The sensory neuron classes described in the literature are promiscuous and can be activated by presentation of an individual ligand (Bargmann and Kaplan, 1998; Julius and Basbaum, 2001; Kaplan and Horvitz, 1993; Patapoutian et al., 2009). While co-presentation could alter neuronal activity, it is not required to reach the threshold of activation. In contrast, stylet Integrator neurons were not reliably activated by presentation of any individual ligand. Co-presentation of any two ligands was sufficient to cross the activation threshold, with the maximal response occurring with co-presentation of all three ligands.

It will be of great interest to determine if this coding strategy is used more broadly by the mosquito and other species to assign an additional level of information to taste or other sensory modalities. Of note, much of the current taste literature has been conducted in model organisms and has focused on processing separate taste qualities as opposed to complex mixtures. Investigation of specialist species, who have extraordinary behavioral adaptations to maximize nutrient acquisition from particular food sources, may reveal additional examples of polymodal integration or entirely novel taste coding strategies. Finally, we speculate that further exploration of physiologically relevant mixtures that incorporate non-canonical taste qualities may provide new insight into the subtilties and complexities of taste coding across both generalists and specialists.

CHAPTER 8. METHODS

RESOURCE AVAILABILITY

Materials Availability

All plasmids described in this thesis are available at Addgene. Genetically modified mosquitoes are available upon request to Leslie Vosshall (leslie@rockefeller.edu).

Data and Code Availability

All data are available on Github at https://github.com/VosshallLab/Jove_Vosshall_2020. Sequencing reads have been deposited at the NCBI Sequence Read Archive (SRA) under BioProject PRJNA605870. Custom Python code for biteOscope data analysis is available on Github at https://github.com/felixhol/biteOscope. Custom R scripts for merged genome annotation and calcium imaging analysis are available on Github at https://github.com/VosshallLab/Jove_Vosshall_2020.

EXPERIMENTAL MODEL AND SUBJECT DETAILS

Human and Animal Ethics Statement

Blood-feeding procedures with live mouse and human hosts were approved and monitored by The Rockefeller University Institutional Animal Care and Use Committee

(IACUC protocol 17108) and Institutional Review Board (IRB protocol LV-0652), respectively. Human subjects gave their written informed consent to participate.

Mosquito Rearing and Maintenance

Ae. aegypti wild-type and genetically-modified strains were maintained and reared at 25 - 28^{o}C, 70–80% relative humidity with a photoperiod of 14 hours light: 10 hours dark (lights on at 7 a.m.) as previously described (DeGennaro et al., 2013). Adult females were blood-fed on mice for stock maintenance, and occasionally on human subjects in the early stages of generating genetically modified strains. Approximately the same number of female and male pupae were placed in one cage prior to eclosion. Adults were allowed to mate freely for at least 7 days prior to performing experiments. Adult mosquitoes were provided constant access to 10% sucrose. 14 – 24 hours prior to behavioral experiments, mosquitoes were briefly anesthetized at 4^{o}C and females were sorted into groups of 15-20 females and were placed into a 32 oz. HDPE plastic cup (VWR #89009-668). Upon returning to the insectary, females were fasted by replacing 10% sucrose with a water source. All behavior experiments were carried between ZT6 and ZT13 and ended before the lights off time based on the photoperiod.

METHOD DETAILS

Generation of Genetically-Modified Mosquito Strains

All CRISPR-Cas9 and transgene injections followed previously established methods (Kistler et al., 2015; Matthews et al., 2019) and were carried out at the Insect Transformation Facility (ITF) at the University of Maryland Institute for Bioscience & Biotechnology Research.

All new strains generated in this paper were generated in the Vosshall Lab using the wild-type Liverpool strain of *Ae. aegypti*. *Brp-QF2w* was generated in the McBride Lab using the wild-type Orlando strain of *Ae. aegypti* (Zhao et al., 2020). We back-crossed *Brp-QF2w* to wild-type Liverpool for at least 4 generations before crossing to *QUAS-dTomato-T2A-GCaMP6s*, which was generated in the Liverpool background.

For instances where a transgene was integrated into the genome using homologous recombination, proper payload integration was confirmed using polymerase chain reaction (PCR). Animals were then back-crossed to wild-type Liverpool for at least three generations before crossing to corresponding QF2 or QUAS for experimental use. Details of plasmid construction are below. All homology arms for homology-directed integration were isolated by PCR from genomic DNA isolated from the Liverpool strain, except for *Brp-QF2w*, which was derived from the Orlando strain. When Gibson assembly was utilized in plasmid construction, oligonucleotide sequences are displayed

in lower case to indicate homology to the adjacent fragment and upper case to indicate the target sequence.

For instances of a gene-disrupting insertion/deletion at a specific locus, a frame-shift mutation was confirmed using PCR and Sanger DNA sequencing (Genewiz). Mutants were then back-crossed to wild-type Liverpool for 3 total generations before inbred to generate a stable homozygous mutant line.

3xP3-eYFP-SV40-15xQUAS-dTomato-T2A-TRPV1-SV40 (Addgene plasmid#140945)

This plasmid was generated using NEBuilder HiFi DNA Assembly (New England Biolabs #E5520S), using the following fragments generated by PCR from the indicated template with the indicated primers:

[1] Plasmid backbone with pBAC arms from *15xQUAS-dTomato-T2A-GCaMP6s* (Addgene plasmid #130666) (Matthews et al., 2019) (Primers: Forward, 5'-GATCTTTGTGAAGGAACCTTACTTCTGTGGTGTG-3'; Reverse, 5'-ATCCCCCGGGCTGCAGGA-3')

[2] *QUAS-dTomato-T2A* from *15xQUAS-dTomato-T2A-GCaMP6s* (Primers: Forward, 5'-tcaatgtatcttaACTAGAGCGGCCGCCACC-3'; Reverse, 5'-cccgttgttccatAGGGCCGGGATTCTCCTC-3')

[3] *3xP3-eYFP-SV40* with YFP open reading frame from Addgene plasmid #62291 (Primers: Forward,

5’-atcgaattcctgcagcccgggggatGTTCCCACAATGGTTAATTC-3’; Reverse, 5’-ggccgctctagtTAAGATACATTGATGAGTTTGG-3’).

[4] *Rattus norvegicus* TRPV1 (Genbank accession NM_031982.1) from *ASH:TRPV1* (Bargmann Lab plasmid #10.33.42, with permission from Dr. David Julius of UCSF) (Tobin et al., 2002)(Primers: Forward, 5’-aatcccggccctATGGAACAACGGGCTAGC-3’; Reverse, 5’-gaagtaaggttccttcacaaagatcACCCAGATAACGTCAACC-3’).

200 embryos were injected with 200 ng/μL plasmid and 200 ng/μL pBAC mRNA. Two independent transgenic lines were recovered, one of which was sex-linked. In pilot experiments, both lines showed qualitatively similar behavioral effects in the *Gr4>TRPV1* capsaicin experiments. All subsequent behavior and expression pattern experiments were performed using the non-sex-linked line.

Gr4, Ir7a, and Ir7f QF2 strains

These knock-in/knock-out strains were generated through CRISPR-mediated homologous recombination of the QF2 transcription factor (Matthews et al., 2019; Potter et al., 2010; Riabinina et al., 2016) into the endogenous locus of the *Ae. aegypti* genome. *In vitro* transcription was performed using HiScribe Quick T7 kit (New England Biolabs #E2050S) following the manufacturer’s directions and incubating for 3 hr at 37°C. Following transcription and DNAse treatment for 15 min at 37°C, sgRNA was purified using RNAse-free SPRI beads (Ampure RNAclean, Beckman-Coulter #A63987), and eluted in Ultrapure water (Invitrogen #10977–015). For each line, 2000 embryos were injected with 600 ng/μL plasmid, 300 ng/μL Cas9 protein, and 40 ng/μL

sgRNA. sgRNA DNA template was prepared by annealing oligonucleotides as previously described (Kistler et al., 2015). For all plasmids, fragments were generated by PCR from the indicated template with the indicated primers and assembled using NEBuilder HiFi DNA Assembly as detailed below.

Gr4-T2A-QF2 -SV40-3xP3-dsRed (Addgene plasmid#140944)

[1] Plasmid backbone from pUC19 (Primers: Forward, 5'-CTAGAGTCGACCTGCAGGC -3'; Reverse, 5'- CCCGGGTACCGAGCTCGA -3').

[2] *Gr4* left homology arm (NCBI LOC5563657) (Primers: Forward, 5'-agtgaattcgagctcggtacccgggACTCTCCTAAAATCTCAAGTATAC-3'; Reverse, 5'-tctgccctctccTGCACGTTTGGGATACTTG-3').

[3] *Gr4* right homology arm (NCBI LOC5563657) (Primers: Forward, 5'-caatgtatcttaCAGGGAAAACTGGATCCATG-3'; Reverse, 5'-ttgcatgcctgcaggtcgactctagGTGTATTTGGAGCCTCAG-3').

[4] *T2A- QF2-SV40-3xP3-dsRed* with QF2 and dsRed open reading frame from *ppk301-T2A-QF2* (Addgene plasmid #130667) (Matthews et al., 2019) (Primers: Forward, 5'- tcccaaacgtgcaGGAGAGGGCAGAGGAAGTC-3'; Reverse, 5'-ccagttttccctgTAAGATACATTGATGAGTTTGGACAAAC-3). The sgRNA targeted exon 2 of the *Gr4* locus, target sequence with protospacer adjacent motif (PAM) underlined: GTATCCCAAACGTGCAACCAGGG.

Ir7a-T2A-QF2 -SV40-3xP3-dsRed (Addgene plasmid#140943)

[1] Plasmid backbone from pUC19 (Primers: Forward, 5'-cgatcaactataaCTAGAGTCGACCTGCAGGC -3'; Reverse, 5'-aatttgctttttaCCCGGGTACCGAGCTCGA-3'.

[2] *Ir7a* left homology arm (Primers: Forward, 5'-cggtacccgggTAAAAAGCAAATTTCACCATG-3'; Reverse, 5'-tctgccctctccATATACGTGACCCCAAATATC-3').

[3] *Ir7a* right homology arm (Primers: Forward, 5'-caatgtatcttaATCCAGAACGGGTGCGGTAG-3'; Reverse, 5'-ggtcgactctagTTATAGTTGATCGAGGAATTTCCGAATCC-3').

[4] T2A- QF2-SV40-3xP3-dsRed with QF2 and dsRed open reading frame from *ppk301-T2A-QF2* (Addgene plasmid #130667) (Matthews et al., 2019) (Primers: Forward, 5'- gggtcacgtatatGGAGAGGGCAGAGGAAGTC-3'; Reverse, 5'-acccgttctggatTAAGATACATTGATGAGTTTGGACAAAC-3'). The sgRNA targeted exon 1 of the *Ir7a* locus, target sequence with PAM underlined: TGGGGTCACGTATATCCAAATGG.

Ir7a was not annotated in the AaegL5 NCBI RefSeq Annotation version 101 (Matthews et al., 2018). Genomic coordinates (NC_035107.1:37734383-37736188; FASTA file available on GitHub) were identified using the manual chemoreceptor annotation (Matthews et al., 2018). See the "Transcript abundance and differential expression analysis" section below for additional annotation information.

Ir7f-T2A-QF2 -SV40-3xP3-dsRed (Addgene plasmid#140942)

[1] Plasmid backbone from pUC19 (Primers: Forward, 5'-attttgaggcgggCTAGAGTCGACCTGCAGGC-3'; Reverse, 5'-aatcagccagtcaCCCGGGTACCGAGCTCGA-3').

[2] *Ir7f* left homology arm (NCBI LOC5565007) (Primers: Forward, 5'-ctcggtacccgggTGACTGGCTGATTAGCTCATCCTATATAAGAA-3'; Reverse, 5'-ctctgccctctccACGCTCGCCACGCATCGAGAAACACCCGG-3').

[3] *Ir7f* right homology arm (NCBI LOC5565007) Primers: Forward, 5'-tcaatgtatcttaTGTCGGTGATGAGGTCCAG -3'; Reverse, 5'-aggtcgactctagCCCGCCTCAAAATGTGCAC-3').

[4] T2A- QF2-SV40-3xP3-dsRed with QF2 and dsRed open reading frame from ppk301-T2A-QF2 (Addgene plasmid #130667) (Matthews et al., 2019) (Primers: Forward, 5'-gcgtggcgagcgtGGAGAGGGCAGAGGAAGTC-3'; Reverse, 5'-ctcatcaccgacaTAAGATACATTGATGAGTTTGGACAAAC-3'). The sgRNA targeted exon 1 of the *Ir7f* locus, target sequence with PAM underlined: GATGCGCGGTGAACGCATGTCGG.

Brp-QF2w strain

This knock-in strain was generated in the McBride Lab (Zhao et al., 2020) in the wild-type Orlando strain background using CRISPR-mediated homologous recombination of the QF2w transcription factor (Riabinina et al., 2015) into the endogenous *bruchpilot* locus (NCBI LOC5570381) of the *Ae. aegypti* genome.

Ir7a$^{-/-}$ and Ir7f$^{-/-}$ loss-of-function strains

These mutant strains were generated using CRISPR-Cas9 as described previously (Kistler et al., 2015) except that 4 sgRNA (instead of 2) were targeted to Exon 1 in *Ir7a* or *Ir7f,* respectively, to increase the probability of cutting. *In vitro* transcription was performed using HiScribe Quick T7 kit (New England Biolabs #E2050S) following the manufacturer's directions and incubating for 3 hr at 37°C. Following transcription and DNAse treatment for 15 min at 37°C, sgRNA was purified using RNAse-free SPRI beads (Ampure RNAclean, Beckman-Coulter #A63987), and eluted in Ultrapure water (Invitrogen #10977–015). For each line, 400 embryos were injected with 200 ng/μL ssODN, 4x 40 ng/μL sgRNA, and 300 ng/μL Cas9. Although a ssODN was injected into both strains, the recovered loss-of-function strains did not have successful integration. Both strains contain a frame-shift deletion.

Ir7a$^{-/-}$ 70 base pair frame-shift

[1] ssODN:

TTGAAGACAGAAAAAGGCGGCTGGTTCTTCGGGGAGTCGAAGGAGATATGCTG
ACGATCATTTCAAGAAGAATGAACTTCTCGATTTAGGTTAGAGTTCCCACGGGT
GAAGATATTTGGGGTCACGTATATCCAGTCATGGCTAATTAATTAAGCTGTTGTA
GCGGTGGTTGTCGGTACGGCATACTTAGTTATACTCATATTCAGTTGTCCGCTA
ATGGGGTACTTCAACCATTCTCCAGCATTGACTCTGTATCGGACAACTATTGGG
GATTCCCTCCCATCACTTCCAACAGGAAACTT

[2] All sgRNA targeted exon 1 of the *Ir7a* locus, target sequences with PAM underlined:

CACCCGTGGGAACTCTAACCTGG

TGGGGTCACGTATATCCAAATGG

GATTTGGATAGGCATGGCGGTGG

ACTCATATTCAGTTGTCCGCTGG

[3] PCR primers for Sanger DNA sequencing and genotyping:

Forward, 5'- GAGATATGCTGACGATCATTTCAAG-3'; Reverse, 5'-TAGAACATTTGTAGCTCTCCCTTAT-3'.

To control for genetic background, *Ir7a*$^{+/-}$ females were mated to *Ir7a*$^{+/-}$ males to generate animals for the behavior experiments in Figure 4.8A. This allowed *Ir7a*$^{+/-}$ females to be directly compared to *Ir7a*$^{-/-}$ females. All animals were genotyped after behavior experiments so that the experimenter was blind to genotype during the experiment.

Ir7f$^{-/-}$ *260 base pair frame-shift mutation*

[1] ssODN:

CACTCCAGCGCCAGCCAACGTGTACAATTTCACCATCATCCAGGTGACAGCAC

TAAACGGTCGGAACATCTTCTCGAACGCCGTGTAGGGCCTTCCCTAATAAGGA

TCCATAACCTAAGGTACGTGAAGTTCAGCTCCGAGGAAATCATGTTCAGCATGT

CGCCTTCTATTTTACGTAGTCTTCGGCGACCTCCAATCCA

[2] All sgRNA targeted exon 1 of the *Ir7f* locus, target sequences with PAM underlined:

AGCGCCAGCCAACGTGTACAAGG

GCCGTGTAGGGCCTTCCCGGTGG

GGAGCTGAACTTCACGTACGAGG

GGAGGTCGCCGAAGACTACGTGG

[3] PCR primers for Sanger DNA sequencing and genotyping:

Forward, 5'-ATA CGT TGA ACA TCA CTG TGA ACA T-3'; Reverse, 5'-AGCCAACGTGTACAAGGTC-3'

To control for genetic background, *Ir7f*$^{+/-}$ females were mated to *Ir7f*$^{+/-}$ males to generate animals for the behavior experiments in Figure 4.8B. This allowed *Ir7f*$^{+/-}$ females to be directly compared to *Ir7f*$^{-/-}$ females. All animals were genotyped after behavior experiments so that the experimenter was blind to genotype during the experiment.

Ligands for Feeding Experiments

Sheep blood: (Hemostat Laboratories #DSB100) was used within 1 week of arrival.

Nucleotides: ATP (Adenosine 5′-triphosphate disodium salt hydrate, Sigma #A6419), AMP-PNP (b,g-imidoadenosine 5'-triphosphate lithium salt hydrate, Millipore Sigma #10102547001), AMP-CPP (α,b-methyleneadenosine 5'-triphosphate lithium salt, Jena Bioscience #NU-421-25), AMP-PCP (β,γ-Methyleneadenosine 5′-triphosphate disodium salt, Millipore Sigma #M7510). ATP and non-hydrolyzable analogues were reconstituted and aliquoted in 25 mM $NaHCO_3$.

Sugars: sucrose (Fisher Scientific #S5-3), cellobiose [D-(+)-cellobiose, Millipore Sigma #22150], fructose [D-(-)-Fructose, Millipore Sigma #F0127], glucose [D-(+)-Glucose, Millipore Sigma #G7528].

Additional blood components: NaCl (Millipore Sigma #S6546), $NaHCO_3$ (Fisher Scientific #S233), albumin (human serum, Millipore Sigma #A9511), hemoglobin (human, Millipore Sigma #G4386), gamma-globulin (human blood, Millipore Sigma, #H7379).

Capsaicin: (E)-capsaicin (Tocris #0462)

Blood-Feeding Assay (Glytube)

7 to 21 day-old female mosquitoes were anesthetized at 4^{o}C and sorted into groups of 15-20 females, and placed into a 32 oz. HDPE plastic cup (VWR #89009-668). The cup was prepared by cutting a 10 cm hole in the lid with a razor blade, covering the cup

with a 20 cm x 20 cm piece of white 0.8 mm polyester mosquito netting (American Home & Habit Inc. #F03A-PONO-MOSQ-M008-ZS) and securing the mesh to the cup by snapping on the modified lid. Animals recovered overnight at 25 - 28^{o}C, 70–80% relative humidity with access to water. The assay chamber was a modification of previously published methods (McMeniman et al., 2014) and used a translucent polypropylene storage box 36 cm L x 31 cm W x 32 cm H with a removable lid. One 1.5 cm hole was made on the chamber wall and was used to introduce silicone tubing for CO_2 delivery. The CO_2 diffusion pad (8.9 cm x 12.7 cm; Tritech Research) was affixed to the inner center of the lid to allow delivery of purified air and CO_2 to condition the chamber atmosphere during the trial. Up to 4 cups were placed in the chamber per trial and feeding positions were randomized according to meal during assays. Females were fed sheep blood or test ligands using Glytube membrane feeders exactly as described (Costa-da-Silva et al., 2013), except the Parafilm feeding surface was not rubbed on human skin prior to offering the Glytube to mosquitoes to avoid introducing contact chemosensory cues as secondary stimuli in our experiments. In Figure 2.2, 2.3, 2.4, and Figure 4.8, the saline meal contained 110 mM NaCl and 20 mM $NaHCO_3$. All meals and Glytubes were preheated for at least 15 min in a 45^{o}C water bath and, if required, ATP or non-hydrolyzable ATP analogues were added to meals immediately before feeding and mixed by vortexing. At the start of each trial, cups were placed in the assay chamber and allowed to acclimate for 5 min before 1 Glytube containing 1.5 mL of a given meal was placed on top each cup and CO_2 was turned on for 15 min. In Figure 2.2C, Figure 2.3A,C,E, and Figure3.4A,B, fed females were scored by eye for engorgement of the abdomen. In the rare cases that females partially fed they were

counted as non-fed and discarded. To sample the weights of these females (Figure 2.2B and Figure 2.3B,D,E), a selection of engorged individuals was weighed in groups of 5 females and the resulting weight in mg was divided by 5 to report the average weight per female.

In Figure 2.1E and Figure 5.2B, Glytube feeding was performed as described, except that fluorescein (Amresco #0681) was added as a fluorescent tracer to each meal (blood, sucrose, fructose, glucose, or water) at a final concentration of 0.002%. After feeding, females were frozen at -20^{o}C until they were processed for fluorescence reading. A 96-well PCR plate was prepared with one 3 mm diameter borosilicate solid-glass bead (Millipore Sigma #Z143928) and 100 µl PBS in each well. 8 wells were used to generate a reference standard curve. These wells contained a single unfed mosquito and the following volumes of the same fluorescent meal fed to test mosquitoes: 5, 2.5, 1.25, 0.625, 0.3125, 0.15625, 0.078125, or 0 µL. One test group mosquito was added to each of the remaining wells. Tissue was disrupted using TissueLyser II (Qiagen) and briefly centrifuged at 2000 rpm for 1 – 2 min. 20 µL of tissue lysate from each well was added to 180 µL PBS in a well of a black 96-well plate (ThermoFisher #12-566-09). Fluorescent intensity for each well was measured using the 485/520 excitation/emission channel of a Varioskan Lux (ThermoFisher #VL0000D0) plate reader. Using the reference dilution curve, fluorescent measurements were converted to volume (µL) of solution ingested. Measurements below the level of detection were quantified as 0 for plotting and statistical analysis.

Nectar-Feeding Assay

Animals were prepared exactly as described for the Glytube assay. Consumption of nectar was quantified by supplementing the meal with 0.002% fluorescein. A cotton ball (Fisher Scientific #22456880) was soaked in each test meal, the cotton ball was briefly dabbed on a Kimwipe to prevent excess liquid from dripping through the mesh, and placed on top of the mesh covering the cup. Animals were allowed to feed for 4 hours. After feeding, animals were frozen at -20^{o}C and fluorescence reading was performed as described.

Meal Size Quantification

In Figure 2.1E,F, we analyzed the average meal size of mosquitoes that fed on blood or sugar respectively. Mosquitoes that did not feed were excluded from meal size analysis. To set a cut-off for whether or not a mosquito fed, we included unfed control groups that were not offered a meal and therefore reflected a true 0. We detected fluctuations in baseline from 0 – 0.0304 µL. We therefore set a cut-off at 0.05 µL and excluded animals in the blood or sugar experimental group that measured < 0.05 µL. We then applied this 0.05 µL cut-off for statistical analysis in subsequent meal size quantification experiments in Figure 5.2A,B, and Figure 6.3: all values < 0.051 were replaced with 0.05. This cut-off was also applied to determine whether or not a female fed in Figure 5.2C,D.

Chemogenetic Capsaicin Feeding Assays

Chemogenetic experiments using capsaicin to activate *Gr4>TRPV1* sensory neurons were carried out exactly as the nectar-feeding experiments except that 50 μM capsaicin in 0.1% DMSO or 0.1% DMSO only-control was added to the meals. Chemogenetic experiments using capsaicin to activate *Ir7a>TRPV1* and *Ir7f>TRPV1* sensory neurons were carried out exactly as the blood-feeding (Glytube) experiments except that 50 μM capsaicin in 0.1% DMSO or 0.1% DMSO only-control was added to the meals.

biteOscope Assay

Stylet piercing behavior was characterized using the biteOscope (Hol et al., 2020). Briefly, all meals were prepared exactly as for the Glytube experiments. The meal was applied on the rectangular section on the outside of a 70 mL Falcon cell culture flask and covered with parafilm. To maintain meal temperature, the flask was filled with warm water maintained at 37^{o}C using a Raspberry Pi controlled Peltier element. The flask was mounted in the floor of a 10 cm x 10 cm x 10 cm acrylic cage. A camera (Basler #acA2040-90um) and two white LED arrays for illumination (Vidpro #LED-312) were mounted outside the cage to image mosquitoes interacting with the bite substrate. At least 12 hours prior to the experiment, females were fasted by replacing 10% sucrose with a water source. At the start of each trial, an individual female was introduced into the cage and the experimenter (F.J.J.H.) blew on the cage 2 times 10 sec to provide human cues. Images were acquired at 10 frames/sec using Basler Pylon 5 software

running on Ubuntu 18.04. Each female was recorded for 700 sec regardless of engorgement status. Images were processed using custom code written in Python (available from Github: https://github.com/felixhol/biteOscope) using SciPy (Virtanen et al., 2019), TrackPy (Allan et al., 2019), and OpenCV (Bradski, 2000) packages to determine the presence and location of a mosquito. Engorgement status of a mosquito was determined by measuring abdominal size by fitting an active contour model to its abdomen. Stylet piercing events were scored by manual visual analysis of the images.

Tissue Fixation Protocol

Tissue fixation followed modification of previously published methods (Matthews et al., 2019) as follows. Heads were carefully removed from the body by pinching at the neck with sharp forceps. Heads were placed in a 1.5 mL tube for fixation with 4% paraformaldehyde, 0.1 M Millonig's Phosphate Buffer (pH 7.4), 0.25% Triton X-100, and nutated for 3 hour at 4^{o}C. Samples were dissected and samples of the same tissue were grouped into a cell strainer cap (Fisher Scientific #08-771-23) that was cut to fit into 1 well of a 24-well plate containing PBS with 0.25% Triton X-100 (PBT). All subsequent steps were performed on a low-speed orbital shaker at room temperature. Samples were washed at least 5 times 20 min and transferred to PBT. All dissections were performed using this protocol unless otherwise noted.

TO-PRO-3 Staining

7 to 14 day-old animals were anesthetized on ice. Heads were removed and fixed prior to tissue dissection according to the tissue fixation protocol. Samples were transferred to a well of PBT with 1:400 TO-PRO-3 (ThermoFisher #T3605) for 2 days. Samples were washed at least 5 times 20 min in 0.25% PBT. After washing, tissues were briefly transferred to a well of SlowFade diamond (ThermoFisher #S36972) to eliminate excess PBT. Samples were then mounted in SlowFade. Within each experiment, all image acquisition parameters were maintained across both sexes.

dTomato Visualization

7 to 14 day-old mosquitoes were anesthetized on ice. Heads were removed and fixed prior to tissue dissection according to the tissue fixation protocol. Samples were briefly transferred to a well of Vectashield (Vector Laboratories #H-1000) to remove excess PBT. Samples were then mounted in Vectashield. Within each genotype, all image acquisition parameters were maintained across tissue types. At higher laser power, we observed very faint cells in *Ir7f>dTomato-T2A-GCaMP6s* female labiums but we suspect that they are not neurons because we did not observe nerve fibers exiting the labium or projecting to the posterior subesophageal zone where labium neurons normally terminate.

Phalloidin, DAPI, and FITC Staining

7 to14 day-old mosquitoes were anesthetized on ice. Stylets were dissected and placed directly into a 24 well-plate containing 4% paraformaldehyde, 0.1 M Millonig's Phosphate Buffer (pH 7.4) and 0.25% Triton X-100. All subsequent steps were performed on a low-speed orbital shaker at room temperature. Samples were washed at least 4 times 15 min in PTx.2 (for 1L: 100 mL PBS 10x, 2 mL TritonX-100) before placed overnight in iDISCO permeabilization solution (for 500 mL: 400 mL PTx.2, 11.5 g glycine, 100 mL DMSO) (Renier et al., 2014). Samples were then incubated in iDISCO PTwH solution (for 1L: 100 mL 10x PBS, 2mL Tween-20, 1 mL of 10mg/mL Heparin stock solution) with 5% DMSO for at least 2 days at room temperature with the following reagents: (1) 1:20 AlexaFluor 594 phalloidin (ThermoFisher #A12381) (Figure 2.6F) or (2) 1:20 AlexaFluor 488 phalloidin (ThermoFisher #A12379) and 1:500 DAPI (Millipore Sigma #D9542) (Figure 2.5D) or (3) 1:20 AlexaFluor 647 phalloidin (ThermoFisher #A22287) (Figure 2.6H) or (4) 2 mg/mL FITC (Millipore Sigma #1.24546) (Figure 2.5A). Samples were then washed at least 4 times 15 min with PTx.2 solution and mounted in Vectashield. If a sample contained AlexaFluor 647, it was mounted in SlowFade instead of Vectashield because this fluorophore was better preserved in this mounting medium.

Dextran Dye-Fills

7 to 14 day-old mosquitoes were anesthetized on ice. The labium was separated from the stylet using forceps. Mosquitoes were affixed on their side to a plastic dish (Falcon #353001) using UV-curable glue (Bondic, Amazon #B0181BEHQU) or double-

sided tape so that the stylet and labium were flat on the dish and distal tips were separated. For stylet dye-fills, a scalpel was used to cut approximately 300-750 µm away from the distal tip and 1 µL of Dextran, Texas Red, 3000 MW, Lysine Fixable (ThermoFisher #D3328) diluted to 1 mg/10 µL in External Saline was added immediately. The External Saline recipe (Matthews et al., 2019) is based on *D. melanogaster* imaging saline: 103 mM NaCl, 3 mM KCl, 5 mM 2-[Tris(hydroxymethyl)methyl]-2-aminoethanesulfonic acid (TES), 1.5 mM $CaCl_2$, 4 mM $MgCl_2$, 26 mM $NaHCO_3$, 1 mM NaH_2PO_4, 10 mM trehalose, 10 mM glucose, pH 7.3, osmolality adjusted to 275 mOsm/kg. The mosquito was left on ice and covered for approximately 3-5 min before excess dye was removed by pipette. Mosquitoes were left at 4^{o}C overnight in a closed Petri dish with a moist Kimwipe placed in the corner to prevent desiccation. Heads were then removed and fixed prior to tissue dissection according to the tissue fixation protocol.

For double dye-fills of stylet and labium, the mosquito was prepared as described for single dye-fills above. The labium was cut at the base of the labellar lobes using a scalpel and 1 µL of Dextran, Texas Red diluted to 1 mg/10 µL in External Saline was added immediately. The mosquito was left on ice and covered for approximately 3-5 min before excess dye was removed by pipette. The stylet was cut approximately 300 – 750 µm away from the distal tip and 1 µL of Dextran, Fluorescein and Biotin, 3000 MW, Lysine Fixable (ThermoFisher #D7156) diluted to 1 mg/10 µL in External Saline was immediately added. The mosquito was left on ice and covered for approximately 3-5 min before excess dye was pipetted up. Mosquitoes were left at 4^{o}C overnight with a moist

Kimwipe to prevent desiccation. Heads were then removed and fixed prior to tissue dissection according to the tissue fixation protocol.

Fixed heads of both single and double dye-fill preparations were then dissected and brains were placed in cell-strainer caps (Falcon #352235) in a 24 well-plate. Brains were stained using a modification of previously published methods (Matthews et al., 2019). All subsequent steps were performed on a low-speed orbital shaker. Brains were washed at room temperature in PBT for at least 4 times 15 min. Brains were permeabilized with 4% Triton X-100 with 2% normal goat serum (Jackson ImmunoResearch #005-000-121) in PBS at 4^{o}C for 2 days. Brains were washed at least 5 times 15 min with PBT at room temperature before being incubated in PBT plus 2% normal goat serum for 3 days at 4^{o}C degrees. The following primary antibodies at the following dilutions were used: rabbit anti-fluorescein (ThermoFisher #A889) 1:500 and mouse anti-*Drosophila* Brp (nc82) 1:50. The nc82 hybridoma developed by Erich Buchner of Universitätsklinikum Würzburg was obtained from the Developmental Studies Hybridoma Bank, created by the NICHD of the NIH and maintained at The University of Iowa, Department of Biology, Iowa City, IA 52242. Following primary antibody incubations, brains were washed at least 5 times 15 min with PBT at room temperature. Brains were incubated with secondary antibody for 3 days at 4^{o}C with secondary antibodies at 1:500: goat anti-rabbit Alexa Fluor 488 (ThermoFisher #A-11008) and goat anti-mouse Alexa Fluor 647 (ThermoFisher #A-21236). Brains were then washed PBT and mounted in Vectashield.

Brain Immunostaining

8 to 9 day-old mosquitoes were anaesthetized on ice. Heads were then removed and fixed prior to tissue dissection according to the tissue fixation protocol. Primary antibodies were used at the following dilutions: rat anti-mCD8 (Invitrogen #14008185) 1:100, and a concentrated aliquot of mouse anti-*Drosophila* Brp 1:5000 generated in-house with the nc82 hybridoma obtained from DHSB. Brains were then washed 5x for at least 30 min at room temperature. Brains were then incubated with secondary antibodies in PBT with 2% normal goat serum for 2 days at 4˚C. The following secondary antibodies were used at 1:500 dilutions: goat anti-rat Alexa Fluor 647 (Invitrogen #A21247) and goat anti-mouse Alexa Fluor 555 (Invitrogen #A32727). Brains were then washed 6 times in PBT at room temperature for at least 30 min then mounted in SlowFade diamond. 3xP3 was used as a promoter to mark transgene insertion as previously described (Matthews et al., 2019). To avoid any interference from possible 3xP3 signal, we used a different laser excitation/secondary antibody for monitoring *Ir7a*, *Ir7f*, and *Gr4* expression. Within each genotype, all image acquisition parameters were maintained across both sexes. *Ir7a* and *Ir7f* are expressed in a maximum of 2 and 4 neurons (Figure 4.5A,B), respectively, which is far fewer neurons than *Gr4* (Figure 5.4A). We also noted that it was easier to detect processes in the subesophageal zone of *Gr4 > CD8-GFP* animals (Figure 5.4B) compared to *Ir7a > CD8-GFP* or *Ir7f > CD8-GFP* animals (Figure 4.5C,D), leading us to use a higher laser power to acquire these images. Upon generating the max projections for Figure 4.5C,D, we noted that the background signal from tissue autofluorescence is higher in *Ir7a > CD8-*

GFP and *Ir7f* > *CD8-GFP* animals. However, this background signal is not correlated with innervation from stylet neurons since females and males from the same genotype were both imaged at the same settings and both have similar background, but only females have subesophageal zone innervation (Figure 4.5C-E).

Confocal Image Acquisition

Images were acquired with a Zeiss Axio Observer Z1 Inverted LSM 880 NLO laser scanning confocal microscope (Zeiss) with a 25x/0.8 NA immersion-corrected objective at a resolution of 2048 x 2048 or 1024 x 1024 pixels. When necessary, tiled images were stitched with 10% overlap. Confocal images were processed in ImageJ (NIH).

Ex-Vivo Stylet Prep for Calcium Imaging

Calcium imaging was performed on an inverted Ti-2E wide-field microscope (Nikon) with a dual FITC/TRITC bandpass cube and alternating emission wheel with 520/40 GFP and 628/40 RFP bandpass filters. A nd2 filter was added with the 628/40 RFP bandpass filter to attenuate dTomato signal. Images were acquired with a 25x/0.9 N.A. water-immersion objective (Nikon) and Zyla 4.2 Plus camera. Calcium imaging experiments were performed on female mosquitoes that were 7–14 days post-eclosion.

Prior to dissection, the imaging chamber was prepared by affixing a Gold Seal Cover Glass, No. 1 22 x 40 mm coverslip (Ted Pella #260353) to a recording chamber using

silicone lubricant (Dow Molykote 111 O-Ring Silicone Lubricant). A fast exchange recording chamber (Warner Instruments #64-0230) was used for perfusion-only experiments and a low-profile large bath recording chamber (Warner Instruments #640236) was used to accommodate the BioPen apparatus. A drop of silicone lubricant approximately 100-200 μm in diameter was placed slightly off-center on the coverslip.

After preparing the chamber, females were anesthetized briefly at 4˚C for dissection. The labium was removed to expose the stylet, and then the stylet was detached at the proximal end using a scalpel (Feather disposable scalpel, No. 11, Fisher Scientific #FH/CX7281A). The severed end was immediately placed in the drop of silicone lubricant with the stylet tip facing the center of the coverslip. Great care was taken to place the stylet flat along the coverslip so that all stylet neurons could be imaged in one plane. This process often involved carefully removing the maxillae and mandibles without damaging the stylet. However, if the stylet was already flat, it was not necessary to remove additional appendages as they did not interfere with image acquisition. The most distal 300 μm of the stylet tip remained free of silicone lubricant to prevent interference with ligand delivery. Once the stylet was secured to the coverslip, the chamber was filled with MilliQ water and the perfusion and/or BioPen fluidics were inserted into the chamber.

dTomato fluorescence was examined before and throughout imaging to verify that the stylet nerves were intact. The sample remained stable during the duration of the imaging session in all animals that were included in this study. Each image acquisition

captured one GCaMP image and one dTomato image separated by less than the 100 ms required to switch the filter wheel. Image acquisition was triggered at a rate of approximately 2 frames per sec for each channel (2 sets of GCaMP/dTomato images per sec).

Perfusion Ligand Delivery

Two independent ValveBank8 Pinch Valve perfusion systems (Automate Scientific #13-pp-54) with BubbleStop8 60 mL Syringe Heater (Automate Scientific #10-8-60-G) were automatically controlled by NIS-Elements software (Nikon). To ensure full perfusion chamber exchange, ligands were perfused for 30 sec followed by a 45 sec recovery period before the next ligand. Ligand delivery switched from water (baseline) to ligand of interest with the following exceptions. Since ATP is rapidly hydrolyzed in water, ATP was always delivered in a buffer of 25 mM $NaHCO_3$. 25 mM $NaHCO_3$ was delivered for 30 sec to establish a baseline, after which ATP dissolved in 25 mM $NaHCO_3$ was applied. Responses above the baseline were considered ATP responses. In control experiments, we demonstrated that ATP dissolved in PBS activated these same neurons after pre-equilibration in PBS. In Figure 5.5 and Figure 5.6A, stylets were pre-equilibrated in 298 mM cellobiose for 30 sec prior to the isomolar sugar of interest to control for osmotic effects. 298 mM cellobiose was behaviorally inactive in both the blood- and nectar-feeding assays (Matthews et al., 2019) (see raw data at https://github.com/VosshallLab/Jove_Vosshall_2020).

Ligands were delivered in the following order for the indicated experiment: (“>” indicates water recovery before adding next ligand)

Figure 3.3A-C: The stimulus order alternated between the following options so that each animal experienced at least one of each: 1. water > 1st blood > 2nd blood > 3rd blood and 2. 1st blood >2nd blood > 3rd blood > water

Figure 3.4C-F: The stimulus order alternated between the following options so that each animal experienced at least one of each: 1. blood > mix+ATP and 2. mix+ATP > blood

Figure 3.5: The stimulus order alternated between the following options: 1. Blood > NaCl > glucose > $NaHCO_3$ > $NaHCO_3$, ATP > Mix+ ATP > Mix and 2. Blood > Mix > NaCl > glucose > $NaHCO_3$ > $NaHCO_3$, ATP > Mix+ATP

Figure 5.5 and Figure 5.6A: The stimulus order alternated between the following options so that each animal experienced one of each: 1. cellobiose, glucose > cellobiose, sucrose > cellobiose, fructose and 2. cellobiose, fructose > cellobiose, sucrose > cellobiose, glucose and 3. cellobiose, sucrose > cellobiose, fructose > cellobiose, glucose

Microfluidic Ligand Delivery Using the BioPen

The BioPen tip holder (Fluicell) was secured using a MP-285 micromanipulator (Sutter #SU-MP-285). Each BioPen tip was prepared according to the manufacturer’s

instructions with the following exceptions. First, the initial “New Tip” protocol was run with MilliQ water in each well to prime the microfluidic channels. Once the protocol was completed, water was removed from each BioPen well and replaced with test ligands. 0.0002% fluorescein was added to each test ligand to visualize the size and location of ligand delivery in each trial. For solutions containing $NaHCO_3$, the fluorescein signal was much brighter, so 0.00002% fluorescein was used instead. For each ligand, the BioPen stimulus was ON for 20 sec with a 60 sec recovery before the next stimulus.

Analysis of GCaMP6s Data

All calcium imaging data were processed with Nikon Elements software. Regions of interest (ROIs) were selected based on the dTomato fluorescence intensity and used for analysis of GCaMP6s signal. Great care was taken to draw ROIs on the cell body of interest and not on *en passant* processes or slightly overlapping cell bodies. To exclude background noise, a cut-off of 0.25 peak $\Delta F/F_0$ was set as the minimum threshold for activation. This cut-off intentionally filters for clear activation and does not distinguish between background noise and weak activation. Occasionally (less than 1 cell body per animal) it was difficult to avoid the halo, especially if baseline GCaMP fluorescence was very low in a given cell body. In these rare cases, the cell body was not considered to be activated. All traces with sample motion, as determined by dTomato fluorescence instability, were discarded.

Once raw fluorescence values were extracted for each neuron/stimulus (ligand) pair, $\Delta F/F_0$ calculations were performed using a custom R script (R version 3.6.0) where $\Delta F/F_0 = (F - F_0)/F_0$. To determine the baseline fluorescence (F_0) 5 frames (~2 fps) were averaged before stimulus presentation. To determine peak F to a given stimulus, the average of 3 frames at the peak during stimulus delivery was determined for each stimulus. This process was repeated twice for each stimulus so that the peak $\Delta F/F_0$ value represented in all plots is the average peak $\Delta F/F_0$ for 3 independent stimulus presentations. Stimulus trains were delivered so that each stimulus was only presented once per trial. Therefore, the final value represents the average peak stimulus response collected from three trials. Once all averages had been calculated, the dataset from individual females were analyzed and represented in multiple ways. Heat maps for GCaMP imaging data were generated using a custom R script available at https://github.com/VosshallLab/Jove_Vosshall_2020. Each box represents average peak $\Delta F/F_0$ to a given stimulus as described above. The heat map color scale is log2 to increase dynamic range and the minimum and maximum color value was set to 0.25 and 3 respectively. “% neurons activated” plots were plotted using Prism 8 (GraphPad) and a neuron was considered activated if peak $\Delta F/F_0 > 0.25$. “peak $\Delta F/F_0$” scatter plots were generated using Prism 8 (GraphPad) except the scatter plots (Figure 3.6B) and box plots (Figure 3.6C) of peak $\Delta F/F_0$ for neurons within a given cluster were plotted in base R.

Hierarchical Clustering

In Figure 3.6 134 individual neurons from the 5 females in Figure 3.5 were pooled and subjected to hierarchical clustering using Euclidean distance with complete linkage and visualized with the pheatmap R package v 1.0.12 (https://CRAN.R-project.org/package=pheatmap). Clustering was based on each neuron's response profile to 7 ligands: blood, mix+ATP, mix, ATP, NaCl, $NaHCO_3$, glucose. The peak $\Delta F/F_0$ of each neuron in response to each ligand was recorded 3 times to calculate an average peak $\Delta F/F_0$ per ligand per neuron, similar to the protocol described in Figure 3.2. In Figure 3.8A suitability of the normalized response measurements to clustering was assessed by the Hopkins statistic (h) (Lawson and Jurs, 1990) using the factoextra R package v 1.0.7 and the get_clust_tendency function (https://CRAN.R-project.org/package=factoextra). To show the significance of this clustering tendency, the p-value for the Hopkins statistic, 4.0126e-39, was calculated using the beta distribution in base R. In Figure 3.8B the optimal number of clusters to be drawn for the data was established by the Silhouette method (Rousseeuw, 1987) using the NbClust R package v 3.0 (Charrad et al., 2014) with potential cluster numbers in the range of 2 to 10. 5 was the optimal cluster number with the highest mean silhouette value 0.769 across clusters. The factoextra package was used to visualize the silhouette analysis results and show the distribution of silhouette widths for all members of each cluster (Kassambara and Mundt, 2020). In Figure 3.8C, the stability of the 5 clusters was assessed by the bootstrap distribution of the Jaccard coefficient of resampled versus original data (Hennig, 2007, 2008). To calculate the Jaccard bootstrap mean for all clusters, we used the fpc v 2.2-5 R package's clusterboot function following the recommendations of 100 bootstraps (https://CRAN.R-project.org/package=fpc). In

Figure 3.8D-F, principal component analysis (PCA) was applied to neuronal responses using base R and the FactoMineR package (Lê et al., 2008) to visualize the contribution of female or cluster to derived principal components. To determine which ligand(s) robustly activate the neuronal subpopulation belonging to each cluster, we performed the one-sample Wilcoxon signed rank test (wilcox.test in R) on each subpopulation's average response to each ligand in Figure 3.6C. A cluster was considered activated by a given ligand if $p < 0.05$ when compared to the hypothetical value 0.25: wilcox.test(GroupA_Values, mu = 0.25, alternative = "greater") because a neuron was considered activated if peak $\Delta F/F_0 > 0.25$.

Custom R scripts for all analyses are available at https://github.com/VosshallLab/Jove_Vosshall_2020. A comprehensive supplementary document on clustering methods is available at https://github.com/VosshallLab/Jove_Vosshall_2020/tree/master/Clustering_validation

Tissue Dissection and RNA Extraction

7 to 11 day-old mosquitoes were cold-anesthetized and kept on ice for up to 30 min or until dissections were complete. For labium samples, the labium was removed by forceps and immediately flash-frozen in DNA Lo-bind nuclease-free tubes (Fisher Scientific #13-698-790) contained in a CoolRack (Biocision #BCS0137) in dry ice for snap-freezing tissue. For female and male stylet samples, the labium was removed first. The stylet was detached half-way from the tip using a scalpel and immediately flash-

frozen as described above. Extreme caution was taken during the tissue dissection and RNA extraction process to ensure that there was no contamination from other mosquito tissues or RNases. Each dish, forcep, and scalpel was carefully cleaned with 70% ethanol and RNase-away (ThermoFisher #7003) after every dissection or dissection attempt. Once the labium was removed, the stylet was discarded if there was any contact between the stylet and any surface other than the cleaned dish, forceps, or scalpel. A dedicated pair of stylet-only forceps was used to place the detached stylet into the collection tube. The following number of mosquitoes was used for each female library: female stylet, 25; male stylet, 25; female labium, 4. Each sample group was dissected in parallel to avoid batch effects. Dissected tissue was stored at −80°C until RNA extraction.

RNA extraction was performed using the PicoPure Kit (ThermoFisher #KIT0204) with the following exception for homogenizing tissue: instead of lysis buffer, 240 µL of TRIzol (ThermoFisher #15596018) was added to the collection tube on ice. Custom-order molecular biology grade, low-binding zirconium beads in 100 µm, 200 µm and 800 µm were used to disrupt tissue (OPS diagnostics). An RNase free spatula (Corning #CLS3013) was used to add 1 scoop each of 100 µm and 200 µm beads and ~100 µL of 800 µm beads to collection tube. Tubes were briefly spun down in a tabletop centrifuge before disruption in a TissueLyser II (Qiagen #85300) for 2 min 30 sec at 30 Hz. Tubes were briefly spun down again in tabletop centrifuge and returned to the TissueLyser II for an additional 2 min at 30 Hz. The remaining TRIzol extraction steps were performed in a chemical fume hood according to manufacturer's instructions:

tubes stood at room temperature for 5 min before 48 µL of chloroform:isoamyl alcohol 24:1 was added (Sigma #C0549). Tubes were hand-shaken for 30 sec and left to stand for 2 min before centrifuging at 12,000 x *g* for 15 min at 4°C. The aqueous Trizol layer was then removed and added into the PicoPure column, up to 180 µL at one time. Subsequent steps were performed according to PicoPure manufacturer's instructions, including DNase treatment.

RNA-seq Library Preparation and Sequencing

Labium samples were run on Bioanalyzer RNA Pico Chip (Agilent #5067-1513) to determine RNA quantity and quality and were used as a proxy for overall sample integrity because female and male stylet samples fell below the level of detection. Labium samples were diluted 1:10 before cDNA amplification to more closely approximate stylet samples. cDNA synthesis was performed using SMART-Seq v4 Ultra Low Input RNA Kit for Sequencing (Takara #634894) according to the manufacturer's instructions except that 10 µL instead of 9 µL was used to optimize for low RNA input. The number of PCR amplification cycles was adjusted for each sample group based on the number of cycles needed to detect RNA in the lowest input sample as determined by the Bioanalyzer High Sensitivity DNA Kit (Agilent #5067-4627). Negative controls for each group were run in parallel to ensure that additional cycles did not result in unspecific background product. All samples within one group were subjected to the same number of PCR amplification cycles. The female labium and female stylet samples underwent 20 cycles and male stylet 22 cycles. The full-length cDNA output

was processed with Nextera XT DNA library preparation kit (Illumina #FC-131-1024) according to manufacturer's instructions. Library quantity and quality were evaluated using High Sensitivity DNA ScreenTape Analysis (Agilent #5067-5585) prior to pooling. Bar-coded samples from all tissues were pooled in an equal ratio before distributing the pool across 3 sequencing lanes. Sequencing was performed at The Rockefeller University Genomics Resource Center on a NextSeq 500 sequencer (Illumina). All reads were 1 x 75 bp. Data were de-multiplexed and delivered as fastq files for each library. Sequencing reads have been deposited at the NCBI Sequence Read Archive (SRA) under BioProject PRJNA605870.

Transcript Abundance and Differential Expression Analysis

All reads were trimmed using TrimGalore version 0.4.2 (https://github.com/FelixKrueger/TrimGalore) with minimum read length of 35 base pairs. Reads from individual libraries were mapped to the AaegL5 genome (Matthews et al., 2018) using STAR version 2.5.2a (Dobin et al., 2013). All raw data use gene names with the LOCXXX naming format derived from the most recent NCBI RefSeq annotation of the *Aedes aegypti* genome (https://www.ncbi.nlm.nih.gov/assembly/GCF_002204515.2/) (Matthews et al., 2018). Gene names with the legacy AAELXXX naming format are easily cross-referenced to the new gene names by searching Vectorbase.

A custom gene annotation was generated by merging AaegL5 with the more recent manual chemoreceptor annotation for *OR*s, *GR*s and *IR*s (Matthews et al., 2018). This merged annotation and the R script used to generate it is available at https://github.com/VosshallLab/Jove_Vosshall_2020. For each of these chemoreceptors, the manual annotation replaced the AaegL5 RefSeq annotation. If the chemoreceptor did not previously exist in AaegL5 RefSeq, it was added. Reads mapping to each were mapped to transcript coding regions (UTRs and multi-mappers were excluded) using featureCounts version 1.5.0-p3 (Liao et al., 2014). For abundance visualization, raw counts were converted to TPM. RNA-seq TPM plots were generated using ggplot2 version 3.2.0 (R Development Core Team, 2017) in RStudio R 3.6.0. Raw counts were used for differential expression analysis in R using DESeq2 version 1.24.0 (Love et al., 2014). Sweet GRs analyzed in Figure 5.3 were derived from the *Ae. aegypti* genome reannotation (Matthews et al., 2018). TPM data from the stylet RNA-seq experiment are available for all predicted coding transcripts on GitHub.

Filtering for Stylet-Specific Transcripts

To obtain the 53 transcripts enriched in the female stylet compared to the female labium and male stylet (Figure 4.2C), we examined TPM values for non-mouthpart tissues that were previously profiled in a comprehensive dataset (Matthews et al., 2018; Matthews et al., 2016). A transcript was considered female stylet-specific if the average TPM expression across a given tissue was < 0.5 TPM for all tissues profiled by Matthews and colleagues, except for the Proboscis and Rostrum samples because

these samples included mouthparts. To calculate average TPM, we used the most recent dataset aligned to the L5 genome and quantified using NCBI RefSeq Annotation version 101(Matthews et al., 2018). If a transcript was present in the NCBI RefSeq annotation and the manual chemoreceptor annotation published alongside in Matthews, et al. 2018, we used the TPM value quantified using the manual chemoreceptor annotation because the NCBI RefSeq annotation is missing a handful of chemoreceptors, including *Ir7a*. A DESeq2 results table and a TPM table filtered for these 53 transcripts are provided on Github.

Quantification and Statistical Analysis

All statistical analysis was performed using Graphpad Prism Version 8 and RStudio R 3.6.0. For experiments where data were quantified as percent of females engorged, non-parametric tests were performed. For all other analyses, we first tested whether the values were normally distributed using D'Agostino–Pearson omnibus and Shapiro–Wilk normality tests. When data were normally distributed, we used parametric tests and when data were not normally distributed, we used non-parametric tests. Data collected as raw values are shown as mean ± SEM or mean ± SD. Details of statistical methods are reported in the figure legends.

CHAPTER 9. APPENDIX

In addition to P2X ionotropic receptors, adenine nucleotides can also be recognized by two types of metabotropic G-protein coupled receptors: P2Y (ATP or ADP ligands) and adenosine receptors (adenosine ligand) (Zarrinmayeh and Territo, 2020). Although adenosine receptors have been described in insects, experimental evidence for P2Y receptors in insects has remained elusive thus far (Burnstock and Verkhratsky, 2009). As part of a comprehensive screen to deorphanize G-protein coupled receptors in *Ae. aegypti* (Duvall et al., 2019), we used BLAST to identify putative orthologs to insect adenosine receptors and mammalian P2Y receptors that have been experimentally demonstrated to respond to ATP (von Kugelgen, 2006). We successfully cloned 11 putative orthologs from the *Ae. aegypti* genome (Figure 10.1, legend). HEK293T cells were transfected with a plasmid expressing a candidate ATP receptor, GCaMP6s, and mouse Gqα15 as previously described (Duvall et al., 2019). We included a No Receptor negative control to measure the endogenous baseline response of HEK293T cells to adenine nucleotides and the ATP-sensitive mouse P2Y2R as a positive control. Based on the behavioral dose response curves (Figure 2.3C,D) (Galun, 1987; Galun et al., 1985b), we reasoned that the receptor mediating ATP detection in blood-feeding behavior should be sensitive to ATP and its non-hydrolyzable analog AMP-PNP. In our preliminary experiments we did not identify a receptor that elicited a significant response to both ATP and the non-hydrolyzable ATP analog (Figure 10.1C,D). However, it is important to note that endogenous responses to adenine nucleotides in HEK293T cells

rendered the data more difficult to interpret. As a result, we did not further pursue this assay for ATP receptor identification.

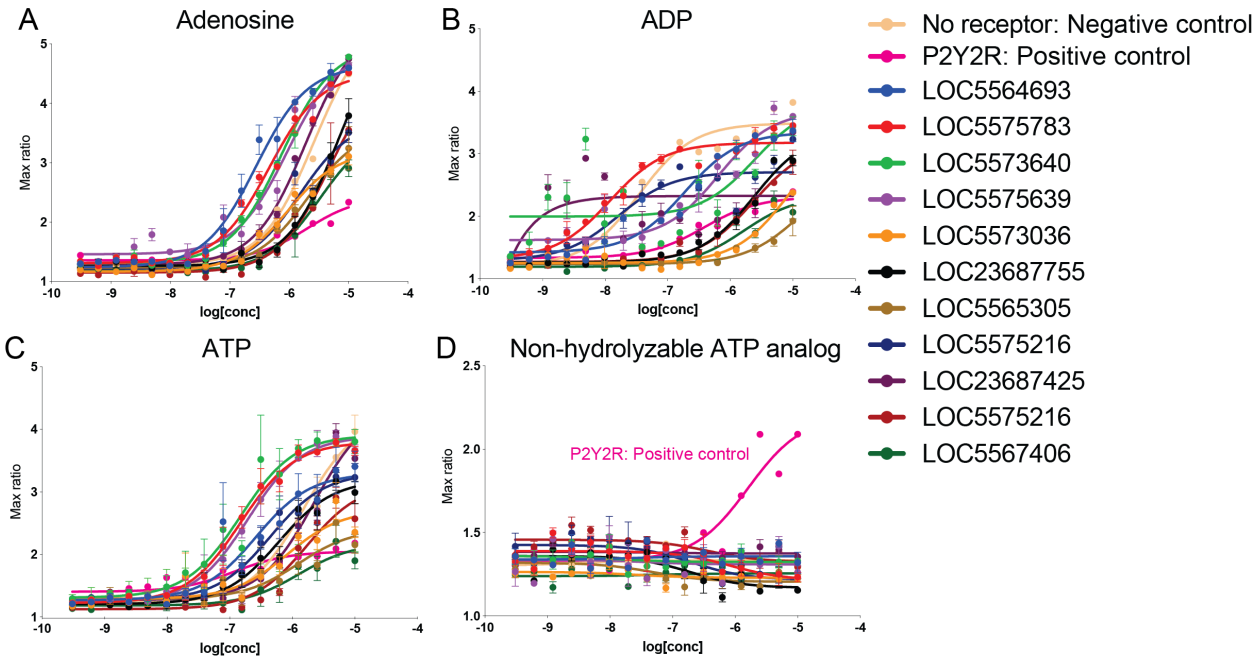

Figure 9.1 Heterologous expression screen for ATP-sensitive G-protein coupled receptors.

(A-D) *In vitro* dose-response curve for the indicated receptor to adenosine (A), ADP (B), ATP (C), and non-hydrolyzable ATP analog (D). Methods were performed as previously described (Duvall et al., 2019).

CHAPTER 9. REFERENCES

Ahn, J.E., Chen, Y., and Amrein, H. (2017). Molecular basis of fatty acid taste in *Drosophila*. Elife *6*.

Allan, D., van der Wel, C., Keim, N., Caswell, T.A., Wieker, D., Verweij, R., Reid, C., Thierry, G., L., , Grueter, L., Ramos, K.*, et al.* (2019). soft-matter/trackpy: Trackpy v0.4.2. DOI:105281/zenodo3492186.

Baldwin, M., Toda, Y., Nakagita, T., O'Connell, M.J., Klasing, K.C., Edwards, S.V., and Liberles, S.D. (2014). Evolution of sweet taste perception in hummingbirds by transformation of the ancestral umami receptor. Science *345*, 929-933.

Bargmann, C., and Kaplan, J.M. (1998). Signal Transduction in the *Caenorhabditis elegans* Nervous System. Annu Rev Neurosci *21*, 279-308.

Barretto, R.P., Gillis-Smith, S., Chandrashekar, J., Yarmolinsky, D.A., Schnitzer, M.J., Ryba, N.J., and Zuker, C.S. (2015). The neural representation of taste quality at the periphery. Nature *517*, 373-376.

Bauder, J.A., Lieskonig, N.R., and Krenn, H.W. (2011). The extremely long-tongued neotropical butterfly *Eurybia lycisca* (Riodinidae): proboscis morphology and flower handling. Arthropod Struct Dev *40*, 122-127.

Bavan, S., Farmer, L., Singh, S.K., Straub, V.A., Guerrero, F.D., and Ennion, S.J. (2011). The penultimate arginine of the carboxyl terminus determines slow desensitization in a P2X receptor from the cattle tick *Boophilus microplus*. Mol Pharmacol *79*, 776-785.

Benton, R. (2017). The neurobiology of gustation in insect disease vectors: progress and potential. Curr Opin Insect Sci *20*, 19-27.

Benton, R., Vannice, K.S., Gomez-Diaz, C., and Vosshall, L.B. (2009). Variant Ionotropic Glutamate Receptors as Chemosensory Receptors in *Drosophila*. Cell *136*, 149-162.

Bishop, A., and Gilchrist, B.M. (1946). Experiments upon the feeding of *Aedes aegypti* through animal membranes with a view to applying this method to the chemotherapy of malaria. Parasitology *37*, 85-100.

Born, G.V., and Kratzer, M.A. (1984). Source and concentration of extracellular adenosine triphosphate during haemostasis in rats, rabbits and man. J Physiol *354*, 419-429.

Bradski, G. (2000). The OpenCV Library. Dr Dobb's Journal of Software Tools.

Burnstock, G., and Verkhratsky, A. (2009). Evolutionary origins of the purinergic signalling system. Acta Physiol (Oxf) *195*, 415-447.

Centor, R.M. (1990). Serum Total Carbon Dioxide. In Clinical Methods: The History, Physical, and Laboratory Examinations.

Chandrashekar, J., Yarmolinksy, D., von Buchholtz, L., Oka, Y., Sly, W., Ryba, N.J.P., and Zuker, C.S. (2009). The Taste of Carbonation. Science *326*, 443-445.

Charrad, M., Ghazzali, N., Boiteau, V., and Niknafs, A. (2014). NbClust: An R Package for Determining the Relevant Number of Clusters in a Data Set. J Stat Soft *61*, 1-36.

Chen, X., Gabitto, M., Peng, Y., Ryba, N.J., and Zuker, C.S. (2011). A gustotopic map of taste qualities in the mammalian brain. Science *333*, 1262-1266.

Choi, H.M.T., Schwarzkopf, M., Fornace, M.E., Acharya, A., Artavanis, G., Stegmaier, J., Cunha, A., and Pierce, N.A. (2018). Third-generation in situ hybridization chain reaction: multiplexed, quantitative, sensitive, versatile, robust. Development *145*.

Choumet, V., Attout, T., Chartier, L., Khun, H., Sautereau, J., Robbe-Vincent, A., Brey, P., Huerre, M., and Bain, O. (2012). Visualizing non infectious and infectious *Anopheles gambiae* blood feedings in naive and saliva-immunized mice. PLoS One *7*, e50464.

Clyne, P.J., Warr, C.G., and Carlson, J.R. (2000). Candidate Taste Receptors in *Drosophila*. Science *287*, 1830-1834.

Costa-da-Silva, A.L., Navarrete, F.R., Salvador, F.S., Karina-Costa, M., Ioshino, R.S., Azevedo, D.S., Rocha, D.R., Romano, C.M., and Capurro, M.L. (2013). Glytube: a conical tube and parafilm M-based method as a simplified device to artificially blood-feed the dengue vector mosquito, *Aedes aegypti*. PLoS One *8*, e53816.

Croset, V., Rytz, R., Cummins, S.F., Budd, A., Brawand, D., Kaessmann, H., Gibson, T.J., and Benton, R. (2010). Ancient protostome origin of chemosensory ionotropic glutamate receptors and the evolution of insect taste and olfaction. PLoS Genet *6*, e1001064.

Day, M.F. (1954). The mechanism of food distribution to midgut or diverticula in the mosquito. Aust J biol Sci *7*, 515-524.

DeGennaro, M., McBride, C.S., Seeholzer, L., Nakagawa, T., Dennis, E.J., Goldman, C., Jasinskiene, N., James, A.A., and Vosshall, L.B. (2013). orco mutant mosquitoes lose strong preference for humans and are not repelled by volatile DEET. Nature *498*, 487-491.

Dekker, T., Geier, M., and Carde, R.T. (2005). Carbon dioxide instantly sensitizes female yellow fever mosquitoes to human skin odours. J Exp Biol *208*, 2963-2972.

Dennis, E.J., Goldman, O.V., and Vosshall, L.B. (2019). *Aedes aegypti* Mosquitoes Use Their Legs to Sense DEET on Contact. Curr Biol *29*, 1551-1556 e1555.

Deutsch, J.A., Moore, B.O., and Heinrichs, S.C. (1989). Unlearned specific appetite for protein. Physiol Behav *46*, 619-624.

Devineni, A.V., Sun, B., Zhukovskaya, A., and Axel, R. (2019). Acetic acid activates distinct taste pathways in *Drosophila* to elicit opposing, state-dependent feeding responses. Elife *8*.

Dobin, A., Davis, C.A., Schlesinger, F., Drenkow, J., Zaleski, C., Jha, S., Batut, P., Chaisson, M., and Gingeras, T.R. (2013). STAR: ultrafast universal RNA-seq aligner. Bioinformatics *29*, 15-21.

Duvall, L.B., Ramos-Espiritu, L., Barsoum, K.E., Glickman, J.F., and Vosshall, L.B. (2019). Small-Molecule Agonists of Ae. aegypti Neuropeptide Y Receptor Block Mosquito Biting. Cell *176*, 687-701 e685.

Fischler, W., Kong, P., Marella, S., and Scott, K. (2007). The detection of carbonation by the *Drosophila* gustatory system. Nature *448*, 1054-1057.

Forsyth, A.M., Wan, J., Owrutsky, P.D., Abkarian, M., and Stone, H.A. (2011). Multiscale approach to link red blood cell dynamics, shear viscosity, and ATP release. Proc Natl Acad Sci U S A *108*, 10986-10991.

Fosque, B.F., Sun, Y., Dana, H., Yang, C., Ohyama, T., Tadross, M.R., Patel, R., Zlatic, M., Kim, D.S., Ahrens, M.B.*, et al.* (2015). Labeling of active neural circuits in vivo with designed calcium integrators. Science *347*.

Fountain, S.J. (2013). Primitive ATP-activated P2X receptors: discovery, function and pharmacology. Front Cell Neurosci *7*, 247.

Galun, R. (1987). The evolution of purinergic receptors invovled in recognition of a blood meal by hematophagous insects. Intern Symp on Insects *82*, 5-9.

Galun, R., Avi-Dor, Y., and Bar-Zeev, M. (1963). Feeding Response in *Aedes aegypti*: stimulation by Adenosine Triphosphate. Science *142*, 1674-1675.

Galun, R., Friend, W.G., and Nudelman, S. (1988). Purinergic reception by culicine mosquitoes. J Comp Physiol A *163*, 665-670.

Galun, R., Koontz, L.C., and Gwadz, R.W. (1985a). Engorgement response of anopheline mosquitoes to blood fractions and artificial solutions. Physiological Entomology *10*, 145-149.

Galun, R., Koontz, L.C., Gwadz, R.W., and Ribeiro, J.M.C. (1985b). Effect of ATP analogues on the gorging response of *Aedes aegypti* Physiol Entomol *10*, 275-281.

Galun, R., Oren, N., and Zecharia, M. (1984). Effect of plasma components on the feeding response of the mosquito *Aedes aegypti* L. to adenine nucleotides. Physiological Entomology *9*, 403-408.

Gonzales, K.K., Rodriguez, S.D., Chung, H.N., Kowalski, M., Vulcan, J., Moore, E.L., Li, Y., Willette, S.M., Kandel, Y., Van Voorhies, W.A*., et al.* (2018). The Effect of SkitoSnack, an Artificial Blood Meal Replacement, on *Aedes aegypti* Life History Traits and Gut Microbiota. Sci Rep *8*, 11023.

Gordon, R.M., Lumsden, W. H. R. (1939). A study of the behavior of the mouth-parts of mosquitoes when taking up blood from living tissue: together with some observations on the ingestion of microfilariae. Annals of Tropical Medicine and Parasitology *33*, 259-278.

Gorman, M.W., Feigl, E.O., and Buffington, C.W. (2007). Human plasma ATP concentration. Clin Chem *53*, 318-325.

Griffiths, R.B., and Gordon, R.M. (1952). An apparatus which enables the process of feeding by mosquitoes to be observed in the tissues of a live rodent; together with an account of the ejection of saliva and its significance in Malaria. Ann Trop Med Parasitol *46*, 311-319.

Harris, D.T., Kallman, B.R., Mullaney, B.C., and Scott, K. (2015). Representations of Taste Modality in the *Drosophila* Brain. Neuron *86*, 1449-1460.

Hennig, C. (2007). Cluster-wise assessment of cluster stability. Computational Statistics & Data Analysis *52*, 258-271.

Hennig, C. (2008). Dissolution point and isolation robustness: Robustness criteria for general cluster analysis methods. Journal of Multivariate Analysis *99*, 1154-1176.

Hol, F.J., Lambrechts, L., and Prakash, M. (2020). BiteOscope, an open platform to study mosquito biting behavior. Elife *9*.

Hosoi, T. (1959). The identification of blood components which induce gorging of the mosquito J Insect Physiol *3*, 191-218.

Ignell, R., and Hansson, B.S. (2005). Projection patterns of gustatory neurons in the suboesophageal ganglion and tritocerebrum of mosquitoes. J Comp Neurol *492*, 214-233.

Inagaki, H.K., Ben-Tabou de-Leon, S., Wong, A.M., Jagadish, S., Ishimoto, H., Barnea, G., Kitamoto, T., Axel, R., and Anderson, D.J. (2012). Visualizing neuromodulation in vivo: TANGO-mapping of dopamine signaling reveals appetite control of sugar sensing. Cell *148*, 583-595.

Isoe, J., Collins, J., Badgandi, H., Day, W.A., and Miesfeld, R.L. (2011). Defects in coatomer protein I (COPI) transport cause blood feeding-induced mortality in Yellow Fever mosquitoes. Proc Natl Acad Sci U S A *108*, E211-217.

Ito, K., Shinomiya, K., Ito, M., Armstrong, J.D., Boyan, G., Hartenstein, V., Harzsch, S., Heisenberg, M., Homberg, U., Jenett, A.*, et al.* (2014). A systematic nomenclature for the insect brain. Neuron *81*, 755-765.

Jaeger, A.H., Stanley, M., Weiss, Z.F., Musso, P.Y., Chan, R.C., Zhang, H., Feldman-Kiss, D., and Gordon, M.D. (2018). A complex peripheral code for salt taste in *Drosophila*. Elife *7*.

Johnson, R.N., O'Meally, D., Chen, Z., Etherington, G.J., Ho, S.Y.W., Nash, W.J., Grueber, C.E., Cheng, Y., Whittington, C.M., Dennison, S.*, et al.* (2018). Adaptation and conservation insights from the koala genome. Nature Genetics *50*, 1102-1111.

Julius, D., and Basbaum, A.I. (2001). Molecular mechanisms of nociception. Nature *413*, 203-210.

Jung, J.W., Baeck, S.J., Perumalsamy, H., Hansson, B.S., Ahn, Y.J., and Kwon, H.W. (2015). A novel olfactory pathway is essential for fast and efficient blood-feeding in mosquitoes. Sci Rep *5*, 13444.

Kaplan, J.M., and Horvitz, H.R. (1993). A dual mechanosensory and chemosensory neuron in *Caenorhabditis elegans*. Proc Natl Acad Sci U S A *90*, 2227-2231.

Kassambara, A., and Mundt, F. (2020). factoextra: Extract and Visualize the Results of Multivariate Data Analyses.

Kent, L.B., and Robertson, H.M. (2009). Evolution of the sugar receptors in insects. BMC Evol Biol *9*, 41.

Kirti, J.S., Kaur, N., and Kaur, S. (2015). Scanning electron microscopic studies on cibarium of *Aedes albopictus* (Skuse) & *Aedes aegypti* (Linnaeus). International Journal of Mosquito Research *2*, 14-16.

Kistler, K.E., Vosshall, L.B., and Matthews, B.J. (2015). Genome engineering with CRISPR-Cas9 in the mosquito *Aedes aegypti*. Cell Rep *11*, 51-60.

Klapoetke, N.C., Murata, Y., Kim, S.S., Pulver, S.R., Birdsey-Benson, A., Cho, Y.K., Morimoto, T.K., Chuong, A.S., Carpenter, E.J., Tian, Z.*, et al.* (2014). Independent optical excitation of distinct neural populations. Nat Methods *11*, 338-346.

Kogan, P.H. (1990). Substitute blood meal for investigating and maintaining *Aedes aegypti* (Diptera: Culicidae). J Med Entomol *27*, 709-712.

Kong, X.Q., and Wu, C.W. (2010). Mosquito proboscis: an elegant biomicroelectromechanical system. Phys Rev E Stat Nonlin Soft Matter Phys *82*, 011910.

Kwon, H.W., Lu, T., Rutzler, M., and Zwiebel, L.J. (2006). Olfactory responses in a gustatory organ of the malaria vector mosquito *Anopheles gambiae*. Proc Natl Acad Sci U S A *103*, 13526-13531.

Lahondere, C., Vinauger, C., Okubo, R.P., Wolff, G.H., Chan, J.K., Akbari, O.S., and Riffell, J.A. (2020). The olfactory basis of orchid pollination by mosquitoes. Proc Natl Acad Sci U S A *117*, 708-716.

Lawson, R.G., and Jurs, P.C. (1990). New index for clustering tendency and its application to chemical problems. . J Chem Inf Comput Sci *30*, 36-41.

Lê, S., Josse, J., and Husson, F. (2008). FactoMineR: AnRPackage for Multivariate Analysis. Journal of Statistical Software *25*.

LeDue, E.E., Chen, Y.C., Jung, A.Y., Dahanukar, A., and Gordon, M.D. (2015). Pharyngeal sense organs drive robust sugar consumption in *Drosophila*. Nat Commun *6*, 6667.

Lee, R. (1974). Structure and function of the fascicular stylets, and the labral and cibarial sense organs of male and female *Aedes aegypti* (L.) Quaestiones entomologicae *10*, 187-215.

Lee, R.M.K.W., and Craig, D.A. (1983). The labrum and labral sensilla of mosquitoes (Diptera: Culicidae): a scanning electron microscope study. Can J Zool *61*, 1568-1579.

Leitao-Goncalves, R., Carvalho-Santos, Z., Francisco, A.P., Fioreze, G.T., Anjos, M., Baltazar, C., Elias, A.P., Itskov, P.M., Piper, M.D.W., and Ribeiro, C. (2017). Commensal bacteria and essential amino acids control food choice behavior and reproduction. PLoS Biol *15*, e2000862.

Li, X., Li, W., Wang, H., Cao, J., Maehashi, K., Huang, L., Bachmanov, A.A., Reed, D.R., Legrand-Defretin, V., Beauchamp, G.K.*, et al.* (2005). Pseudogenization of a sweet-receptor gene accounts for cats' indifference toward sugar. PLoS Genet *1*, 27-35.

Li, X., Yang, J., Pu, Q., Peng, X., Xu, L., and Liu, S. (2019). Serine hydroxymethyltransferase controls blood-meal digestion in the midgut of *Aedes aegypti* mosquitoes. Parasit Vectors *12*, 460.

Liao, Y., Smyth, G.K., and Shi, W. (2014). featureCounts: an efficient general purpose program for assigning sequence reads to genomic features. Bioinformatics *30*, 923-930.

Liesch, J., Bellani, L.L., and Vosshall, L.B. (2013). Functional and genetic characterization of neuropeptide Y-like receptors in *Aedes aegypti*. PLoS Negl Trop Dis *7*, e2486.

Lima, S.Q., and Miesenbock, G. (2005). Remote control of behavior through genetically targeted photostimulation of neurons. Cell *121*, 141-152.

Liman, E.R., Zhang, Y.V., and Montell, C. (2014). Peripheral coding of taste. Neuron *81*, 984-1000.

Liu, M.Z., and Vosshall, L.B. (2019). General Visual and Contingent Thermal Cues Interact to Elicit Attraction in Female *Aedes aegypti* Mosquitoes. Curr Biol *29*, 2250-2257 e2254.

Liu, Q., Tabuchi, M., Liu, S., Kodama, L., Horiuchi, W., Daniels, J., Chiu, L., Baldoni, D., and Wu, M.N. (2017). Branch-specific plasticity of a bifunctional dopamine circuit encodes protein hunger. Science *356*, 534-539.

Love, M.I., Huber, W., and Anders, S. (2014). Moderated estimation of fold change and dispersion for RNA-seq data with DESeq2. Genome Biol *15*, 550.

Marella, S., Fischler, W., Kong, P., Asgarian, S., Rueckert, E., and Scott, K. (2006). Imaging taste responses in the fly brain reveals a functional map of taste category and behavior. Neuron *49*, 285-295.

Matthews, B.J., Dudchenko, O., Kingan, S.B., Koren, S., Antoshechkin, I., Crawford, J.E., Glassford, W.J., Herre, M., Redmond, S.N., Rose, N.H.*, et al.* (2018). Improved reference genome of *Aedes aegypti* informs arbovirus vector control. Nature *563*, 501-507.

Matthews, B.J., McBride, C.S., DeGennaro, M., Despo, O., and Vosshall, L.B. (2016). The neurotranscriptome of the *Aedes aegypti* mosquito. BMC Genomics *17*, 32.

Matthews, B.J., Younger, M.A., and Vosshall, L.B. (2019). The ion channel ppk301 controls freshwater egg-laying in the mosquito *Aedes aegypti*. eLife *8*.

McBride, C.S. (2016). Genes and Odors Underlying the Recent Evolution of Mosquito Preference for Humans. Curr Biol *26*, R41-46.

McBride, C.S., Baier, F., Omondi, A.B., Spitzer, S.A., Lutomiah, J., Sang, R., Ignell, R., and Vosshall, L.B. (2014). Evolution of mosquito preference for humans linked to an odorant receptor. Nature *515*, 222-227.

McKellar, C.E. (2016). Motor control of fly feeding. J Neurogenet *30*, 101-111.

McMeniman, C.J., Corfas, R.A., Matthews, B.J., Ritchie, S.A., and Vosshall, L.B. (2014). Multimodal integration of carbon dioxide and other sensory cues drives mosquito attraction to humans. Cell *156*, 1060-1071.

Mishra, D., Thorne, N., Miyamoto, C., Jagge, C., and Amrein, H. (2018). The taste of ribonucleosides: Novel macronutrients essential for larval growth are sensed by *Drosophila* gustatory receptor proteins. PLoS Biol *16*, e2005570.

Miyamoto, T., Slone, J., Song, X., and Amrein, H. (2012). A fructose receptor functions as a nutrient sensor in the *Drosophila* brain. Cell *151*, 1113-1125.

Murphy, M., Peters, K.Z., Denton, B.S., Lee, K.A., Chadchankar, H., and McCutcheon, J.E. (2018). Restriction of dietary protein leads to conditioned protein preference and elevated palatability of protein-containing food in rats. Physiol Behav *184*, 235-241.

Ohla, K., Yoshida, R., Roper, S.D., Di Lorenzo, P.M., Victor, J.D., Boughter, J.D., Fletcher, M., Katz, D.B., and Chaudhari, N. (2019). Recognizing Taste: Coding Patterns Along the Neural Axis in Mammals. Chem Senses *44*, 237-247.

Owen, W.B. (1963). The Contact Chemoreceptor Organs of the Mosquito and Their Function in Feeding Behaviour. J Insect Physiol *9*, 73-87.

Pappas, L.G., and Larsen, J.R. (1978). Gustatory mechanisms and sugar-feeding in the mosquito, Culiseta inornata. Physiol Entomol *3*, 115-119.

Patapoutian, A., Tate, S., and Woolf, C.J. (2009). Transient receptor potential channels: targeting pain at the source. Nat Rev Drug Discov *8*, 55-68.

Peng, Y., Gillis-Smith, S., Jin, H., Trankner, D., Ryba, N.J., and Zuker, C.S. (2015). Sweet and bitter taste in the brain of awake behaving animals. Nature *527*, 512-515.

Potter, C.J., Tasic, B., Russler, E.V., Liang, L., and Luo, L. (2010). The Q system: a repressible binary system for transgene expression, lineage tracing, and mosaic analysis. Cell *141*, 536-548.

Ramasubramanian, M.K., Barham, O.M., and Swaminathan, V. (2008). Mechanics of a mosquito bite with applications to microneedle design. Bioinspir Biomim *3*, 046001.

Riabinina, O., Luginbuhl, D., Marr, E., Liu, S., Wu, M.N., Luo, L., and Potter, C.J. (2015). Improved and expanded Q-system reagents for genetic manipulations. Nat Methods *12*, 219-222, 215 p following 222.

Riabinina, O., Task, D., Marr, E., Lin, C.C., Alford, R., O'Brochta, D.A., and Potter, C.J. (2016). Organization of olfactory centres in the malaria mosquito *Anopheles gambiae*. Nat Commun *7*, 13010.

Ribeiro, C., and Dickson, B.J. (2010). Sex peptide receptor and neuronal TOR/S6K signaling modulate nutrient balancing in *Drosophila*. Curr Biol *20*, 1000-1005.

Rose, N.H., Sylla, M., Badolo, A., Lutomiah, J., Ayala, D., Aribodor, O.B., Ibe, N., Akorli, J., Otoo, S., Mutebi, J.P.*, et al.* (2020). Climate and Urbanization Drive Mosquito Preference for Humans. Curr Biol *30*, 3570-3579 e3576.

Rousseeuw, P.J. (1987). Silhouettes: a graphical aid to the interpretation and validation of cluster analysis. J Comput Applied Math *20*, 53-65.

Rowe, A.H., Xiao, Y., Rowe, M.P., Cummins, T.R., and Zakon, H.H. (2013). Voltage-gated sodium channel in grasshopper mice defends against bark scorpion toxin. Science *342*, 441-446.

Ruckert, C., and Ebel, G.D. (2018). How Do Virus-Mosquito Interactions Lead to Viral Emergence? Trends Parasitol *34*, 310-321.

Ruta, V., Datta, S.R., Vasconcelos, M.L., Freeland, J., Looger, L.L., and Axel, R. (2010). A dimorphic pheromone circuit in *Drosophila* from sensory input to descending output. Nature *468*, 686-690.

Rytz, R., Croset, V., and Benton, R. (2013). Ionotropic receptors (IRs): chemosensory ionotropic glutamate receptors in *Drosophila* and beyond. Insect Biochem Mol Biol *43*, 888-897.

Sanchez-Alcaniz, J.A., Silbering, A.F., Croset, V., Zappia, G., Sivasubramaniam, A.K., Abuin, L., Sahai, S.Y., Munch, D., Steck, K., Auer, T.O.*, et al.* (2018). An expression atlas of variant ionotropic glutamate receptors identifies a molecular basis of carbonation sensing. Nat Commun *9*, 4252.

Sanford, J.L., Shields, V.D., and Dickens, J.C. (2013). Gustatory receptor neuron responds to DEET and other insect repellents in the yellow-fever mosquito, *Aedes aegypti*. Naturwissenschaften *100*, 269-273.

Scott, K. (2018). Gustatory Processing in *Drosophila melanogaster*. Annu Rev Entomol *63*, 15-30.

Simpson, S.J., Le Couteur, D.G., and Raubenheimer, D. (2015). Putting the balance back in diet. Cell *161*, 18-23.

Slone, J., Daniels, J., and Amrein, H. (2007). Sugar receptors in *Drosophila*. Curr Biol *17*, 1809-1816.

Sparks, J.T., Vinyard, B.T., and Dickens, J.C. (2013). Gustatory receptor expression in the labella and tarsi of *Aedes aegypti*. Insect Biochem Mol Biol *43*, 1161-1171.

Steck, K., Walker, S.J., Itskov, P.M., Baltazar, C., Moreira, J.M., and Ribeiro, C. (2018). Internal amino acid state modulates yeast taste neurons to support protein homeostasis in *Drosophila*. Elife *7*.

Stocker, R.F. (1994). The organization of the chemosensory system in *Drosophila melanogaster*: a review. Cell Tissue Res *275*, 3-26.

Takken, W., and Verhulst, N.O. (2013). Host preferences of blood-feeding mosquitoes. Annu Rev Entomol *58*, 433-453.

Talay, M., Richman, E.B., Snell, N.J., Hartmann, G.G., Fisher, J.D., Sorkac, A., Santoyo, J.F., Chou-Freed, C., Nair, N., Johnson, M.*, et al.* (2017). Transsynaptic Mapping of Second-Order Taste Neurons in Flies by trans-Tango. Neuron *96*, 783-795 e784.

Tauber, J.M., Brown, E.B., Li, Y., Yurgel, M.E., Masek, P., and Keene, A.C. (2017). A subset of sweet-sensing neurons identified by IR56d are necessary and sufficient for fatty acid taste. PLoS Genet *13*, e1007059.

Thorne, N., Chromey, C., Bray, S., and Amrein, H. (2004). Taste perception and coding in *Drosophila*. Curr Biol *14*, 1065-1079.

Tobin, D., Madsen, D., Kahn-Kirby, A., Peckol, E., Moulder, G., Barstead, R., Maricq, A., and Bargmann, C. (2002). Combinatorial Expression of TRPV Channel Proteins Defines Their Sensory Functions and Subcellular Localization in *C. elegans* Neurons. Neuron *35*, 307-318.

Trembley, H.L. (1952). The distribution of certain liquids in the esophageal diverticula and stomach of mosquitoes. Am J Trop Med Hyg *1*, 693-710.

Van Handel, E. (1972). The Detection of Nectar in Mosquitoes. Mosquito News *32*, 458.

Van Handel, E. (1984). Metabolism of nutrients in the adult mosquito. Mosquito News *44*, 573-579.

Virtanen, P., Gommers, R., Oliphant, T.E., Haberland, M., Reddy, T., Cournapeau, D., Burovski, E., Peterson, P., Weckesser, W., Bright, J.*, et al.* (2019). SciPy 1.0--Fundamental Algorithms for Scientific Computing in Python. arXiv https://arxiv.org/abs/1907.10121.

von Kugelgen, I. (2006). Pharmacological profiles of cloned mammalian P2Y-receptor subtypes. Pharmacol Ther *110*, 415-432.

Walker, S.J., Corrales-Carvajal, V.M., and Ribeiro, C. (2015). Postmating Circuitry Modulates Salt Taste Processing to Increase Reproductive Output in *Drosophila*. Curr Biol *25*, 2621-2630.

Wang, Z., Singhvi, A., Kong, P., and Scott, K. (2004). Taste representations in the *Drosophila* brain. Cell *117*, 981-991.

Werner-Reiss, U., Galun, R., Crnjar, R., and Liscia, A. (1999a). Factors modulating the blood feeding behavior and the electrophysiological responses of labral apical chemoreceptors to adenine nucleotides in the mosquito *Aedes aegypti* (Culicidae). J Insect Physiol *45*, 801-808
.

Werner-Reiss, U., Galun, R., Crnjar, R., and Liscia, A. (1999b). Sensitivity of the mosquito *Aedes aegypti* (Culicidae) labral apical chemoreceptors to blood plasma components. J Insect Physiol *45*, 485-491.

Werner-Reiss, U., Galun, R., Crnjar, R., and Liscia, A. (1999c). Sensitivity of the mosquito *Aedes aegypti* (Culicidae) labral apical chemoreceptors to phagostimulants. J Insect Physiol *45*, 629-636.

Wu, A., Dvoryanchikov, G., Pereira, E., Chaudhari, N., and Roper, S.D. (2015). Breadth of tuning in taste afferent neurons varies with stimulus strength. Nat Commun *6*, 8171.

Yamaguchi, S. (1967). The Synergistic Taste Effect of Monosodium Glutamate and Disodium 5'-Inosinate. Journal of Food Science *32*, 473-478.

Yapici, N., Cohn, R., Schusterreiter, C., Ruta, V., and Vosshall, L.B. (2016). A Taste Circuit that Regulates Ingestion by Integrating Food and Hunger Signals. Cell *165*, 715-729.

Yarmolinsky, D.A., Zuker, C.S., and Ryba, N.J. (2009). Common sense about taste: from mammals to insects. Cell *139*, 234-244.

Zarrinmayeh, H., and Territo, P.R. (2020). Purinergic Receptors of the Central Nervous System: Biology, PET Ligands, and Their Applications. Mol Imaging *19*, 1536012120927609.

Zhang, J., Jin, H., Zhang, W., Ding, C., O'Keeffe, S., Ye, M., and Zuker, C.S. (2019). Sour Sensing from the Tongue to the Brain. Cell *179*, 392-402 e315.

Zhao, Z., Tian, D., and McBride, C.S. (2020). Development of a pan-neuronal genetic driver in *Aedes aegypti* mosquitoes. bioRxiv *https://doi.org/10.1101/2020.08.22.262527*.